UNIVERSITÉ DU QUÉBEC À CHICOUTIMI

THÈSE PRÉSENTÉE À L'UNIVERSITÉ DU QUÉBEC À CHICOUTIMI COMME EXIGENCE PARTIELLE DU DOCTORAT EN INGÉNIERIE

PAR

XIAOMING QIAN

COMPORTEMENT À LA DÉFORMATION À CHAUD D'ALLIAGES D'ALUMINIUM 6XXX

SEPTEMBRE 2019

UNIVERSITY OF QUEBEC AT CHICOUTIMI

A DISSERTATION PRESENTED TO THE UNIVERSITY OF QUEBEC AT CHICOUTIMI IN PARTIAL FULFILLMENT OF THE REQUIREMENTS FOR THE DOCTOR OF PHILOSOPHY IN ENGINEERING

BY

XIAOMING QIAN

HOT DEFORMATION BEHAVIOR OF 6XXX ALUMNIUM ALLOYS

SEPTEMBER 2019

Résumé

Au cours des dernières décennies, la consommation et la demande d'alliages d'aluminium ont augmenté rapidement en raison de leur légèreté, de leur rapport élevé de résistance/poids et de leur facilité de recyclage. Les alliages d'aluminium 6xxx (Al-Mg-Si) sont très largement utilisés dans les secteurs de la construction, de l'automobile et de l'aérospatiale en raison de leurs propriétés mécaniques attrayantes soit à la température ambiante, soit à des températures élevées (250-300 °C). La production des alliages d'aluminium corroyés 6xxx se déroule en plusieurs étapes, consistant principalement à couler des billettes/lingots par refroidissement direct (DC), puis à effectuer un traitement thermique d'homogénéisation, puis à subir des processus de déformation à chaud, tels que l'extrusion, le laminage ou le forgeage suivi d'un recuit. Pour les alliages 6xxx, le manganèse (Mn) est un élément d'alliage important pour modifier la microstructure et augmenter la résistance ainsi que pour contrôler la structure du grain. Lorsqu'il était présenté sous forme de matrice d'aluminium, de composés intermétalliques ou de dispersoïdes, l'addition de Mn avait une influence significative sur l'évolution des microstructures, le comportement à la déformation à chaud et les propriétés mécaniques.

Dans la présente étude, les effets de l'homogénéisation et du micro-alliage avec Mn sur l'évolution de la microstructure et la maniabilité à chaud de l'AA6060 ont été systématiquement examinés; Les effets du Mn et de ses dispersoïdes contenant du Mn sur le comportement à la déformation à chaud et la résistance à la recristallisation lors du recuit de l'alliage d'aluminium 6082 ont également été étudiés. Des travaux

expérimentaux ont été effectués à l'aide de la microscopie optique, du MEB, de l'EBSD électronique, du MET, de la mesure de la conductivité électrique et des tests de compression à chaud. Les résultats obtenus ont été divisés en quatre parties.

Dans la première partie, l'effet du traitement d'homogénéisation et du micro-alliage de Mn sur l'évolution de la microstructure et la maniabilité à chaud des alliages d'aluminium AA6060 a été étudié. Différents traitements d'homogénéisation ont été réalisés avec des températures allant de 520 à 610 ℃ et des durées de trempage de 2 à 16 h. L'évolution de la microstructure et l'ouvrabilité à chaud ont été évaluées par des tests de microscopie optique, SEM, de conductivité électrique et de compression à chaud. Les résultats ont révélé que la β-AlFeSi était la phase dominante de la microstructure à la coulée des alliages expérimentaux. Au cours de l'homogénéisation, des composés intermétalliques se sont fragmentés et le β-AlFeSi en forme de plaque s'est transformé en α-AlFeSi en forme de tige. Le comportement à la contrainte d'écoulement des alliages AA6060 homogénéisés a été principalement déterminé par le niveau de la solution solide. L'augmentation des températures d'homogénéisation a entraîné une contrainte d'écoulement plus élevée en raison de l'augmentation du nombre d'atomes de soluté dans la matrice en aluminium, mais a également favorisé la fragmentation et la transformation des composés intermétalliques. La croissance des grains s'est produite dans les alliages à faible teneur en Mn (<0,03 Mn) au cours de l'homogénéisation à haute température (580 à 610 ℃), ce qui a entraîné des baisses soudaines des contraintes d'écoulement et une forme irrégulière de l'échantillon après la déformation. Le micro-alliage de Mn (>

0,06%) peut empêcher efficacement la croissance des grains à de telles températures. Pour l'alliage avec micro-alliage de Mn (0,1%), une homogénéisation à 550-580 ℃ pendant 6 h pourrait constituer les conditions optimales pour équilibrer la contrainte d'écoulement et la microstructure souhaitable.

Dans la deuxième partie, trois vitesses de refroidissement post-homogénéisation et trois températures d'homogénéisation ont été appliquées aux alliages AA6060 coulés à froid. L'évolution de la microstructure dans différentes conditions d'homogénéisation et le comportement des contraintes d'écoulement lors de la déformation à chaud ont été systématiquement étudiés. Lors du refroidissement post-homogénéisation, du Mg_2Si a précipité dans la matrice d'aluminium, ce qui a eu une influence importante sur le niveau de la solution solide et la contrainte d'écoulement à haute température. Les résultats ont révélé que la diminution des vitesses de refroidissement réduisait considérablement la contrainte d'écoulement dû à la précipitation de Mg_2Si et de la réduction du niveau de solution solide. Le micro-alliage avec 0,1% en poids de Mn a généré une distribution de dispersoïdes d'α-Al(FeMn)Si au cours de l'homogénéisation, la densité en taille et en nombre diminuent et le Mn en solution solide augmentent à des températures d'homogénéisation plus élevées. Les études TEM ont confirmé que les dispersoïdes α-Al(FeMn)Si agissaient comme des sites de nucléation favorables de Mg_2Si et favorisaient donc grandement la précipitation de Mg_2Si lors du refroidissement ultérieur. En conséquence, la contrainte d'écoulement à haute température était contrôlée par les niveaux résiduels de Mg, Si et Mn dans la solution solide résultant

des interactions entre la formation de dispersoïde et la précipitation de Mg_2Si. La combinaison de l'addition de Mn, d'une faible vitesse de refroidissement et d'une basse température d'homogénéisation a permis d'obtenir la contrainte d'écoulement la plus faible et une densité en nombre élevée de Mg_2Si fin. Cette combinaison améliore la maniabilité à chaud et devrait favoriser la dissolution rapide de Mg_2Si lors de l'extrusion.

Dans la troisième partie, le comportement à la déformation à chaud des alliages d'aluminium 6082 contenant différentes teneurs en Mn (0,05 à 1,0% en poids) a été systématiquement étudié à l'aide des essais de compression uniaxiale à des températures comprises entre 400 et 550 °C et un taux de contrainte de 0,001 à 1. s-1. Avant la déformation à chaud, les billettes coulées par refroidissement direct ont été traitées à travers une homogénéisation à basse température à 450 °C pendant 6 h pour favoriser la précipitation des dispersoïdes contenant du Mn. Les résultats révèlent que la présence d'une grande quantité de dispersoïdes dans les alliages contenant du Mn a entraîné une augmentation significative des contraintes d'écoulement à haute température par rapport à l'alliage de base dépourvu de dispersoïdes. Les constantes des matériaux et l'énergie d'activation pour la déformation à chaud ont été déterminées à l'aide de l'équation constitutive hyperbolique-sinus et des données expérimentales sur les contraintes de débit maximales. L'énergie d'activation est passée de 191 kJ/mol pour l'alliage de base à 286 kJ/mol pour l'alliage à 0,5% Mn. Avec l'augmentation continue de la teneur en Mn, l'énergie d'activation n'a augmenté que modérément jusqu'à 315 kJ/mol pour l'alliage à 1,0% de Mn. Les influences des

niveaux de Mn et des conditions de déformation sur la restauration dynamique et la recristallisation ont été analysées quantitativement. La précipitation de dispersoïdes dans les alliages contenant du Mn a favorisé le retard de la récupération dynamique et l'inhibition de la recristallisation en raison de leur fort effet de blocage sur le mouvement de dislocation et la migration du sous-grain.

Dans la quatrième partie, l'effet de différentes teneurs en Mn (0,05 à 1% en poids) et de ses dispersoïdes sur la résistance à la recristallisation de 6082 alliages d'aluminium lors du recuit post-déformation a été étudié. Un traitement d'homogénéisation à basse température (450 ℃/6h) a été réalisé pour favoriser la précipitation de grandes quantités de dispersoïdes. Les échantillons ont été comprimés à chaud, puis recuits à 500 ℃ pendant 8 heures. Les évolutions microstructurales dans des conditions homogénéisées et déformées et après le recuit post-déformation ont été étudiées à l'aide de microscopes optiques, à balayage et électroniques à transmission et de la technique de diffraction à rétrodiffusion d'électrons. Les résultats ont révélé que la présence d'une grande quantité de dispersoïdes d'α-Al(Mn, Fe)Si dans des alliages contenant du Mn améliorait de manière significative la résistance à la recristallisation. Dans l'alliage de base dépourvu de Mn et de dispersoïdes, une recristallisation statique partielle s'est produite après 2 h et la croissance anormale des grains est apparue après un recuit de 4 h, alors que dans les alliages 6082 contenant du Mn, même après un recuit de 8 h à 500 ℃, la structure restaurée des grains était bien retenue. L'alliage à 0,5% de Mn présentait la meilleure résistance à la recristallisation, tandis que l'augmentation supplémentaire du taux de Mn à 0,75% et 1% entraînait une

réduction progressive de la résistance à la recristallisation malgré la densité plus élevée en nombre de dispersoïdes. La raison en était que la recristallisation ne se produisait que dans les zones dépourvues de particules (PFZ) et que la fraction de ces zones (PFZ) accrue avec la teneur en Mn, ce qui entraînait une augmentation de la fraction de recristallisation. La variation de la densité en nombre de dispersoïdes et leurs grossissements lors du recuit ont une influence limitée sur la recristallisation statique dans les alliages contenant du Mn.

Abstract

Over the last decades, the consumption and demand for aluminum alloys have rapidly grown owing to their light weight, high strength-to-weight ratio, and easy recyclability. 6xxx (Al-Mg-Si) aluminum alloys are very widely used in construction, automotive and aerospace industries due their due to their attractive mechanical properties at both room and elevated temperatures (250-300 ℃). The production of 6xxx wrought aluminum alloys involves many steps, mainly starting with direct chill (DC) casting of billets/ingots, processing with a homogenization heat treatment then subjected to hot deformation processes, such as extrusion, rolling or forging followed by an annealing. For 6xxx alloys, Manganese (Mn) is an important alloying element to modify the microstructure and increase the strength as well as control the grain structure. When presented in Al matrix, intermetallics or dispersoids, Mn addition gave significant influences on the evolution of microstructures, hot deformation behavior and mechanical properties.

In the present study, the effects of the homogenization and micro-alloying with Mn on the evolution of the microstructure and hot workability of AA6060 were investigated systematically; Effects of Mn and its related Mn-containing dispersoids on the hot deformation behavior and recrystallization resistance during annealing of 6082 aluminum alloy were also studied. Experimental work were carried out using optical microscopy, SEM, electron EBSD, TEM, electrical conductivity measurements and hot compression tests. The results obtained were divided into following four parts.

In the first part, the effect of the homogenization treatment and micro-alloying of Mn on the evolution of microstructure and hot workability of AA6060 aluminum alloys were investigated. Various homogenization treatments with temperatures ranging from 520 to 610 ℃ and soaking times from 2 to 16 h were conducted. Microstructure evolution and hot workability were evaluated by optical microscopy, SEM, electrical conductivity and hot compression tests. The results revealed that β-AlFeSi was the dominant phase in the as-cast microstructure of experimental alloys. During homogenization, fragmentation of intermetallics occurred and the plate-like β-AlFeSi transformed to rod-like α-AlFeSi. The flow stress behavior of the homogenized AA6060 alloys was mainly determined by the solid solution level. Increasing homogenization temperatures resulted in higher flow stress due to the increase of solute atoms in aluminum matrix but also promoted the fragmentation and transformation of the intermetallics. Grain growth occurred in the low Mn containing alloys (<0.03Mn) during high temperature homogenization (580-610 ℃), which resulted in sudden drops of flow stresses and irregular sample shape after deformation. The micro-alloying of Mn (>0.06%) can effectively prevent grain growth at such temperatures. For the alloy with micro-alloying of Mn (0.1%), homogenization at 550-580 ℃ for 6 h could be the optimum conditions to balance the flow stress and the desirable microstructure.

In the second part, three post homogenization cooling rates and three homogenization temperatures were applied to direct chill cast AA6060 alloys. The microstructure evolution for different homogenization conditions and the flow stress

behavior during hot deformation were systematically studied. During post homogenization cooling, Mg_2Si precipitated in the aluminum matrix, which had an important influence on the solid solution level and the high temperature flow stress. Results revealed that decreasing cooling rates reduced the flow stress significantly due to the precipitation of Mg_2Si and the reduction of the solid solution level. Micro-alloying with 0.1wt% Mn generated a distribution of α-Al(FeMn)Si dispersoids during homogenization with the size and number density decreasing and the Mn in solid solution increasing at higher homogenization temperatures. TEM studies confirmed that α-Al(FeMn)Si dispersoids acted as favorable nucleation sites of Mg_2Si and thus greatly promoted the precipitation of Mg_2Si during subsequent cooling. As a result the high temperature flow stress was controlled by the residual solid solution levels of Mg, Si and Mn resulting from the interactions between dispersoid formation and Mg_2Si precipitation. The combination of the Mn addition, a low cooling rate and a low homogenization temperature provided the lowest flow stress and a high number density of fine Mg_2Si. This combination improved the hot workability and should promote ready dissolution of Mg_2Si during extrusion.

In the third part, the hot deformation behavior of 6082 aluminum alloys containing different Mn contents (0.05-1.0 wt%) was systematically investigated using the uniaxial compression tests at the temperature range of 400-550 ℃ and strain rate range of 0.001-1 s^{-1}. Prior to hot deformation, direct chill cast billets were treated at a low temperature homogenization at 450 ℃ for 6 h to promote the precipitation of Mn-containing dispersoids. The results reveal that the presence of a large amount of

dispersoids in the Mn-containing alloys resulted in a significant increase in high temperature flow stresses compared to the base alloy free of dispersoids. The materials constants and activation energy for hot deformation were determined using the hyperbolic-sine constitutive equation and experimental peak flow stress data. The activation energy increased from 191 kJ/mol for the base alloy to 286 kJ/mol for the 0.5% Mn alloy. With further increasing Mn content, the activation energy increased only moderately to 315 kJ/mol for the 1.0% Mn alloy. The influences of Mn levels and deformation conditions on the dynamic recovery and recrystallization were quantitatively analyzed. The precipitation of dispersoids in the Mn-containing alloys promoted the retardation of dynamic recovery and the inhibition of recrystallization due to their strong pinning effect on dislocation movement and subgrain migration.

In the fourth part, the effect of different Mn contents (0.05–1 wt%) and its related dispersoids on recrystallization resistance of 6082 aluminum alloys during post-deformation annealing was investigated. A low temperature homogenization treatment (450 ℃/6h) was conducted to promote the precipitation of large amount of dispersoids. Samples were hot-compressed and then annealed at 500 ℃ up to 8 h. The microstructural evolution at homogenized and as-deformed conditions and after post-deformation annealing were studied using optical, scanning electron and transmission electron microscopes and the electron backscattered diffraction technique. The results revealed that the presence of a large amount of α-Al(Mn,Fe)Si dispersoids in Mn-containing alloys significantly improved the recrystallization resistance. In the base alloy free of Mn and dispersoids, after 2 h annealing the partial

static recrystallization occurred and the abnormal grain growth appeared after 4 h annealing, whereas in Mn-containing 6082 alloys, even after 8 h at 500 ^{o}C annealing the recovered grain structure was well retained. The alloy with 0.5% Mn exhibited the best recrystallization resistance, while the further increase of Mn level to 0.75% and 1% resulted in a gradual reduction of recrystallization resistance despite of the higher dispersoid number density. The reason was that the recrystallization occurred only in the particle free zones (PFZs) and the increased PFZ fraction with Mn content led to an increase in recrystallization fraction. The variation in dispersoid number density and coarsening of dispersoids during annealing had limited influence on static recrystallization in Mn-containing alloys.

Acknowledgement

First and foremost, it is with immense gratitude that I acknowledge the support and help of my director Prof. X. Grant Chen. He provided me not only the chance to study in Canada and offered the financial support ensuring my living in Chicoutimi, but also introduced me to an academic world and gave great guidance for my Ph. D study. It is his excellent academic knowledge and industrial experiences as well as the innovative ideas that make the continuously ongoing of my Ph. D study. It is hard to imagine that I can finish my Ph. D study without his timely help and valuable advice throughout the four years of research duration.

Secondly, I would like to express my sincere appreciation to my co-director Dr. Nick Parson from Arvida Research & Development Centre (ARDC) of Rio Tinto, for his expertise guidance and suggestions during the planning and development of the research tasks as well as the papers writing.

Thirdly, I am also grateful to Prof. Zhan Zhang, who gave me the training of SEM, EBSD, TEM and also precious comments in detail on the operation of the experimental equipment. And also I thank Professor Sarkar Dilip, who offered me valuable courses and advice during my study. Thanks Prof. Kun Liu, for giving me encouragement to overcome difficulties and heat-warmed smile every time encounter.

Then, I would like to extend my thanks the colleagues in CURAL (Centre Universitaire de Recherche sur L'aluminium) who helped me during the research and lab experiment. Dany Racine helped me a lot on the lab rules training, let me formed the habit to follow the safety rules in the lab. Samuel Dessureault gave me many on

time help when I had difficult on the sample polishing. Thanks Dave Girard for the machining of large amount of Gleeble samples. And my dearest friends in CURAL, who supported me and made my life full of fun. Those includes Chen Li, Wei Xu, Sinan Chen, Siyu Chen, Mengyun Liu, Lanfeng Jin, Zhen Li, Jian Qin, Lei, Pan, Anil Arici, Mohammadreza Mofarrehi, Redouane Farid, Xingli Chen, Zhixing Chen, Jovid Rakhmonov, Siamak Nikzad Khangholi, Ali Elashery, Ahmed Algendy, Mohamed Ahmed, Shuai Wang, Dong Li, Cong Li, Émélie Brideau and Pier-Luc Prive.

Finally, but by no means least, I cannot find words to express my gratitude to my wife Shanshan Qian whose love are always with me, and sharing summer and winter during the four years in Chicoutimi.

This project was financially supported by Natural Science and Engineering Research Council of Canada (NSERC) and Rio Tinto Aluminum through the NSERC Industry Research Chair in the Metallurgy of Aluminum Transformation at Université du Québec à Chicoutimi (UQAC). I would like to thank both organizations for their support for my research.

Publications

Journal papers:

1. Xiaoming Qian, Nick Parson, X. Grant Chen, Effect of homogenization treatment and micro-alloying of Mn on the microstructure and hot workability of AA6060 aluminum alloys, Journal of Materials Engineering and Performance, https://doi.org/10.1007/s11665-019-04232-7.

2. Xiaoming Qian, Nick Parson, X. Grant Chen, Effect of post homogenization cooling rate and Mn contenton Mg2Si precipitation and hot workability of AA6060 alloys (To be summit in 2019).

3. Xiaoming Qian, Nick Parson, X. Grant Chen, Effect of Mn addition and its related Mn-containing dispersoids on the hot deformation behavior of 6082 aluminum alloy, Materials Science & Engineering A 764 (2019) 138253.

4. Xiaoming Qian, Nick Parson, X. Grant Chen, Effect of Mn and dispersoids on recrystallization resistance of 6082 aluminum alloys during post-deformation annealing (To be summit in 2019).

Posters:

1. Xiaoming Qian, Nick Parson, X. Grant Chen, Effect of homogenization regime and Mn on microstructure and electrical conductivity of AA6060 alloys. REGAL student's day, Quebec, Canada, October. 2016. (Dynamic Concept awarded)

2. Xiaoming Qian, Nick Parson, X. Grant Chen, Effect of homogenization treatment on the hot workability of AA6060 alloys, REGAL student's day, Montreal, Canada,

September. 2017.

3. Xiaoming Qian, Nick Parson, X. Grant Chen, Effect of cooling rate and Mn on the Mg_2Si precipitation during homogenization cooling of AA6060 alloys, REGAL student's day, Montreal, Canada, June. 2018. . (Aluminerie Alouette prize awarded)

Presentation:

Effect of homogenization treatment on the hot workability of AA6060 alloys, REGAL student's day, Montreal, Canada, September. 2017. (1^{st} prize best speaker of AAC awarded)

Table of Contents

List of Tables

List of Figures

Chapter 1 Introduction

1.1 Background

The 6xxx (Al-Mg-Si) aluminum alloys are one of the most popular wrought alloys with a wide range of applications in the aerospace, aircraft, automotive and construction industries due to their high strength to weight ratio, excellent corrosion resistance and low cost [1-3].

Among 6xxx alloys, 6060 aluminum alloys have comparable low contents of Mg and Si and are featured as medium strength, excellent formability, good corrosion resistance and anodizing properties. The advantage in the aspect of formability makes 6060 alloys ideal materials used for extrusion parts with complex cross sections. Industrially, 6060 alloys are mostly produced by the direct chill (DC) casting in term of extrusion billets, during which the non-equilibrium solidification induces inhomogeneous microstructure such as micro-segregation and a network of brittle Fe-bearing intermetallics, causing a low formability [4, 5]. In general, a homogenization heat treatment is conducted before extrusion to eliminate such negative effects.

Industrial homogenization consists of the following steps: heating, soaking and cooling at the predetermined rates. During soaking stage of homogenization, the microsegregation of alloying elements at dendrite boundaries can be diminished, leading to a more uniform elements distribution in in the aluminum matrix [6]. On the other hand, the interdendritic network of the plate-like β-AlFeSi intermetallics is

gradually replaced by the more rounded and discrete α-AlFeSi intermetallic particles [7-9]. The precipitation of secondary particles (dispersoids) can also occur in Mn- or Cr-containing alloys [3, 10]. The proper homogenization regime can significantly increase the extrusion productivity and give a great benefit on the surface finish [11, 12].

At the cooling step, precipitation of Mg_2Si usually occurs. Depending on the cooling regime, the Mg_2Si precipitation differs. A rapid cooling tends to trap the Mg and Si in solid solution with little or no Mg_2Si precipitation produced while a slow cooling tends to produce coarse Mg_2Si particles [13, 14]. Fine or no precipitation of Mg_2Si results in the increase in the flow stress since Mg and Si are trapped in the solution, while coarse Mg_2Si precipitation lead to the lower flow stress due to the reduced Mg and Si solution level in the matrix [15]. Re-dissolution of these Mg_2Si is desired during the extrusion process for the purpose of fulfilling the demand of as high as possible Mg and Si solution level for the subsequent T5 ageing. However, if the Mg_2Si particles were too coarsen to dissolve, this could result in the partially loss of potential strengthening of subsequent T5 ageing. For these consideration, the number of particles should be high to reduce the solid solution strengthening during hot working [16], but the particles are not too large for enhanced dissolution during extrusion [17].

6082 alloys have been receiving an increasing attention recently owing to their superior room temperature mechanical properties and their potential in the applicationsat elevated temperatures [18, 19]. The mechanical properties at elevated

temperatures of 6082 alloy were mainly based on the dispersoids-strengthening mechanism. 6082 alloys have high level of dispersoids-forming elements of Mn and Si, which are supersaturated in the as-cast state and follow the decomposition of the supersaturated solid solution during heat treatment to precipitate the dispersoids [10, 20]. In a recent work of Li [19], it is found that α-Al(FeMn)Si dispersoids in 6082 alloys started to precipitate at 350 ℃ and reached the highest number density at 400-450 ℃. While at temperature higher than 500 ℃, the disperosoids coarsened and the number density decreased sharply with time.

The production of aluminum wrought alloys involves many steps, mainly starting with direct chill (DC) casting of billets/ingots, processing with a homogenization heat treatment and followed by hot deformation processes, such as extrusion, rolling or forging. During hot deformation, the high temperature flow stress is one of the most significant factors for the design of hot deformation regime due to its substantial impact on the required deformation load and the kinetics of metallurgical transformation [21]. It is known that the high temperature flow stress was closely related to the alloy chemistry, homogenization heat treatment history and microstructure [21-23]. In general, Al-Mg-Si 6082 alloys prior to hot deformation are subjected a high temperature homogenization treatment (550-580 ℃) [22], where the dispersoids could precipitate during heating process. The size and number density of dispersoids plays an important role on the high temperature flow stress, the retardation of dynamic recovery and the inhibition of recrystallization. However, after such high temperature homogenization treatment, Mn-containing dispersoids in 6082

alloys were coarsened and dissolved, leaving a limited amount of dispersoids in the aluminum matrix [22, 24, 25]. To date, several studies have conducted to investigate the effect of Zr and V and their related dispersoids on the flow stress behavior and the inhibition of dynamic recrystallization [26-28]. However, a systematical investigation of the effect of Mn and its related Mn-containing dispersoids on the hot deformation behavior and deformed microstructure in Al-Mg-Si 6xxx alloys has not been found in the literature.

To study the hot deformation of aluminum alloys, different types of constitutive equations have been applied to analyze and predict the hot deformation behavior. Among many equations and models, the hyperbolic-sine Arrhenius-type equation proposed by Sellars and McTegart [29] is widely used for constitutive analysis over a wide range of temperatures and strain rates. Using this constitutive equation, the activation energy for hot deformation Q could be derived from a series of flow stress data. The Q values were often used to compare the difficulty degree of plastic deformation between different aluminum alloys [30-32]. Recent works discovered that the Q was not a constant for an alloy but it might vary with deformation conditions (mainly temperature and strain rate) [10, 33, 34]. The changes in hot deformation flow stress and activation energy are closely related to the balance between dynamic work hardening and dynamic softening under a specific hot deformation condition [30]. Dynamic recovery (DRV) and dynamic recrystallization (DRX) are the main softening mechanisms during deformation at high temperature [35-37]. DRV associated with change of the density and distribution of line defects,

while DRX took place by means of progressive transformation of subgrains to the newly formed grains as well as grain boundary migration [30, 31]. The effects of Zr-containing dispersoids (Al_3Zr) and V-containing dispersoids ($Al_{11}V$) on DRV and DRX in 7xxx alloys have been thorough studied [26, 30, 31]. It is reported that the softening mechanism of 7050 alloys shifted from DRV to DRX with decreasing Z (Zener–Hollomon parameter) [30, 38]. However, the influence of Mn-containing dispersoids (α-Al(MnFe)Si) on deformed microstructure of 6xxx alloys due to DRV and DRX is still far being clear.

After deformation, an annealing treatment is necessary to be performed so as to get a stable property [39]. Static recovery (SRV) and static recrystallization (SRX) are usually occurred during annealing. SRV associated with change of the density and distribution of line defects while SRX involved nucleation of new grains and their growth as well as grain boundary migration [30, 34]. The partially recrystallized structures or coarse grains are undesirable due to their detrimental effect not only on strength, toughness, and formability, but also on surface quality and corrosion resistance [40]. Therefore, good recrystallization resistance is of paramount importance for adequate performance. The use of dispersoids in Al alloys is a well-established method of controlling grain growth and recrystallization during annealing treatment. The size, number density, distribution and morphology of dispersoids could have significant influence on the recrystallization resistance. Birol [41] reported that the addition of Zr and Sc was an efficient and applicable approach to improve recrystallization resistance via the formation of Al(Cr,Mn,Fe)Si and (Al,

Si)3Zr dispersoids. L.P. Troeger and E.A. Starke Jr. [42] reported that in an Al-Mg-Si-Cu alloy a homogeneous distribution of micron-size precipitates was necessary for developing a fine and uniform grain structure.

In the first two parts of present study, the effects of the homogenization and micro-alloying with Mn on the evolution of the microstructure, Mg2Si and hot workability of AA6060 alloys were investigated systematically. The as-cast and homogenized microstructures were examined, and the true stress–strain response was obtained by conducting hot-compression tests. The focus of this study is the relation between the microstructure, solid solution levels, and hot workability in term of homogenization and Mn addition.

In the third and fourth parts, research work was centered on the effects of Mn and its related Mn-containing dispersoids on the hot deformation behavior and recrystallization resistance of 6082 aluminum alloy. To accommodate the goal, in contrary to the usual high temperature homogenization, a low temperature homogenization at 450 ℃ for 6 h was applied to DC cast billets to promote the maximum precipitation of Mn-containing dispersoids prior to hot deformation. The influence of different Mn contents (0.05-1.0 wt%) on high temperature flow stresses as a function of the deformation temperature and strain rate were studied. Using the hyperbolic-sine constitutive equation, the materials constants and activation energy for hot deformation were calculated based on the flow stress data. The deformed microstructure was studied using the electron back-scattered diffraction (EBSD) technique to study the the effect of dispersoids on DRV and DRX. The deformed

samples were subjected to a post-deformed annealing treatment. The influence of different Mn contents (0.05-1.0 wt%) on recrystallization as a function of the annealing time was studied. The microstructural evolution of the alloys during hot deformation and annealing was investigated to understand the effect of dispersoids on SRV and SRX.

1.2 Objectives

This research project is divided in four parts. The objectives of each part are detailed as follows:

1) Effect of homogenization temperature, soaking time and micro-alloying of Mn on the microstructure and hot workability of AA6060 aluminum alloys

a) Studying the effect of the homogenization parameter and micro-alloying of Mn (0-0.1%wt.) on the evolution of microstructure;
b) Examined and the true stress–strain response and hot workability on solid solution levels and hot workability;

2) Effect of post homogenization cooling rate and Mn contenton Mg2Si precipitation and hot workability of AA6060 alloys

a) Quantifying the influences of the cooling rate of homogenization and micro-alloying of Mn (0-0.1%wt.) on the Mg_2Si precipitation;
b) Evaluating the ifluences of the homogenization temperature, cooling rate and micro-alloying on high temperature flow stress;

3) Effect of Mn-containing dispersoids on the hot deformation behavior of 6082

alloys

a) Investigating hot deformation flow stress in different alloys;

b) Using the hyperbolic-sine constitutive equation, calculating the materials constants and activation energy;

c) Studying the microstructural evolution of the alloys during hot deformation to understand the effect of dispersoids on DRV and DRX.

4) Effect of Mn-containing dispersoids on the recrystallization resistance of 6082 alloys

a) Evaluating the effects of the Mn-containing dispersoids on the recrystallization resistance during post-deformed annealing;

b) Investigating the mechanism of SRV and SRX during post-deformed annealing.

References

[1] J. Dutkiewicz, L. Litynska, The effect of plastic deformation on structure and properties of chosen 6000 series aluminium alloys. Mater. Sci. Eng., A. 324 (2002) 239-243.

[2] L.P. Troeger, E.A. Starke, Microstructural and mechanical characterization of a superplastic 6xxx aluminum alloy. Mater. Sci. Eng., A. 277 (1) (2000) 102-113.

[3] R. Hu, T. Ogura, H. Tezuka, T. Sato, Q. Liu, Dispersoid Formation and Recrystallization Behavior in an Al-Mg-Si-Mn Alloy. J. Mater. Sci. Technol. 26 (3) 2010 237-243.

[4] J.H. Li, A. Wimmer, G. Dehm & P. Schumacher, Intermetallic phase selection during homogenization for AA6082 alloy, Philosophical Magazine, 94, 8, (2014) 830-846.

[5] S. Kumar, K.A.Q. O'Reilly, Influence of Al grain structure on Fe bearing intermetallics during DC casting of an Al-Mg-Si alloy, Materials Characterization 120 (2016) 311-322.

[6] S.N. Samaras, G.N. Haidemenopoulos, Modelling of microsegregation and homogenization of 6061 extrudable Al-alloy, Journal of Materials Processing Technology 194 (2007) 63–73.

[7] A.L. Dons, The Alstruc homogenization model for industrial aluminum alloys, J. Light Met. 1 (2001) 133–149.

[8] N.C.W. Kuijpers, F.J. Vermolen, K.Vuik and S. van der Zwaag, A Model of the β-AlFeSi to α-Al(FeMn)Si Transformation in Al-Mg-Si Alloys, Materials Transactions, 44, 7 (2003) 1448-1456.

[9] N. Bayat, T. Carlberg, M. Cieslar, In-situ study of phase transformations during homogenization of 6005 and 6082 Al alloys, Journal of Alloys and Compounds 725 (2017) 504-509.

[10] L. Lodgaard, N. Ryum, Precipitation of dispersoids containing Mn and:or Cr in Al–Mg–Si alloys, Materials Science and Engineering A 283 (2000) 144-152.

[11] O. Reiso, Extrusion of AlMgSi Alloys, The 9th International Conference on Aluminium Alloys (2004) 32-46.

[12] Y. Totik, M. Gavgali, The effect of homogenization treatment on the hot

workability between the surface and the center of AA 2014 ingots, Materials Characterization 49 (2003) 261–268 .

[13] E.B. Bjornbakk, The influence of homogenization cooling rate, billet preheating temperature and die geometry on the T5-properties for three 6XXX alloys extruded under industrial conditions, Materials Science Forum 396-402 (2002) 405-410.

[14] N. Dahl, T. Johnsen, B.R. Henriksen, E.K. Jensen, Precipitation of Mg_2Si in Al–Mg–Si‐alloys during cooling from homogenization temperature, Proceedings of 6th International Aluminum Extrusion Technology Seminar 1 (1996) 529-535.

[15] J. Langerweger, Effect of metallurgical factors on productivity in the extrusion of aluminum–magnesium–silicon (AlMgSi) alloys, Aluminum 58(1982) 107-109.

[16] J. van de Langkruis, The effect of thermal treatments on the extrusion behaviour of AlMgSi alloys, Ph.D. Thesis, Delft University of Technology (2000) 61-84.

[17] Y. Birol, The effect of homogenization practice on the microstructure of AA6063 billets, J. Mater. Process. Technol. 148 (2004) 250-258.

[18]. Y. Han, K. Ma, L. Li, W. Chen, H. Nagaumi, Study on microstructure and mechanical properties of Al–Mg–Si–Cu alloy with high manganese content, Materials and Design 39 (2012) 418–424.

[19]. C. Li, Precipitation Behaviors of dispersoids induced from transition elements (Mn, Sc And Zr) and their effect on recrystallization resistance in AA6082 alloys, Master theses, University of Quebec at Chicoutimi, 2018.

[20] C. Liu, PhD thesis, Microstructure evolution during homogenization and its effect on the high temperature deformation behaviour in aa6082 based alloys, The

University of British Columbia (2017) 74−92.

[21] W. Geertruyden, W. Misiolek, P. Wang, Grain structure evolution in a 6061 aluminum alloy during hot torsion, Mater. Sci. Eng. A 419 (2006) 105–114.

[22] C. Shi, W. Mao, X.-G. Chen, Evolution of activation energy during hot deformation of AA7150 aluminum alloy, Mater. Sci. Eng. A 571 (2013) 83–91.

[23] R. Kaibyshev, O. Sitdikov, A. Goloborodko, Grain refinement in as-cast 7475 aluminum alloy under hot deformation, Mater. Sci. Eng. A 344 (2003) 348–356.

[24] C.M. Sellars and W.J. McTegart, La relation entre la resistance et la structure dans la deformation a chaud, Mem. Sci. Rev. Met., (1966)63, 731–746. (in French)

[25] B. Zhang, T. Baker, Effect of the heat treatment on the hot deformation behaviour of AA6082 alloy, J. Mater. Proc. Tech. (2004) 153–154, 881–885.

[26] S. Gourdet, F. Montheillet, An experimental study of the recrystallization mechanism during hot deformation of aluminium, Mater. Sci. Eng. A 283 (2000) 274–288.

[27] D. Tsivoulas, P. Prangnell, The effect of Mn and Zr dispersoid-forming additions on recrystallization resistance in Al–Cu–Li AA2198 sheet, Acta Mater. 77 (2014) 1–16.

[28] M. Rokni, A. Zarei-Hanzaki, A. Roostaei, H. Abedi, An investigation into the hot deformation characteristics of 7075 aluminum alloy, Mater. Des. 32 (2011) 2339–2344.

[29] C. Shi, X. G.-Chen, Effect of vanadium on hot deformation and microstructural evolution of 7150 aluminum alloy, Mater. Sci. Eng. A 613 (2014) 91–102.

[30] D. Tsivoulas, P. Prangnell, The effect of Mn and Zr dispersoid-forming additions on recrystallization resistance in Al–Cu–Li AA2198 sheet, Acta Mater. 77 (2014) 1–16.

[31] M. Rokni, A. Zarei-Hanzaki, A. Roostaei, H. Abedi, An investigation into the hot deformation characteristics of 7075 aluminum alloy, Mater. Des. 32 (2011) 2339–2344.

[32] M. Shakiba, N. Parson, X.-G. Chen, Effect of iron and silicon content on the hot compressive deformation behavior of dilute Al-Fe-Si alloys, J. Mater. Eng. Perform. 24 (2015) 405–415.

[33] C. Liu, H. Azizi-alizamini, N. Parson, W. Poole, Q. Du, Microstructure evolution during homogenization of Al-Mg-Si-Mn-Fe alloys: Modelling and experimental results, Trans. Nonferrous Met. Soc. China 27 (2017) 747−753.

[34] H. J. McQueen, S. Spigarelli, M. Kassner, E. Evagelista, Hot Deformation and Processing of Aluminum Alloys, CRC, Bradenton, FL (2011) 87–233.

[35] D. Samantaray, S. Mandal, C. Phaniraj, A. Bhaduri, Flow behavior and microstructural evolution during hot deformation of AISI Type 316 L(N) austenitic stainless steel, Mater. Sci. Eng. A 528 (2011) 8565.

[36] H. Liao, Y. Wu, K. Zhou, J. Yang, Hot deformation behavior and processing map of Al–Si–Mg alloys containing different amount of silicon based on Gleebe-3500 hot compression simulation, Mater. Des. 65 (2015) 1091–1099.

[37] M. Shakiba, N. Parson, X.-G. Chen, Hot deformation behavior and rate-controlling mechanism in dilute Al–Fe–Si alloys with minor additions of Mn and

Cu, Mater. Sci. Eng. A 636 (2015) 572–581.

[38] S. Spigarelli, E. Evangelista, H. J. McQueen, Study of hot workability of a heat treated AA6082 aluminum alloy, Scr. Mater. 49 (2003) 179–183

[39]. S. Lin, Z. Nie, H. Huang, B. Li, Annealing behavior of a modified 5083 aluminum alloy, Materials and Design 31 (2010) 1607–1612

[40] Y. Birol, Impact of partial recrystallization on the performance of 6005A tube extrusions, Engineering Failure Analysis 17 (2010) 1110–1116.

[41] Y. Birol, Effect of Cr and Zr on the Grain Structure of Extruded EN AW 6082 Alloy, Met. Mater. Int., 20, 4 (2014) 727-732.

[42] L.P. Troeger, E.A. Starke Jr, Particle-stimulated nucleation of recrystallization for grain-size control and superplasticity in an Al–Mg–Si–Cu alloy, Materials Science and Engineering A293 (2000) 19–29.

Chapter 2 Literature review

2.1 Review of Al-Mg-Si (6xxx) alloys

Over the last decades, the consumption and demand for aluminum alloys have rapidly grown owing to their light weight, high strength-to-weight ratio, and easy recyclability. AA6xxx series alloys are widely used in construction and transportation industries due to their attractive combination of mechanical properties, processability and corrosion resistance [1-3].

Mg and Si are the main alloying elements of 6xxx alloys. The contents of Mg and Si range typically from 0.20 to 1.20 wt.% and from 0.20 to 1.25 wt.%, respectively. The Mg and Si could form metastable Mg-Si precipitates which are the source of precipitation hardening in these 6xxx alloys. 6xxx alloys are in general obtained by undergoing T6 heat treatment to achieve adequate strength. Fig. 2.1 shows some typical 6xxx alloys with the different contents of Mg and Si as well as the ranges of strength [4]. The contents of Mg and Si determine the potential strength after the T6 heat treatment. Among the alloys, 6060 alloys have comparable low contents of Mg and Si and thus possessing moderate mechanical properties, while 6082 alloys have higher levels of Mg and Si, and therefore exhibiting higher strength levels.

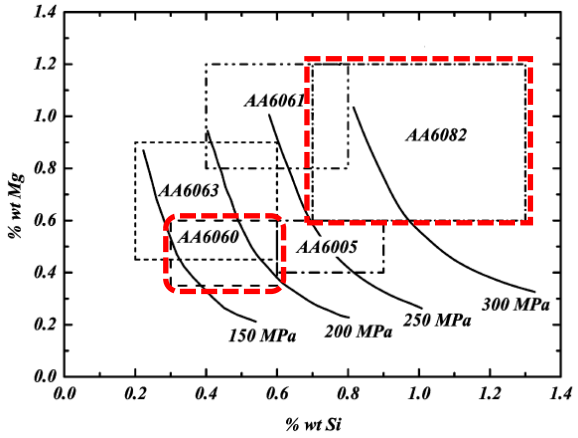

Fig. 2.1 Typical 6xxx alloys with the different contents of Mg and Si as well as the ranges of strength

2.2 Homogenization of 6xxx alloys

The typical heat treatment for the production of 6xxx alloys are shown in Fig. 2.2. Extrusion billets are mostly produced by the direct chill (DC) casting. After that, the homogenization is conducted to eliminate casting negative effects. Subsequently the billets are cooled down and transported to the extrusion press; the billets are then re-heated to the desired temperature and extruded. During extrusion the billets are pressed through a die with a shaped opening. After extrusion, the extrusion profile may be press-quenched to room temperature. Finally, the extrusion profiles are artificially age-hardened to improve the final extruded product properties.

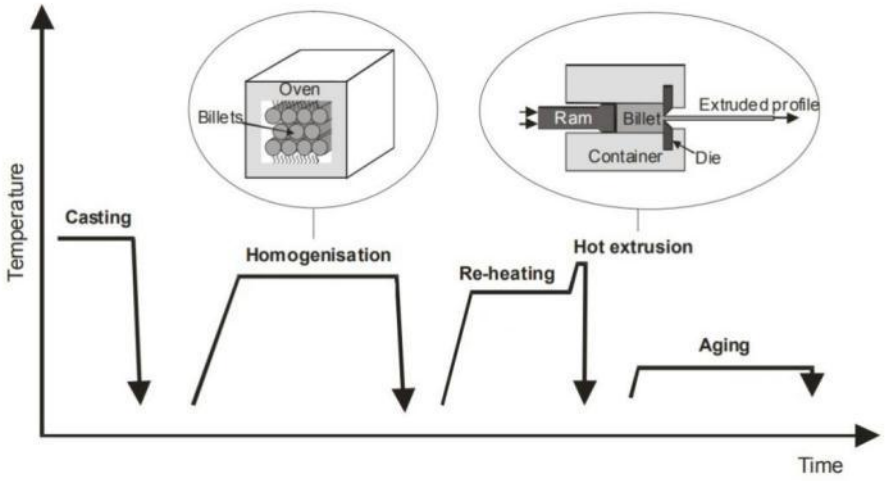

Fig. 2.2 The typical heat treatment for the production of 6xxx extrusion alloys

2.2.1 As-cast billet and benefits of homogenization

6xxx billets are mostly produced by the direct chill (DC) casting, during which the non-equilibrium solidification induces inhomogeneous microstructure as the following [5]:

1) Microsegregation of alloying elements, grain boundary segregation.

2) Low melting point eutectics and brittle intermetallic, such as β-AlFeSi.

3) Supersaturated solutions which lead increases of the deformation flow stress.

This inhomogeneous microstructure was undesirable for the extrusion, because it lead the higher breakout pressures, lower throughput rates, worse surface finish (a surface with streaking, pick-up or die-lines).

These negative effects can be partly or completely eliminated by the homogenization heat treatment of the cast billets. The main benefits of this process are the following [6]

1). Removal of microsegregation.

2). Dissolution of primary Mg_2Si in solid solution before extrusion in order to ensure the age hardening potential.

3). Transformation of β-AlFeSi to α-Al(FeMn)Si constituent, and fragmentation and round-off of intermetallics.

4). Formation of dispersoids for grain size control during extrusion.

2.2.2 The transformation of β to α intermetallic during homogenization

One of the important objectives on applying the homogenization treatment before hot deformation is to modify the intermetallic phase type and morphology in order to improve hot workabiltiy [7].

Table 2.1 shows the three most prevalent types of intermetallics in 6xxx alloys, which are the monoclinic β-AlFeSi phase, the hexagonal α_h-AlFeSi and cubic α_c-Al(FeMn)Si [8-25]. The α_c phase includes three types: an α_c phase containing Fe, an α_c phase containing Fe and Mn, and an α_c phase containing Mn. The stoichiometry of each phase is different and the properties of different phases are reported by different authors.

Table 2.1 The structural variance of the prevalent intermetallic phases in 6xxx alloys

Notation	stoichiometry	Bravais lattice/ Space group	Lattice parameters/ Space group	References
β	Al4.5FeSi [14] Al5FeSi [12]	Monoclinic	a = 6.12 Å b = 6.12 Å c = 41.5 Å β = 91°	[8-12]
α_h (α′)	Al8Fe2Si	Hexagonal/ P63	a = b = 12.3 Å c = 26.2 Å	[8, 13,14]
α_c	(Fe containing) Al12Fe3Si [19], Al12-15Fe3Si1-2[23]	Cubic /Im3	a = 12.56 Å	[8, 15-19]
	(Fe+Mn containing) Al12(FeMn)3Si [24], Al15(FeMn)3Si2 [12]	Cubic/ Im3- Pm3	a = 12.56-12.68 Å	[8,9,14,18,20-23]
	(Mn containing) Al12Mn3Si [24], Al15Mn3Si2 [12], Al9Mn2Si [22]	Cubic /Pm3	a = 12.68 Å	[8,16,18,20,24,25]

In 6xxx alloys, β-AlFeSi generally presented in as-cast microstructures while α-Al(FeMn)Si was the typical phase in as-homogenized condition. The transformation of β-AlFeSi to α-Al(FeMn)Si during the homogenization was an important aspect for the subsequent processing and could be influenced by the specific homogenization regimes.

Kuijpers [26] reported that during homogenization at 540 ℃ for 30 minutes, the dominant intermetallic in 6082 alloy was still needles shape β-AlFeSi (Fig 2.3a). The partial homogenization for 8 hours exhibited the mixture of β and α (Fig 2.3b). The heavy homogenization for 32 hours resulted in the fully transformed α-Al(FeMn)Si phase, which appeared as a string of separate more round α particle with more curvy edges (Fig 2.3c). Results also suggested that the increase of homogenization temperature could significantly raise the transformation rate; the high homogenization temperature of 590 °C for 32 h was necessary in order to transform all the β-AlFeSi phase to the α-Al(FeMn)Si phase [26].

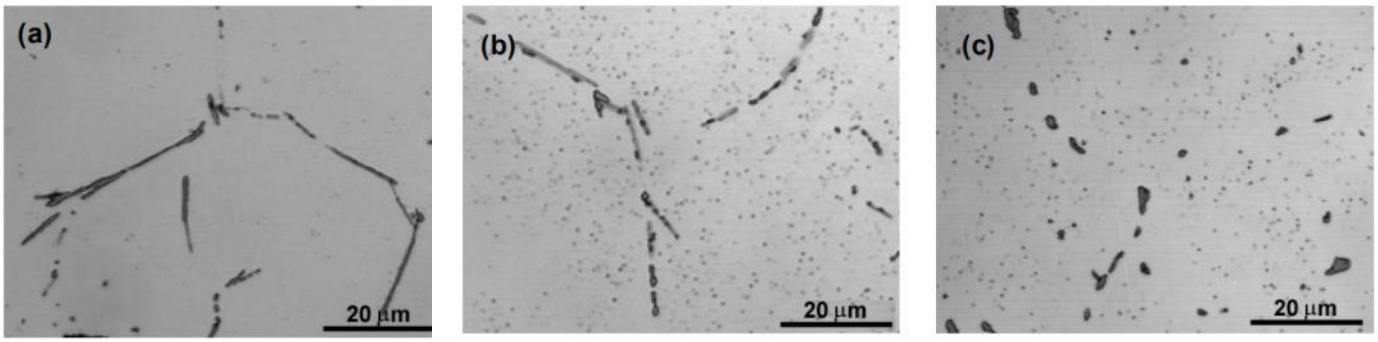

Fig. 2.3 Optical micrographs of the intermetallic structure (a) lightly homogenized for 30 minutes, (b) partially homogenized for 8 hours and (c) heavily homogenized for 32 hours at 540 ℃ of 6082 alloy (For the partially transformed sample the etching produced contrast between the β-Al_5FeSi phase, which appears light grey, and the α_c-$Al_{12}(FeMn)_3Si$ phase, which appears dark grey) [26].

The transformation process from β-AlFeSi to α-Al(FeMn)Si was demonstrated by Kuijpers [26], as shown in Fig. 2.4. In the initial stage α particles nucleate on the face of the β particle. Then α particle starts to grow towards the closest rim of the β particle and the β particle starts to dissolve until the β particle was replaced by α particle, leaving only more rounded α particle.

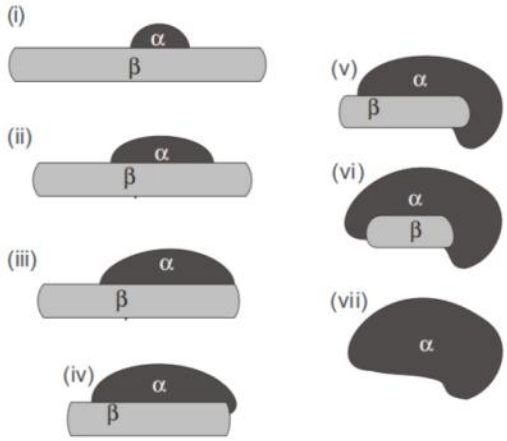

Fig.2.4 Schematic illustration of growing the α particle on the β particle.

It has been found that β-to-α transformation could improve the ductility and surface quality [27, 28, 29], which is closely related to the workability. Research has been conducted on the ductility regarding the β-to-α transformation [30-32]. The coverage ratio, which defined as the area of β particles on the grain boundaries divide by the total area of grain boundaries, correlates with the ductility in extrusion [30]. The β-to-α transformation resulted in lower coverage ratio of the dendrites and leads to an improvement of the ductility. The β plates, with a high coverage of the dendrites, form a network of brittle phase and block dislocations by the interconnected network, causing a low formability, whereas the more rounded small α particles allow the dislocation to move around, making the deformation more easily.

The β-to-α transformation was also found to be beneficial on the reduction of surface defects aspect. Take extrusion as an example, several types of surface defects may occur during the extrusion [28, 29, 33, 34]. One of the most common defects is

the “pick-up", which leads to eyesore scratchs on the profile surface.

The weak adhesion of the β particles to the Al matrix [30] lead the β particles loose from the matrix. During extrusion, these loose β particles tend to stick to the die surface and scratch the Al surface. In contrary, α particles have much better adhesion with Al, which therefore lead to less pick-up defects and better surface quality.

Besides, the sharp edges of the β particles tend to lead micro-cracks during the deformation process, and therefore resulted in cracks on the profile surface. The transformed α particle are more rounded with more curvy edges and therefore gave less micro cracking on the profile surface.

2.2.3 Mg_2Si dissolution and precipitation during homogenization

One of the main objective of the homogenization is to dissolve the coarse primary Mg_2Si, making the Mg and Si elements released in the matrix to provide a high Mg and Si solution level, ensuring the aging potential during the T5 aging. Temperature above the Mg_2Si solvus was mostly applied in the homogenization process. Industrially, as high as possible homogenization temperatures are desirable due to the higher Mg_2Si dissolution rate, which means a shorter processing time. However, a safe limit for the homogenization temperature should be the set preventing the local melting of eutectic region, which can cause severe damage at the alloy microstructure inducing voids, cracks and blistering during extrusion [35].

At the cooling step of homogenization, precipitation of Mg_2Si may usually occur. Depending on the cooling regime, the Mg_2Si precipitation differs. A slow cooling tends to produce coarse Mg_2Si particles while a rapid cooling traps the Mg and Si in

solution with little or no Mg_2Si precipitation produced [36, 37]. Coarse Mg_2Si particles are generally more difficult to dissolve during the subsequent preheating and extrusion process. However, no precipitation of Mg_2Si results in the increase of high temperature flow stress since Mg and Si are trapped in the solution [38]. For these consideration, the number of the particle should be high to reduce the solid solution strengthening during hot working [39], but the particle size should be fine for enhanced dissolution during extrusion [40].

Birol [41] have studied the effect of homogenization practice on the microstructure of AA6063 billets, as shown in Fig. 2.5, the population of the Mg_2Si precipitates was increased drastically as the cooling rate decreased for 2000 ◦C/h to 400 ℃/h, and further to 100 ℃/h.

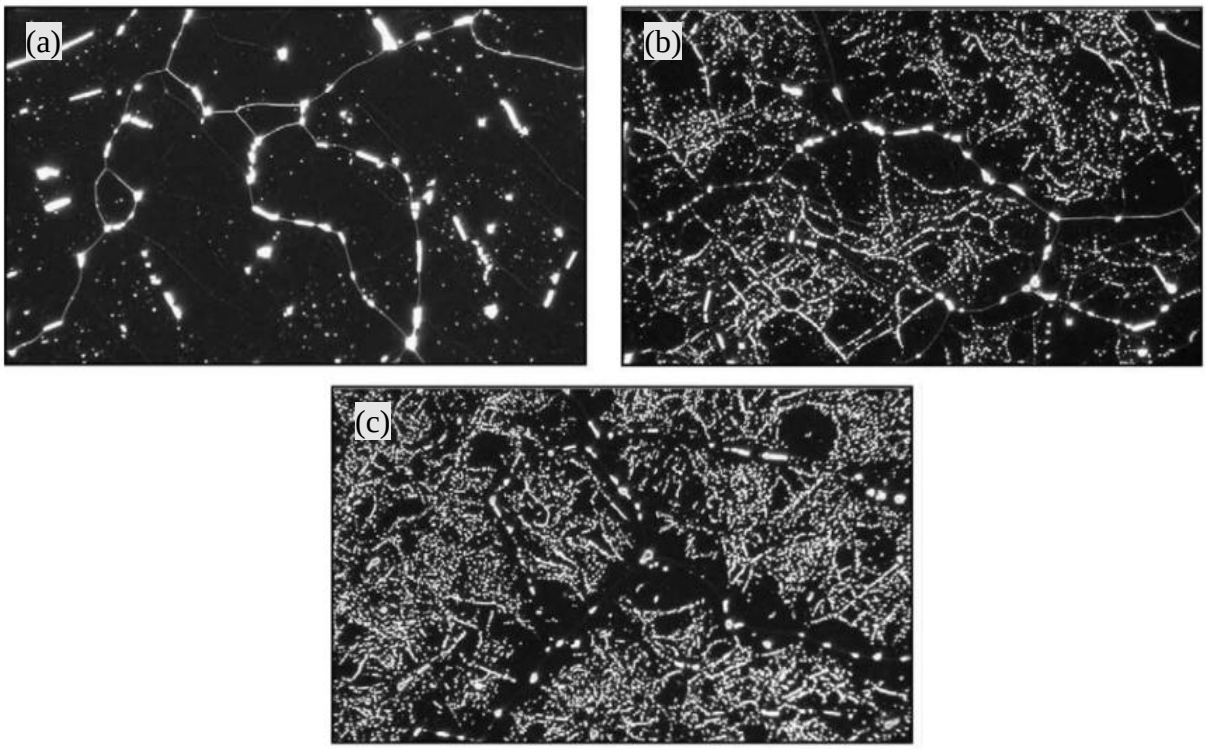

Fig. 2.5 Dark-field optical micrographs showing the distribution of Mg_2Si precipitates in samples soaked at 580 ℃ for 6 h and subsequently cooled to 200 ℃ at the cooling rate (a) 2000 ℃/h, (b) 400 ℃/h, (c) 100 ℃/h

2.2.4 Dispersoids formation during homogenization

In 6xxx alloys, the added transition elements, such as Mn Cr, are partially remained in the aluminum matrix during casting to form a supersaturated solid solution [42, 43]. By conducting homogenization heat treatments, the dispersoids could be formed via the decomposition of the supersaturated solid solution.

The α-Al(MnFe)Si dispersoids are the most common dispersoid formed in the Mn and Si-containing aluminum alloys [44]. There is discussion on whether the type is simple cubic (SC) or body center cubic (BCC). It is well accepted that the unit cell is SC when the Fe/Mn ratio is low and it is BCC as the Fe/Mn ratio increased [45, 46].

Fig 2.6 shows the typical microimages of dispersoids in 6082 alloy after homogenized at 550 ℃ for 2 h [47]. It can be seen that the dispersoids appear with various shapes, which can be attributed to the projections of the plate shaped dispersoids in a 2D image. Besides, the dispersoids may lie under or above the foil surface, which also leads to varying contrast. The morphology of the dispersoids projected in the micrographs varies to a considerable extent.

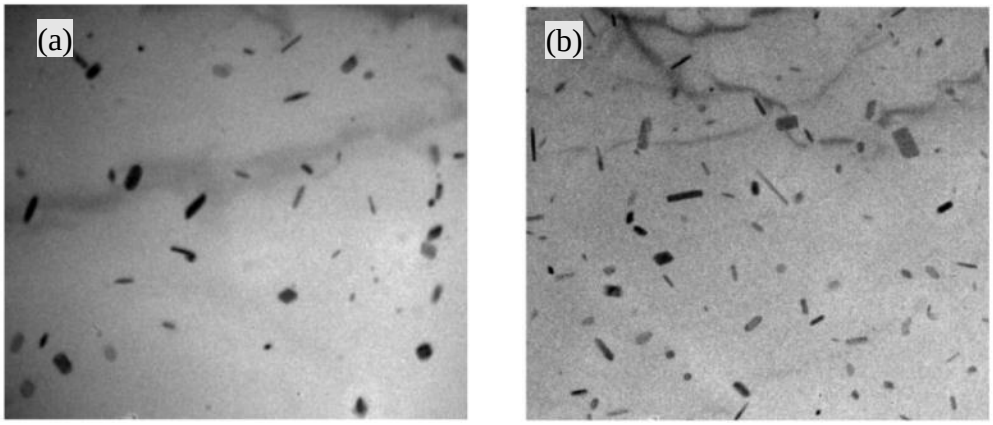

Fig. 2.6 TEM micrographs for the samples homogenized at 550 ℃ for 2 h of (a) 0.25Mn alloy, (b) 0.5Mn alloy [47].

The precipitation behavior of α-Al(FeMn)Si dispersoids in 6082 alloys at lower temperatures was studied by Li et al [48]. It was found that α-Al(FeMn)Si dispersoids precipitation began at 350 ℃ and reached the maximum number density at 400 ℃. At 500 ℃, the dispersoids coarsened quickly and started to dissolve with increasing holding time (Fig. 2.7).

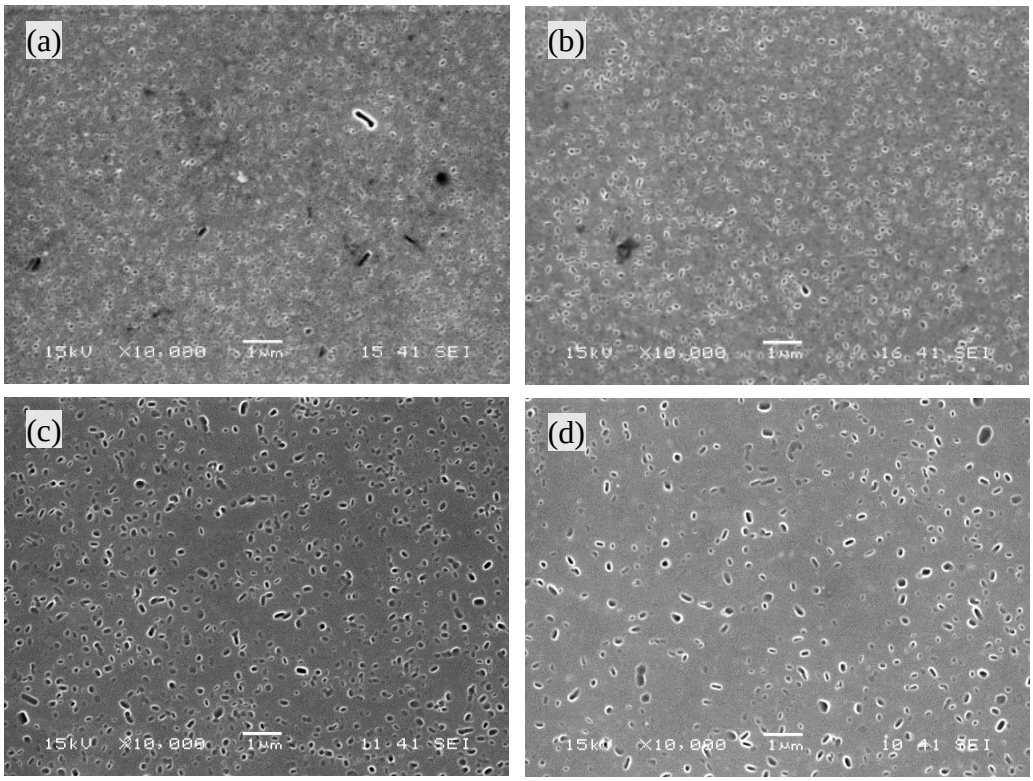

Fig. 2.7 SEM images of 6082 alloy after heat treatment (a) 400 ℃ for 1h, (b) 400 ℃ for 24 hours, (c) 500 ℃ for 1h and (d) 500 ℃ for 24h [48].

Hu et al. [49] reported in the Mn-containing Al-Mg-Si-Mn alloy, the size and distribution of dispersoids formed during the homogenization treatment strongly depend on the heating rate. As shown in Fig. 2.8, a rapid heating rate produces large needle shaped heterogeneously distributed dispersoids, while a slower heating rate produces fine spherical shape dispersoids with a more homogeneous distribution. During homogenization, the β'phase acts as the preferential nucleation site for the Mn-containing dispersoids during heating with the appropriate heating rate.

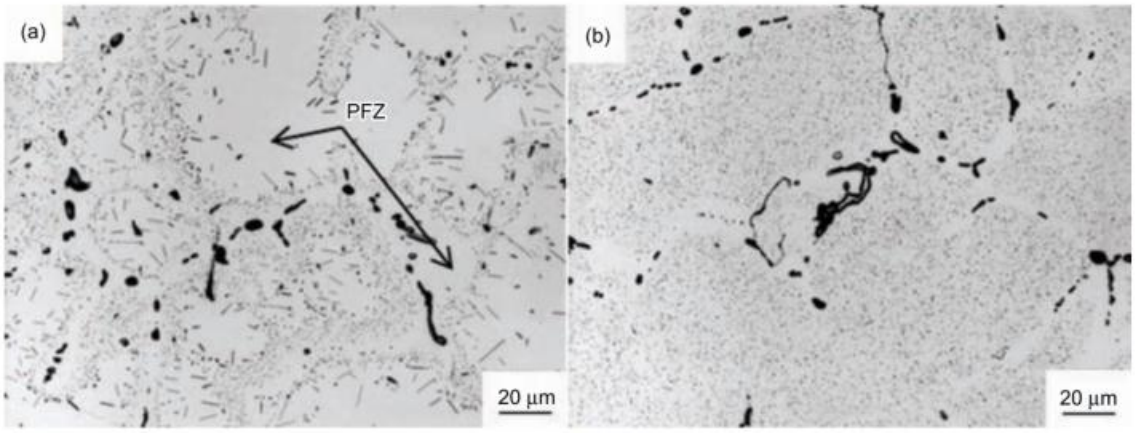

Fig. 2.8 AA6082 alloy after homogenization. (a) rapidly heated specimen in salt bath to 530 ℃, and (b) slowly-heated specimen (40 ℃/h). (PFZ: Precipitation free zone) (Dark particles: constituent particles, grey particles: dipersoids) quenched when the sample reaches 530 ℃ [49].

2.2.5 Solid solution level evolution during homogenization

The solid solution level is a significant factor for the extrude alloys because it is closely related to the subsequent extrusion force. For 6xxx alloys, extrusion billets are mostly produced by the direct chill (DC) casting, during which the non-equilibrium solidification induces supersaturation of alloying elements and inhomogeneous microstructure such as micro-segregation, causing a low formability [50, 51]. Therefore, homogenization is conducted before extrusion to eliminate such negative effects. During homogenization, the supersaturation of alloying elements and inhomogeneous microstructure can be diminished, resulting in a more uniform elements distribution results [52].

Shakiba [53] reported that in dilute Al–Fe–Si system, the as-cast alloys exhibited a high flow stress (Fig. 2.9a) due to the overall high level of supersaturation of

alloying elements formed during DC casting, which was implied by the lower electrical conductivity (Fig. 2.9b). After homogenization at 550℃, the flow stress decreased significantly due to the decreased solid solution by diminished supersaturation condition. However, with further increasing of homogenization temperatures to 580 and 610℃, the flow stress increased again due to the increased levels in the solid solution, which was promoted via intermetallic phase transformation.

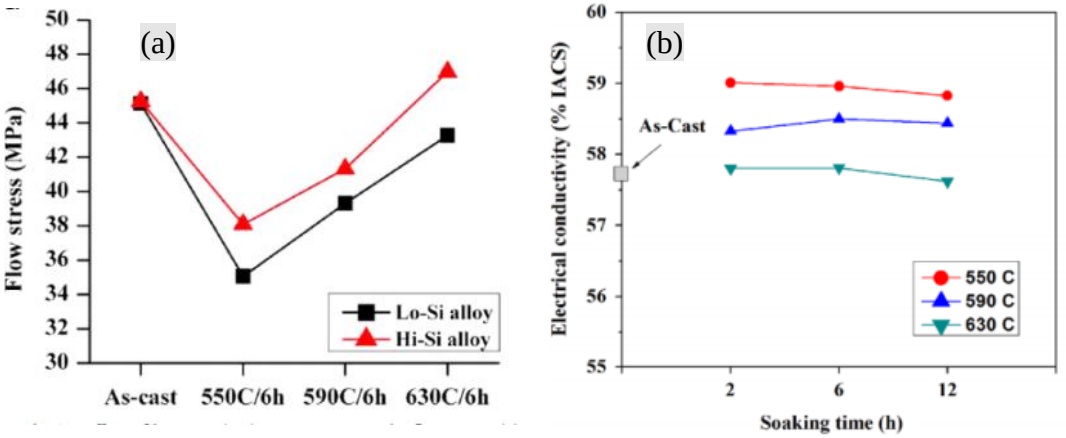

Fig. 2.9 Effect of homogenization treatment on (a) flow stress of hot deformation at ε=1 s^{-1}, T=400 ℃ at a strain of 0.8, (b) the electrical conductivity [53].

2.3 Effect of Mn on 6xxx alloys

It has been long recognized that the addition of Mn in 6xxx aluminum alloys can modify the microstructure in both as-cast and heat treated conditions and thus improve the properties of the alloys [54-56]. In AA6xxx alloys, Mn can be present in the constituent particles and fine dispersoids as well as in solid solution.

2.3.1 Mn in intermetallics

In the Mn-containing 6xxx alloys, Mn was always found to be present in

α-Al(FeMn)Si intermetallics form during solidification. The α-Al(FeMn)Si exhibited as “Chinese-script-like” morphology and was also called “constituents” because they remain as a separate phase in the Al-matrix even after long homogenization times, although they may undergo the change in phase composition and morphology [57].

The α-Al(FeMn)Si could be formed both at solidification and homogenization stage. During solidification, a mixture of intermetallic of β-AlFeSi and α-Al(FeMn)Si was formed and the fraction of β-AlFeSi and α-Al(FeMn)Si depends on the Mn content in alloys. During homogenization, α-Al(FeMn)Si could be formed by the transformation from β-AlFeSi phase [26]. The transformation was highly dependent on the homogenization temperature and time. Fig. 2.10 shows the relative fraction of α-Al(FeMn)Si as a function of time computed by the Finite Element Model and confirmed by experiments in 6005A alloy. As the homogenization temperature increase, the relative fraction of α-phase increased, indicating the high rate of β-AlFeSi to α-Al(FeMn)Si transformation.

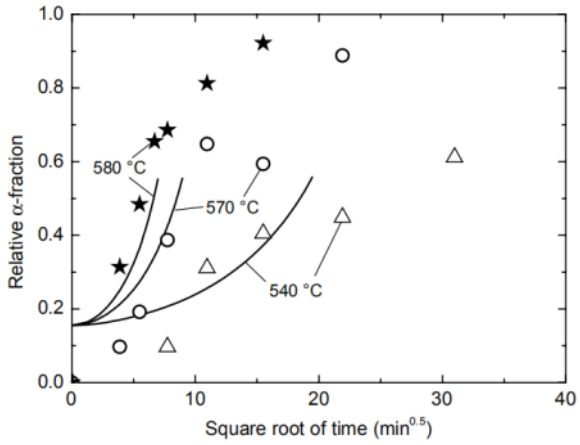

Fig. 2.10 The relative α-Al(FeMn)Si fraction as a function of time derived by the Finite Element Model (presented by the straight lines) compared with the relative α-fractions, measured by experiments (presented by the separate points). The calculations and measurements are performed for three different temperatures [26].

2.3.2 Mn in dispersoids

During the casting process of 6xxx alloys containing Mn, most of Mn element will be retained the aluminum matrix to form a supersaturated solid solution during the casting process. Therefore, dispersoids are likely to precipitate during the heat treatment due to the decomposition of supersaturated solid solution. The dispersoids have a strong effect on the processes, such as recovery, recrystallization and grain growth; moreover, they also affect the high temperature flow stress.

Liu [47] have investigated the α-Al(FeMn)Si dispersoids in 6082 alloy containing 0.25%Mn. It was reported that, the chemical composition of the dispersoids varies with the homogenization parameters (Fig. 2.11). The overall Mn/Fe ratio is higher for samples homogenized for 2 h at either 550 ℃ or 580 ℃ (≈2-4:1)

compared to 12 h at 580 ℃ (less than 2:1).

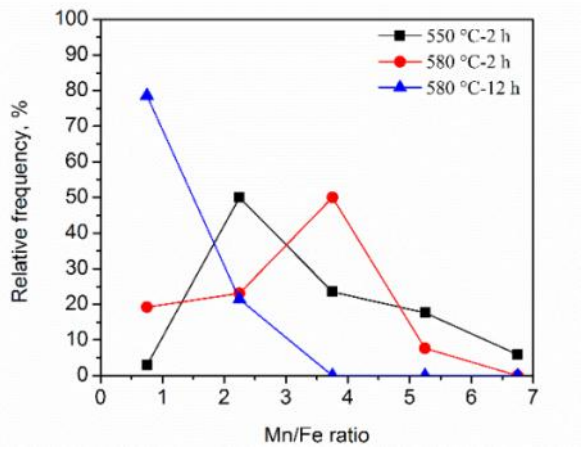

Fig. 2.11 Mn/Fe ratios of dispersoids plotted in histogram for 0.25Mn 6082 alloy from three homogenization conditions [47]

Additionally, the non-homogeneous distribution of chemical composition in a single dispersoid has been observed. As shown in Fig. 2.12 of the high angle annular bright field dispersoids micrographs, combining the TEM results, the Mn/Fe ratio changed in the same single dispersoids [47]. The Mn/Fe ratio exhibited uneven distribution in a single dispersoids, and Mn/Fe ratio was higher at the center region than those at the edge regions.

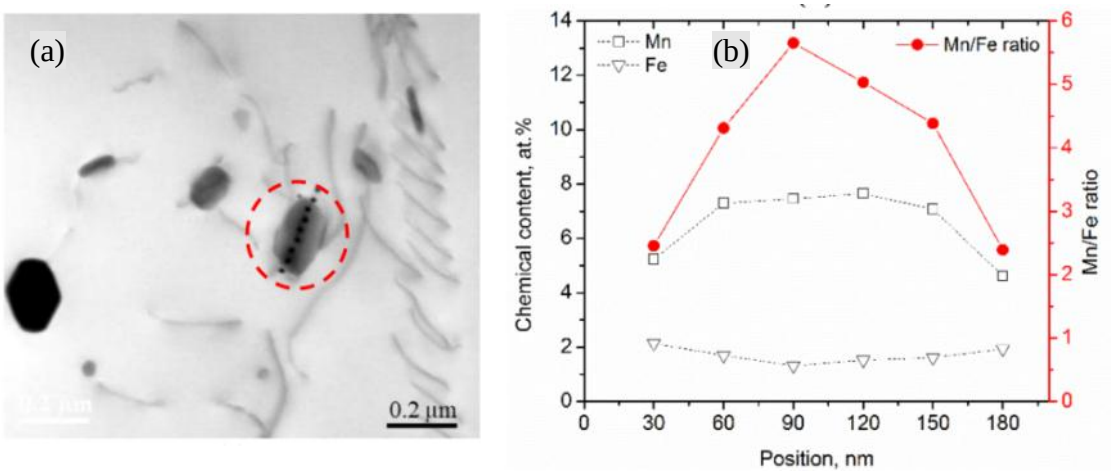

Fig. 2.12 (a) High angle annular bright field image of representative dispersoids in 0.25Mn alloy homogenized at 550 ℃ for 2 h; (b) Mn and Fe contents and also the Mn/Fe ratios measured along the length of a dispersoids [47].

2.3.3 Mn in solid solution

In 6xxx alloys, the added Mn is partially retained in the aluminum matrix during casting and form the supersaturated solid solution [42, 43].

Chen Li [48] have studied the solid solution level of Mn and the hardness of as-cast 6082 alloys. In his study, electrical conductivity was measured to follow the changes of Mn solid solution level for the base alloy without Mn and the 0.5%Mn containing alloy, the electrical conductivity was described in the following equation:

$$1/EC_{Alloy\text{-}A}=0.0267+0.032\,Fe_{ss}\%+0.0068Si_{ss}\%+0.003Mg_{ss}\% \quad (1)$$

While for the 0.5%Mn containing alloy:

$$1/EC_{Alloy\text{-}B}=0.0267+0.032\,Fe_{ss}\%+\mathbf{0.033Mn_{ss}\%}+0.0068Si_{ss}\%+0.003Mg_{ss}\% \quad (2)$$

Where, Fess%, Mnss%, Siss% and Mgss% are the weight percentages of the solute elements Fe, Mn, Si and Mg. The influence of other alloying elements on EC was negligible because the Fe, Si and Mg contents in two alloys were almost the same. Thus the change in the Mn solid solution level could be defined by the change in electrical conductivity. The results revealed that the base alloy without Mn had a 47.7 %IACS of electrical conductivity while the 0.5%Mn containing alloy exhibited a 34.9 %IACS of electrical conductivity, which indicated a considerable Mn was retained in supersaturated solid solution of the aluminum matrix in the 0.5%Mn containing alloy. Correspondingly, the hardness of 0.5%Mn added alloy was 67.0 HV, which was higher than the base alloy of 62.5 HV due to the Mn solid solution strengthening.

The Mn solid solution strengthening was also reported by Ryen et al. [58]. It was suggested that Mn in solid solution had a significant strength effect of both high purity and commercial aluminum alloys. The solid solution strengthening rate was about 50% stronger in the commercially pure aluminum alloys compared to the high purity alloys. This stronger hardening effect was considered to be related to the clustering effect between Mn and trace elements in solid solution.

2.4 Hot deformation of aluminum alloy

The applications of wrought aluminum alloys in aerospace, aircraft, automotive

and construction industries, are usually subjected to hot deformation, such as rolling, forging and extrusion, in order to achieve desirable shapes. When hot deformation occurs in aluminum alloys, the dislocations glide in the lattice structure, the slip plane is the {111} and the slip direction is the <110> [59]. However, other slip systems may operate, which involves slip on {100}, {110}, {112} and {122} planes during high temperature deformation [60]. When the slip of dislocations was active in several slip planes, multi-slip of dislocations occurred. These dislocations could be the resource as the sub-grain boundary as a result of dislocations pile-up. During hot deformation, both the dynamic hardening and dynamic softening could take place continuously, which influence the flow stress. Based on deformation parameters, such as flow stress, deformation temperature, strain rate, the constitutive equations could be used to derive the material constants for hot deformation, such as stress multiplier α and the activation energy Q. [61, 62]

2.4.1 High temperature flow stress

When the hot deformation is performed, the stress required to sustain plastic deformation at a constant temperature with a given strain rate is defined as the flow stress. High temperature flow stress is one of the most significant factors for the design of hot deformation regime due to its substantial impact on the required deformation load and the kinetics of metallurgical transformation [61]. It is known that the high temperature flow stress was closely related to the alloy chemistry, homogenization heat treatment history and microstructure [61, 63, 64].

Shi et al. [65] studied the hot deformation behavior of 7150 alloy. A series of hot

deformation flow stress curved was obtained under various of deformation temperatures and strain rates (Fig. 2.13a). In general, the flow stress curves exhibit a peak at a certain strain, followed by dynamic flow softening until the end of straining. Under normal deformation conditions, the flow stress curves remained fairly constant or decreased to some extent beyond the peak stresses, demonstrating a dynamic equilibrium between work hardening and dynamic softening. In addition, it is obvious that the level of flow stress and peak stress increased with increasing strain rate and decreasing deformation temperature.

Fig. 2.13b illustrates the evolution of the peak flow stresses after different Zr addition based on the base alloy. Under a given deformation condition, no significant variation could be observed in the peak stress between the base alloy and Alloy with 0.04% Zr. With the further addition of Zr, increasing the content from 0.07% to 0.19%, the peak stress levels increased significantly. The values of peak stress showed a gradual rise with increasing content of Zr under the same deformation condition, which was due to the formation of Al_3Zr dispersoids.

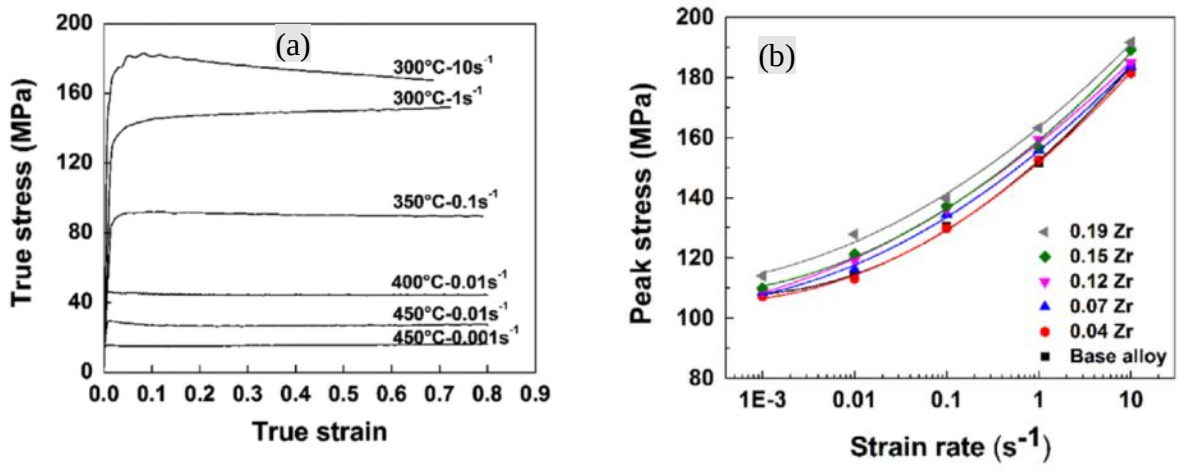

Fig. 2.13 (a) Typical true stress–true strain curves of the base alloy during hot compression deformation; (b) The evolution of peak stresses of base alloy and alloys after Zr addition during hot deformation at 300 ℃;

Shakiba [66] investigated the hot deformation flow stress in dilute Al-Fe-Si alloys (Fig. 2.14), and results revealed that increasing the Fe content in dilute Al-Fe-Si alloys increases the flow stress at all deformation temperatures. This increased flows tress was due to the increased solid solution level produced by the addition of Fe alloy element.

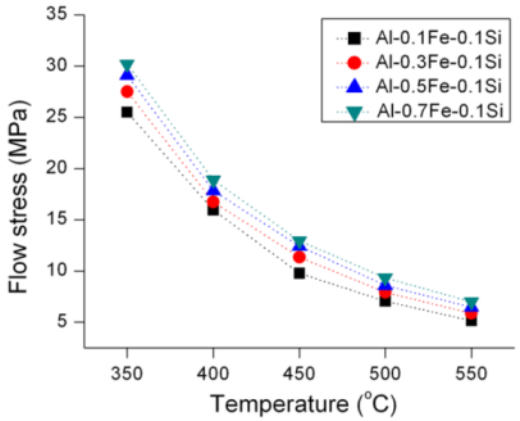

Fig. 2.14 Effect of iron on the flow stress at a strain of 0.8 [66].

Flow stress of 6xxx alloys is very important for the extrusion, especially when the productivity is typically limited by the press capacity. In general, an extrusion press has a specific pressure available to push the billet through the die and this is directly related to the flow stress. Aluminum alloys exhibit a strain rate sensitivity, namely the higher the strain rate (the ram speed), the higher the flow stress is. Hence, under a given press capacity, the flow stress will dictate the maximum ram speed at which the press can operate. A higher flow stress also produces a larger temperature increase during extrusion, which increases the surface exit temperature for a given extrusion speed resulting in an earlier onset of surface defects. In this aspect, as low as possible flow stress could be beneficial for the productivity [53].

2.4.2 Constitutive equations and activation energy Q

Constitutive equations are widely used to describe the plastic flow properties of metals and alloys during hot deformation, which are correlated with the flow stress, strain rate and deformation temperature. At an elevated temperature, the strain rate (ε) is related to the temperature and the flow stress by the Arrhenius type equation [67-72]:

$$\dot{\varepsilon} = Af(\sigma)\exp\left(-\frac{Q}{RT}\right)$$

where $\dot{\varepsilon}$ is the strain rate (s^{-1}), A is a constant, Q is the activation energy for hot deformation (KJ mol^{-1}), R is the universal gas constant (8.314 J mol^{-1} K^{-1}), T is the

absolute temperature (K) and f(σ) is the stress function which can be expressed as [73-79]:

$$f(\sigma) = \begin{cases} \sigma^{n1} & \alpha\sigma < 0.8 \\ \exp(\beta\sigma) & \alpha\sigma > 1.2 \\ [\sinh(\alpha\sigma)]^{n} & \text{for all } \sigma \end{cases}$$

where σ is the flow stress (MPa), n1, β and n are material constant and α = β/n1 [76-78] is a stress multiplier. Substituting the suitable functions of f (σ) into Eq. (1) leads to the power law, exponential and hyperbolic sine law equations, respectively:

$$\dot{\varepsilon} = A_1\sigma^{n_1}\exp\left(-\frac{Q}{RT}\right)$$

$$\dot{\varepsilon} = A_2\exp(\beta\sigma)\exp\left(-\frac{Q}{RT}\right)$$

$$\dot{\varepsilon} = A[\sinh(\alpha\sigma)]^{n}\exp\left(-\frac{Q}{RT}\right)$$

where A1 and A2 are the material constants. Generally, the power law equation breaks down at high stress values, and the exponential equation breaks down at low stress values. However, the hyperbolic-sine law is suitable for constitutive analysis over a wide range of temperatures and strain rates [69-72], which was more widely used for describing the plastic flow properties of metals and alloys during hot deformation.

Moreover, Zener-Holloman parameter (Z) in an exponential equation is used to represent the effect of the temperature and the strain rate on the hot-deformation behavior [80-83]:

$$Z = \dot{\varepsilon}\exp\left(\frac{Q}{RT}\right)$$

Using the constitutive equation, the activation energy for hot deformation Q

could be derived from a series of flow stress data. The Q values were often used to compare the difficulty degree of plastic deformation between different aluminum alloys [65, 66]. Recent works discovered that the Q was not a constant for an alloy but it might vary with deformation conditions (mainly temperature and strain rate) [84-86]. The changes in high temperature flow stress and activation energy are closely related to the balance between dynamic work hardening and dynamic softening under a specific hot deformation condition [65]

Through the constitutive analyses (section 3.3), one expects to have a unique index Q to compare the difficulty levels of hot deformation between the different chemical compositions or between different microstructures. However, the results reveals that the Q is not a constant and the values are highly depended on the hot deformation condition, because the flow stress often changes with the progress of the deformation. Therefore, it is not always easy to assess the hot workability of different aluminum materials only using the Q. Shi et al [85] pointed out that Q mainly reflected the free energy barrier to dislocation movement, which was affected by the deformation temperature and strain. In recent years, some researchers explored the concept of the activation energy map instead of treating Q as a constant to study the hot workability of aluminum alloys [86-88].

2.4.3 Microstructures evolution during hot deformation

During hot deformation processes, the general trend of the flow stress change was closely related to the dynamic balance of work hardening and softening [89].

Microstructures evolution of dynamic recovery (DRV) and dynamic recrystallization (DRX) are the typical softening mechanisms in the hot deformation process of aluminum alloys [90-92]，as shown in Fig. 2.15. DRV reduces the energy stored in the deformed grains by a rearrangement of defects in their crystal structure and is a necessary prerequisite for DRX to take place. DRX is the metallurgical phenomenon that allows replacing deformed grains by small dislocation free equiaxed grains at elevated temperatures.

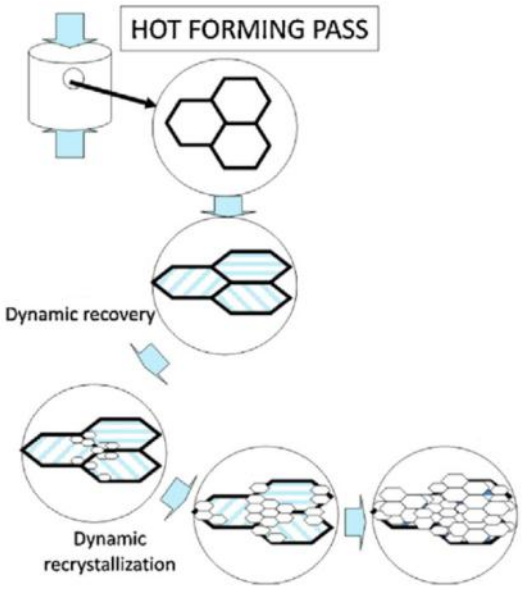

Fig. 2.15 Microstructural evolution of DRV and DRX

2.4.3.1 Dynamic recovery (DRV)

DRV is a thermally activated process which consists of all the processes that lead to annihilation of dislocations and rearrangement of the remaining dislocations into low angle grain boundaries and subgrain structures. Thus both the hot deformation

temperatures and train rate could influence the DRV level and affect the flow stress.

Shi et al. [65] studied the DRV behavior in 7150 Al alloy and reported that the DRV rate increases with increasing temperature and decreasing strain rate, as is shown in Fig. 2.16. When the deformation was performed at 300 ℃ and 1 s^{-1}, Typical DRV was observed, a large amount of dislocations presented (Fig. 2.16a). For the deformation processes conducted at 450 ℃ and 1 s^{-1} and 450 ℃ and 0.01 s^{-1}, the microstructures became more homogeneous and better organized (Fig. 2.16b and c), which presenting a higher DRV level. The rise of DRV level was due to the enhanced dislocation motion as the temperature increased and strain rate decreased.

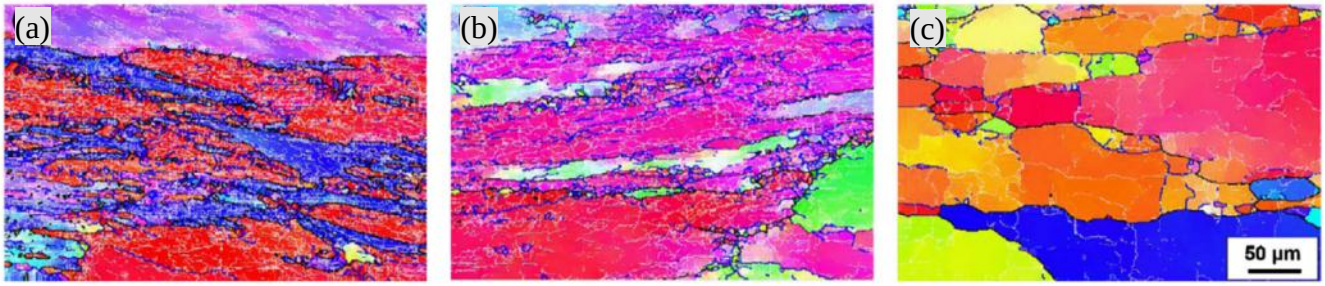

Fig. 2.16 Orientation imaging maps of 7150 Alloy-F (0.19 Zr) under different deformation conditions: (a) 300 ℃ and 1 s^{-1}, (b) 450 ℃ and 1 s^{-1} , (c) 450 ℃ and 0.01 s^{-1} (the boundary misorientation angles of both grains and subgrains can be distinguished as follows: white lines: 1–5 °, blue lines: 5–15 °, thin black lines: 15–30 ° and thick black lines: ＞30 °) [65].

2.4.3.2 Dynamic recovery (DRX),

Dynamic recovery (DRX), known as an important and typical softening mechanisms in the hot deformation process of aluminum alloys, which involves the

production of new grains. DRX presents with the new microstructures result from the production of nuclei, followed by the long-range migration of their boundaries [93-95]. During hot deformation, when high dislocation density can provide enough driving force, recrystallization occurred. DRX is barely observed in metals and alloys with high stacking fault energy such as aluminum and its alloys due to the high rate of dynamic recovery that inhibits the accumulation of sufficient dislocations to sustain dynamic recrystallization [96, 97]. However, there are some reports that the dynamic recrystallization can easily occur in aluminum of very high purity and aluminum alloys containing large particles such as Al-5Mg-0.8Mn [96].

The formation of DRX grains in an aluminum alloy during hot working is illustrated in Fig. 2.17 [98]. When the strain of high temperature deformation was 1 (Fig.2.17a), the original grains were deformed and a large amount of low angle boundaries were induced in the deformed original grains. As the strain increased by 2, the new grains form at the region of grain boundaries as a result of the increase in sub-boundary misorientation and accumulation of the dislocations introduced by the deformation (Fig.2.17b). This is related to the rapid development of strain gradients near grain boundaries and the latter leads to the presence of large misorientations in the vicinities of the boundaries. After the strain reached 12, the original grains were replaced by the new formed ones, the dynamic grain size produced were much smaller than the original ones (Fig.2.17c). The changes in the microstructure during DRX are associated with the formation of high angle grain boundaries due to the accumulation of dislocations. The fraction of such boundaries gradually increases during straining,

until almost all the grains are bounded by high angle grain boundaries at strain reached 12 (Fig.2.17c).

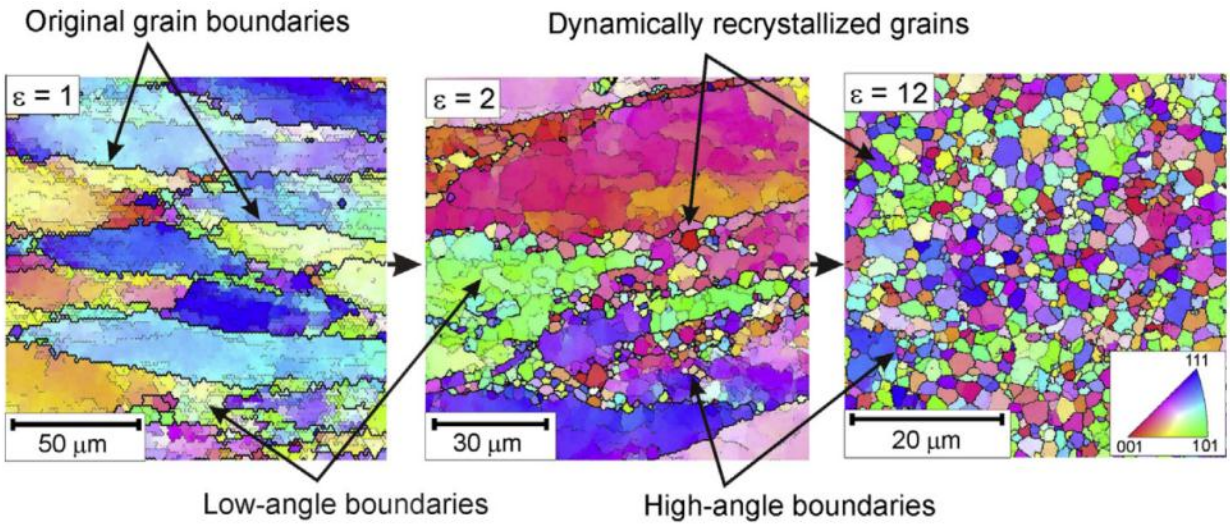

Fig. 2.17 Development process of DRX at different strains in the AA1421 aluminum alloy and the hot deformation was processed at 673 K [98].

2.5 Annealing treatment of aluminum alloys

After deformation, a high density of substructures and internal stress was induced and it is necessary to perform an annealing so as to get a stable property [99]. Annealing treatments employed for aluminum alloys are of several types that differs in the objective. Annealing times and temperatures depend on alloy type as well as on initial structure and temper. Depending on the different purpose, annealing could be departed into: stress-relief annealing, partial annealing and full annealing [100].

Stress-relief annealing was usually conducted on the cold-worked wrought aluminium alloys in order to remove the strain hardening effects formed during cold working. Partial annealing could be performed on the cold worked non-heat-treatable

wrought aluminum alloys aiming to obtain intermediate mechanical properties. Temperatures of partial annealing are below those that produce extensive recrystallization. Incomplete softening is always accomplished by substructural changes in dislocation density and rearrangement into cellular patterns. Full annealing was often performed on the aluminum alloys which are featured as softest, good workability wrought alloys. Work hardened products after full annealing could be recrystallized in case of weak recrystallization resistances. In the case of heat-treatable alloys, the solutes are sufficiently thoroughly precipitated to prevent natural age hardening. A higher temperature and longer soaking time generally are employed [100].

2.5.1 Static recrystallization (SRX) during annealing or solution treatments

During annealing or solution treatments, static recrystallization (SRX) usually took place. Different from the dynamic recrystallization (DRX) during deformation process, the SRX occurred during annealing stage after the hot deformation. SRX usually involved nucleation of new grains and their growth as well as grain boundary migration [101, 102]. The driving force of nucleation and growth for SRX could be provided by the substructures (dislocations and subgrains) formed from initial deformation and the annealing temperature. Fig. 2.18 shows the examples of typical SRX took place during annealing in high purity aluminum [103]. In the as-deformed state (Fig. 2.18 (a)) a typical banded microstructure is observed which is characteristic of rolled sheets. After annealing for 200 s at 360 ℃, the first new recrystallized grains could be detected (Fig. 2.18 (b)). After 300 s the entire specimen was recrystallized

showing an extremely fine grained microstructure with numerous larger grains (Fig. 2.18 (c)). With further annealing, the grain growth is initiated leading to a substantial increase in grain size (Fig. 2.18 (d)).

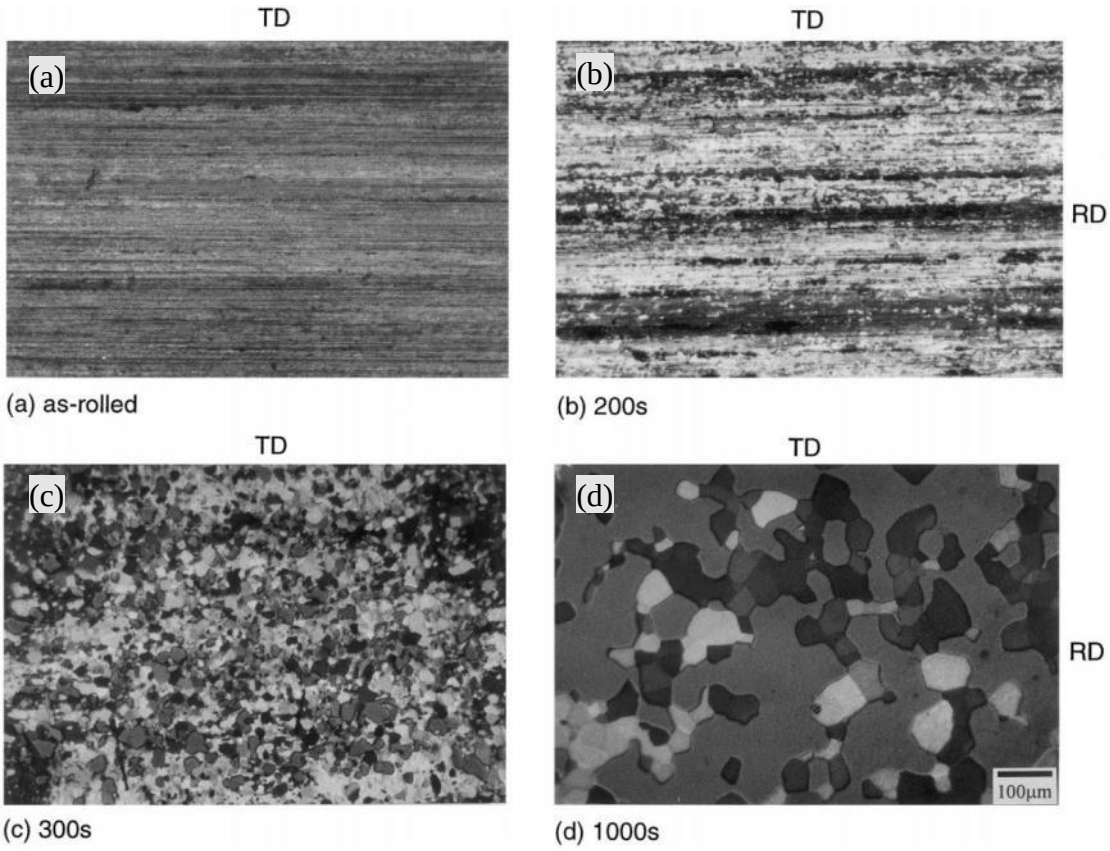

Fig. 2. 18 Evolution of the microstructure in a high purity aluminum at annealing time of 360℃ with increasing annealing time; (a) as-rolled, (b) annealed for 200 s, (c) annealed for 300 s, (d) annealed for 1000 s (optical microscopy) [103].

In some certain conditions, partially recrystallization took place and the structures with coarse grains were formed. Partially recrystallization was undesirable due to their detrimental effect not only on strength, toughness, and formability, but also on surface quality and corrosion resistance [104]. Birol [104] studied the impact

of partial recrystallization on the performance of 6005A tube extrusions and found that the partially recrystallized structures formed the relatively soft zones and acted as the very favorable site for crack initiation (Fig. 2.19).

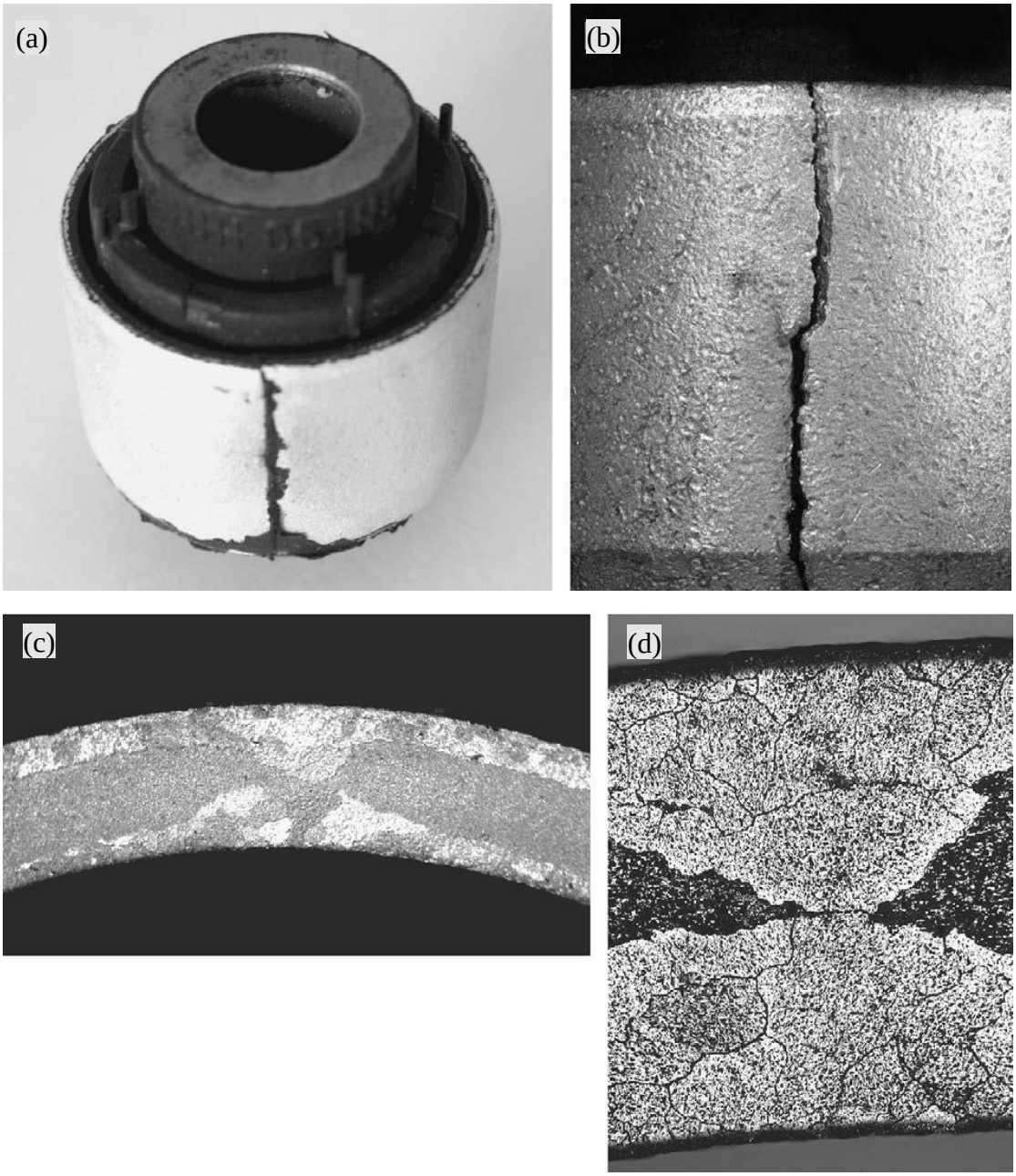

Fig. 2.19 (a) Suspension bushing with a fractured 6005A tube; (b) 6005A tube after cleaning away the rubber that penetrated in between the fracture surfaces; (c) and (d)

recrystallized grains covered the entire section [104].

2.5.2 Recrystallization resistance

The control of SRX plays an important role in some wrought aluminum alloys. It is reported that [13] occurrence of SRX negatively influenced the corrosion resistance in 2xxx alloys; In 5xxx alloys, work hardening effect could be kept only if the unrecrystallized wrought state can be maintained; In 7xxx alloys, a recrystallized structure causes the increasing risk of weld cracking, declined fracture toughness, and detrimental effect on corrosion resistance. Good recrystallization resistance is of paramount importance for adequate performance in industrial aspect.

The use of dispersoids in Al alloys is a well-established method of controlling grain growth and recrystallization during annealing treatment. The size, number density, distribution and morphology of dispersoids could have significant influence on the recrystallization resistance.

Guo et al [105] studied the effects of Al_3Zr dispersoids onrecrystallization resistance in 7150 aluminum alloy. As shown in Fig. 2.20, after sothermally annealed at 470 ℃ for 24 h, samples with Zr contents from 0 to 0.09% show all partially recrystallized microstructures after annealing, and the sample with 0.16% Zr exhibits a main recovery microstructure with few, small and isolated recrystallized grains, indicating the enhanced recrystallization resistance with the increasing Zr addition which enhanced the formation of Al_3Zr dispersoids (as show in the Fig. 2.20c exemplary).

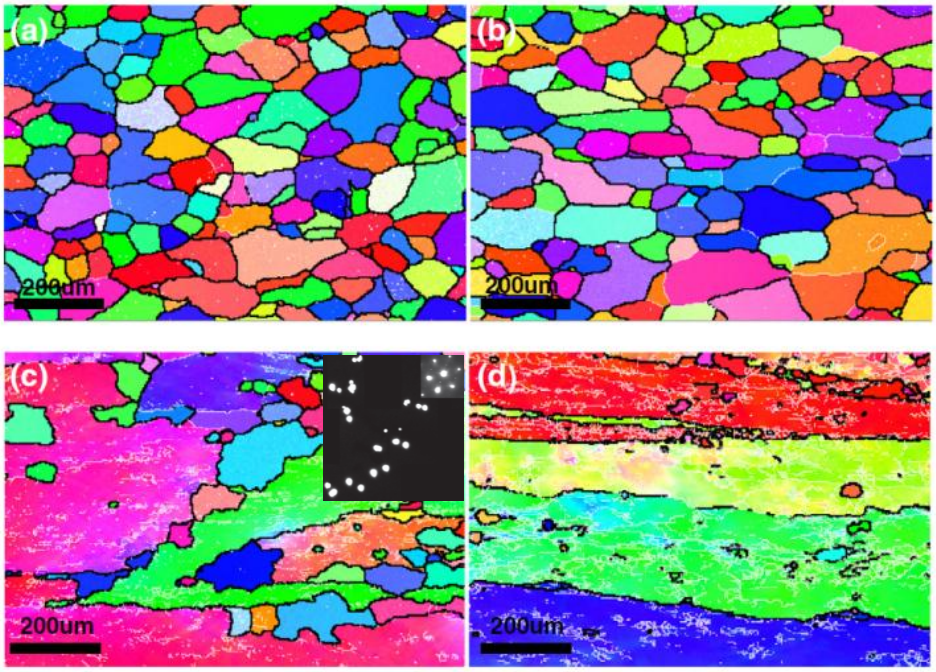

Fig. 2.20 Orientation maps of 7150 alloys with different Zr contents for one-step homogenization: (a) the base alloy (0% Zr); (b) 0.04% Zr; (c) 0.09% Zr; (d) 0.16% Zr. High angle boundaries (over 15°) and low angle boundaries (1 – 15°) shown as black line and white line, respectively, the onset TEM image are the Al_3Zr dispersoids [105].

Li et al. [106] studied the effects of combined addition of Er and Zr on precipitation and recrystallization of pure aluminum and found that combined addition of Er and Zr to pure aluminum results in remarkable recrystallization resistance. The recrystallization temperature of the 0.2Zr addition alloy is about 450 ℃, which is significantly higher than that of Zr free alloy due to the precipitation of Al_3(Er, Zr) precipitates, as shown in Fig. 2.21

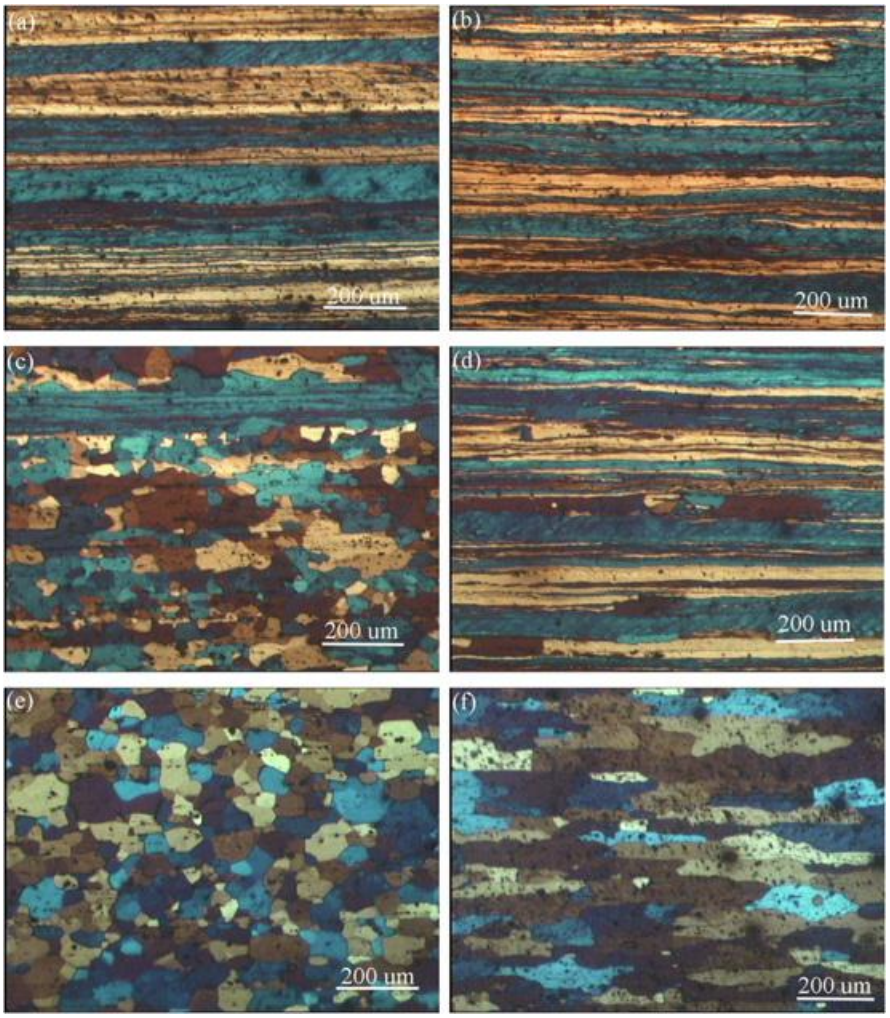

Fig. 2.21 Micrographs of the cold-rolled Zr free alloy heated to: (a) 275 ℃, (c) 350 ℃, (e) 450 ℃; and 0.2Zr addition alloy heated to (b) 275 ℃, (d) 350 ℃, (f) 525 ℃ [106].

Birol [107] reported that the superior recrystallization resistance of a 6082 alloy is obtained via a large population of the Cr-rich Al(Cr,Mn,Fe)Si as well as $(Al, Si)_3Zr$ dispersoids particles. However, the individual addition of Mn or Zr fails to offer any improvement in the recrystallization resistance in 6082 tube extrusions. Tsivoulas [108] investigated the effect of Mn and Zr additions on recrystallization resistance in

Al–Cu–Li AA2198 sheet and suggested that with a constant Zr level recrystallization resistance was seen to diminish with the addition of Mn and became progressively worse with a decrease in Zr content, as more Mn was added.

References:

[1] A. Woźnic ki, D. Leśnia k, G. Włoch , B.Les zczyńska-Made j, A. Wojtyna, The Effect Of homogenization conditions on the structure and properties of 6082 alloy billets, Archives of Metallurgy and Materials, 60, 3 (2015) 1763-1771.

[2] N. Kumar, S. Goel, R. Jayaganthan, Heinz-Günter Brokmeier, Effect of grain boundary misorientaton, deformation temperature and AlFeMnSi-phase on fatigue life of 6082 Al alloy, Materials Characterization 124 (2017) 229-240.

[3] N. Kumar, S. Goel, R. Jayaganthan, Effect of solution treatment on mechanical and corrosion behaviors of 6082-T6 Al alloy, Metallogr. Microstruct. Anal. 4 (2015) 411-422.

[4] S.N. Samaras, G.N. Haidemenopoulos, Modelling of microsegregation and homogenization of 6061 extrudable Al-alloy Journal of Materials Processing Technology 194 (2007) 63–73

[5] K. Laue, H. Stenger, Extrusion: Process Machinery Tooling, ASM International, 1976

[6] A.L. Dons, The Alstruc homogenization model for industrial aluminum alloys, J. Light Met. 1 (2001) 133–149.

[7] J.E. Hatch, Aluminium Properties and Physical Metallurgy, Handb. Alum. Vol. 1 -

Phys. Metall. Process. (1984)

[8] L.F. Mondolfo, Aluminium alloys: structure and properties. Published by Butter Worths & Co Ltd, London-Boston (1976).

[9] G. Phragmen, On the phases occupying in alloys of aluminium with copper, magnesium, manganese, iron, and silicon. J. Inst. Metals 77 (1950) 489-552.

[10] Chr. Rømming, Crystal structure of β-Al4.5FeSi. Acta Cryst. B 50 (1994) 307-312.

[11] P. Skjerpe, Intermetallic phases formed during DC-Casting of an Al-0.25 wt Pct Fe-0.13 Wt Pct Si Alloy. Metall. Trans. A 18 (1987) 189-200.

[12] J. G. Zheng, R. Vincent and J.W. Steeds: Crystal structure of an orthorhombic phase in β-(Al-Fe-Si) precipitates determined by convergent-beam electron diffraction. Phil. Mag. A 80 (2000) 493-500.

[13] A.L. Dons, AlFeSi-particles in commercial pure aluminium. Z. Metallkde 75 (1984) 170-174.

[14] A. Griger, V. Stefániay, A. Lendvai and T. Turmezey: Possible modification of cast structure by continuous casting technology in AlFeSi alloys Part III: Intermetallic phases. Aluminium 65 (1989) 1049-1056.

[15] D. J. Skinner, R. L. Bye, D. Raybould and A. M. Brown: Dispersion strengthened Al-Fe-V-Si alloys. Scripta Met. 20 (1986) 867-872

[16] M. Cooper, The crystal structure of the ternary alloy AlFeSi. Acta Cryst. 23 (1967) 1106.

[17] M.H. Mulazimoglu, A. Zaluska, J.E. Gruzleski, F. Paray, Electron microscope

study of Al-Fe-Si intermetallics in 6201 aluminum alloy. Metall. Mater. Trans. A 27 (1996) 929-936.

[18] P. Donnadieu, G. Lapasset, T.H. Sanders: Mangenese-induced ordering in the α-(Al-Mn-Fe-Si) approximant phase. Philos. Mag. Lett. 70 (1994) 319-326.

[19] Y. Birol, Formation and transformation of intermetallic particles in strip-cast Al-0.8Fe-0.6Si Alloy. Z. Metallkd. 89 (1998) 501-506.

[20] P. Donnadieu, G. Lapasset, B. Thanaboonsombut and T.H. Sanders: α-phase particles in 6xxx aluminium alloys, The 4th international conference on aluminum alloys, Atlanta, Georgia, USA (1994) 668-675.

[21] D.T.L. Alexander and A.L. Greer, Solid-state intermetallic phase transformation in 3xxx aluminium alloys. Acta. Mat. 50 (2002) 2571-2583.

[22] H. Westengen, Formation of intermetallic compounds during DC Casting of a commercial purity Al-Fe-Si alloy. Z. Metallkd. 73 (1982) 360-368.

[23] T. Turmezey, AlFe and AlFeSi intermetallic phases in aluminium alloys. Mater. Sci. Forum. 13-14 (1987) 121-132.

[24] K. Sugiyama, N. Kaji and K. Hiraga, Re-Refinement of α-(AlMnSi). Acta Cryst. C 54 (1998) 445-447.

[25] M. Cooper, K. Robinson, The crystal structure of the ternary Alloy α (A1MnSi), Acta Cryst. 20 (1966) 614.

[26] N.C.W. Kuijpers, Kinetics of the β-AlFeSi to α-Al(FeMn)Si transformation in Al-Mg-Si alloys, Ph. D thesis, Technische Universiteit Delft, (2004) 57-64

[27] O.R. Reiso: The effect of homogenization treatment on the microstructure

properties of aluminium extrusion ingots, Deutsche Gesellschaft für Metallkunde, Germany (1995) 199-208.

[28] M.P. Clode, T. Sheppard: Extrusion limit diagrams containing structural and topological information for AA 6063 aluminium alloy. Mater. Sci. Technol. 9 (1993) 313-318.

[29] M.P. Clode, T. Sheppard, Surface generation and origin of defects during extrusion of aluminium alloys. Proc. Aluminium Technology '86, The Institute of Metals, Carlton House Terrace, London, UK (1986) 230-239.

[30] S. Zajac, L. Gullman, A. Johansson and B. Bengtsson, Hot ductility of some AlMg-Si alloys. Mater. Sci. Forum. 217-222 (1996) 1193-1198.

[31] K.E. Nilsen and P.T.G. Koenis: Quantitative analysis of the homogenizing heat treatment by means of AlFeSi particle analysis and the effect on productivity, ET 2000, Seventh International Aluminum Extrusion Technology Seminar. Chicago, USA, Aluminum Extruders Council (2000) 69-75.

[32] N.C. Parson, H.L. Yiu, The effect of heat treatment on the microstructure and properties of 6000 Series alloy extrusion ingots, Proc. Light Metals, Las Vegas, Nevada, USA (1989) 713-724.

[33] G. Merk, S. E. Naess, Pick-Up formation on aluminium extrusions, Z. Metallkde 68 (1977) 683-687.

[34] T. Minoda, H. Hayakawa and H. Yoshida, A mechanism of pick-up formation on 6063 aluminium alloy extrusions. Mater. Sci. Techn. 7 (1998) 13-17.

[35] P.K. Saha, Aluminum Extrusion Technology, ASM International, 2000

[36] Bjornbakk EB. The influence of homogenization cooling rate, billet preheating temperature and die geometry on the T5-properties for three 6xxx alloys extruded under industrial conditions, Materials Science Forum, 396-402 (2002) 405-410

[37] Dahl N, Johnsen T, Henriksen BR, Jensen EK. Precipitation of Mg_2Si in Al–Mg–Si‐alloys during cooling from homogenization temperature, Proceedings of 6th International Aluminum Extrusion Technology Seminar 1 (1996) 529-535.

[38] Langerweger J. Effect of metallurgical factors on productivity in the extrusion of aluminum–magnesium–silicon (AlMgSi) alloys, Aluminum 58(1982) 107-109.

[39] J. van de Langkruis, The effect of thermal treatments on the extrusion behaviour of AlMgSi alloys, Ph.D. Thesis, Delft University of Technology (2000) 61-84.

[40] D.H. Lee, J.H. Park, S.W. Nam, Enhancement mechanical properties of Al-Mg-Si alloys by means of manganese dispersoids, Mater. Sci. Technol 15 (1999) 450-455.

[41] Y. Birol, The effect of homogenization practice on the microstructure of AA6063 billets, Journal of Materials Processing Technology 148 (2004) 250–258

[42] K. Liu, X.G. Chen, Development of Al–Mn–Mg 3004 alloy for applications at elevated temperature via dispersoid strengthening, Materials and Design 84 (2015) 340–350.

[43] K. Liu, H. Ma, X.G. Chen, Enhanced elevated-temperature properties via Mo addition in Al-Mn-Mg 3004 alloy, Journal of Alloys and Compounds 694 (2017) 354-365

[44] R.G. Buchheit, R.P. Grant, P.F. Hlava, B. Mckenzie and G.L. Zender, Local Dissolution Phenomena Associated with S Phase (Al_2CuMg) Particles in Aluminum

Alloy 2024 - T3, J. Electrochem. Soc. 144, 8 (1997) 2621-2628

[45] L. Lodgaard, N. Ryum, Precipitation of dispersoids containing Mn and/or Cr in Al–Mg–Si alloys, Materials Science and Engineering: A 283 15 (2000) 144-152

[46] M.H. Mulazimoglu, A. Zaluska, J.E. Gruzleski, and F. Paray, Electron microscope study of Al-Fe-Si intermetallics in 6201 Aluminum alloy, Metallurgical And Materials Transactions A 27a (1996) 929

[47] C. Liu, Microstructure evolution during homogenization and its effect on the high temperature deformation behaviour in aa6082 based alloys, Ph. D thesis, University of British Columbia (2017) 76, 99-103

[48] C. Li, Precipitation behaviors of dispersoids induced from transition elements (Mn, Sc And Zr) and their effect on recrystallization resistance in AA6082 Alloys, Master theses, University of Quebec at Chicoutimi, 2018.

[49] R. Hu, T. Ogura, H. Tezuka, T. Sato and Q. Liu, Dispersoid formation and recrystallization behavior in an Al-Mg-Si-Mn Alloy, J. Mater. Sci. Technol. 26(3) (2010) 237-243.

[50] J.H. Li, A. Wimmer, G. Dehm, P. Schumacher, Intermetallic phase selection during homogenization for AA6082 alloy, Philosophical Magazine, 94, 8 (2014) 830-846.

[51] S. Kumar, K.A.Q. O'Reilly, Influence of Al grain structure on Fe bearing intermetallics during DC casting of an Al-Mg-Si alloy, Materials Characterization 120 (2016) 311-322.

[52] S.N. Samaras, G.N. Haidemenopoulos, Modelling of microsegregation and

homogenization of 6061 extrudable Al-alloy, Journal of Materials Processing Technology 194 (2007) 63–73.

[53] M. Shakiba, N. Parson, X-G. Chen, Effect of homogenization treatment and silicon content on the microstructure and hot workability of dilute Al–Fe–Si alloys, Materials Science & Engineering A 619 (2014) 180–1

[54] Y. Han, K. Ma, L. Li, W. Chen, H. Nagaumi, Study on microstructure and mechanical properties of Al–Mg–Si–Cu alloy with high manganese content, Materials and Design 39 (2012) 418–424

[55] A.M.F. Muggerud, E.A. Mortsell, Y.J. Li, R. Holmestad, Dispersoid strengthening in AA3xxx alloys with varying Mn and Si content during annealing at low temperatures, Materials Science & Engineering A 567 (2013) 21-28.

[56] Z. Li, Z. Zhang, X-G. Chen, Effect of magnesium on dispersoid strengthening of Al−Mn−Mg−Si (3xxx) alloys, Trans. Nonferrous Met. Soc. China 26 (2016) 2793-2799.

[57] Y. Wu, J. Xiong, R. Lai, X. Zhang, Z. Guo, The microstructure evolution of an Al–Mg–Si–Mn–Cu–Ce alloy during homogenization, Journal of Alloys and Compounds 475 (2009) 332–338

[58] Ø. Ryen, B. Holmedal, O. Nijs, E. Nes, E. Sjölander, H.-E. Ekström, Strengthening mechanisms in solid solution aluminum alloys, Metall. Mat. Trans. A 37 (2006) 1999-2006.

[59] K.E. Knipling, D.C. Dunand, D.N. Seidman, Acta Mater. 56 (2008) 114-127.

[60] F.J. Humphreys, M. Hatherly, Recrystallization and Related Annealing

Phenomena, second ed., Elsevier Ltd., Oxford (2004) 169-450

[61] H.J. Mcqueen, S. Spigarelli, M.E. Kassner, E. Evagelista, Hot deformation and processing of aluminum alloys. Florida, CRC Press, (2011) 43-89.

[62] H.J. Mcqueen, N.D. Ryan, Constitutive analysis in hot working, Mater. Sci. Eng. A 322 (2002) 43-63.

[63] C. Liu, Q. Du, N. Parson, W. Poole, The interaction between Mn and Fe on the precipitation of Mn/Fe dispersoids in Al-Mg-Si-Mn-Fe alloys, Scripta Mater. 152 (2018) 59–63.

[64] M. Shakiba, N. Parson, X.-G. Chen, Effect of homogenization treatment and silicon content on the microstructure and hot workability of dilute Al–Fe–Si alloys, Mater. Sci. Eng. A 619 (2014) 180–189.

[65] C. Shi, X.-G. Chen, Effect of Zr addition on hot deformation behavior and microstructural evolution of AA7150 aluminum alloy, Materials Science & Engineering A 596 (2014)183–193

[66] M. Shakiba, N. Parson and X.-G. Chen, Effect of Iron and Silicon Content on the Hot Compressive Deformation Behavior of Dilute Al-Fe-Si Alloys, Journal of Materials Engineering and Performance 24 (2015) 404–415

[67] H.J. Mcqueen, N.D. Ryan, Constitutive analysis in hot working, Mater. Sci. Eng. A 322 (2002) 43-63.

[68] Y.C. Lin, X.-M. Chen, A critical review of experimental results and constitutive descriptions for metals and alloys in hot working, Mater. Des. 32 (2011) 1733-59.

[69] S. Banerjee, P.S. Robi, A. Srinivasan, L. Praveen Kumar, High temperature

deformation behavior of Al–Cu–Mg alloys micro-alloyed with Sn, Mater. Sci. Eng. A 527 (2010) 2498-503.

[70] S.B. Brown, K.H. Kim, L. Anand, An internal variable constitutive model for hot working of metals, Int. J. Plast. 5 (1989) 95-130.

[71] F.A. Slooff, J. Zhou, J. Duszczyk, L. Katgerman, Constitutive analysis of wrought magnesium alloy Mg–Al4–Zn1, Scripta Mater. 57 (2007) 759-62.

[72] Y.C. Lin, Y.-C. Xia, X.-M. Chen, M.-S. Chen, Constitutive descriptions for hot compressed 2124-T851 aluminum alloy over a wide range of temperature and strain rate, Comput. Mater. Sci. 50 (2010) 227-33.

[73] C.M. Sellar, W.J.M. Tegart, Hot workability, Int. Met. Rev. 17 (1972) 1-24.

[74] H. Mirzadeh, A. Najafizadeh, M. Moazeny, Flow Curve Analysis of 17-4 PH Stainless Steel under Hot Compression Test, Metall. Mater. Trans. A 40 (2009) 2950-8.

[75] Y.-C. Lin, M.-S. Chen, J. Zhang, Modeling of flow stress of 42CrMo steel under hot compression, Mater. Sci. Eng. A499 (2009) 88-92.

[76] S. Mandal, V. Rakesh, P.V. Sivaprasad, S. Venugopal, K.V. Kasiviswanathan, Constitutive equations to predict high temperature flow stress in a Ti-modified austenitic stainless steel, Mater. Sci. Eng. A 500 (2009) 114-121.

[77] Z.Y. Chen, S.Q. Xu, X.H. Dong, Deformation behavior of AA6063 aluminium alloy after removing friction effect under hot working conditions, Acta Metall. Sin. 21 (2008) 451-458.

[78] W. Li, H. Li, Z. Wang, Z. Zheng, Constitutive equations for high temperature

flow stress prediction of Al–14Cu–7Ce alloy, Mater. Sci. Eng. A528 (2011) 4098-4103.

[79] C.M. Sellars, W.J. Mctegart, La relation entre la résistance et la structure dans la deformation à chaud, Mem. Sci. Rev. Met. 63 (1966) 731-746.

[80] H.R. Rezaei Ashtiani, M.H. Parsa, H. Bisadi, Constitutive equations for elevated temperature flow behavior of commercial purity aluminum, Mater. Sci. Eng. A545 (2012) 61-67.

[81] H.J. Mcqueen, P. Sakaris, Influence of sress multiplier in SINH equation on constitutive constants for Al alloys with Mg and dispersoids In: L. Arnberg, E. Nes, O. Lohne, N. Ryum, editors., Aluminum alloys: Their Physical and Mechanical Properties - Proceedings ICAA3. Trondheim, Norway 179-784.

[82] Y.C. Lin, Q.-F. Li, Y.-C. Xia, L.-T. Li, A phenomenological constitutive model for high temperature flow stress prediction of Al–Cu–Mg alloy, Mater. Sci. Eng. A, 534 (2012) 654-662.

[83] A. Marandi, A. Zarei-Hanzaki, N. Haghdadi, M. Eskandari, The prediction of hot deformation behavior in Fe–21Mn–2.5Si–1.5Al transformation-twinning induced plasticity steel, Mater. Sci. Eng. A 554 (2012) 72-78.

[84] B. Zhang, T. Baker, J. Effect of the heat treatment on the hot deformation behaviour of AA6082 alloy, Mater. Proc. Tech. (2004) 153–154, 881–885.

[85] C. Shi, W. Mao, X.-G. Chen, Evolution of activation energy during hot deformation of AA7150 aluminum alloym, Mater. Sci. Eng. A 571 (2013) 83–91.

[86] X. Peng, W. Su, D. Xiao, G. Xu, Investigation on hot workability of

homogenized Al-Zn-Mg-Cu alloy based on activation energy and processing map, JOM 70 (2018) 993-999.

[87] C. Shi, X.-G. Chen, Evolution of activation energies for hot deformation of 7150 aluminum alloys with various Zr and V additions, Mater. Sci. Eng. A 650 (2016) 97−209.

[88] S. Wang, L. G. Hou, J. R. Luo, J. S. Zhang, L. Z. Zhuang. Characterization of hot workability in AA 7050 aluminum alloy using activation energy and 3-D processing map, Mater. Process. Tech. 225 (2015) 110−121.

[89] C. Shi, X.-G. Chen, Effect of vanadium on hot deformation and microstructural evolution of 7150 aluminum alloy, Materials Science & Engineering A 613 (2014) 91–102.

[90] W.V. Geertruyden, W.Z. Misiolek, P.T. Wang, Grain structure evolution in a 6061 aluminum alloy during hot torsion, Materials Science and Engineering A 419 (2006) 105–114.

[91] R. Kaibyshev, O. Sitdikov, A. Goloborodko, Grain refinement in as-cast 7475 aluminum alloy under hot deformation, Materials Science and Engineering A344 (2003) 348-356.

[92] S. Gourdet, F. Montheillet, An experimental study of the recrystallization mechanism during hot deformation of aluminium, Materials Science and Engineering A283 (2000) 274-288.

[93] Haessner F, editor. Stuttgart, Dr. Riederer-Verlag, Gmbh, Recrystallization of metallic materials. (1978).

[94] F.J Humphreys, M. Hatherly, Recrystallization and related annealing phenomena. 2nd ed. Oxford, Elsevier, (2004).

[95] R. Kaibyshev, K. Shipilova, F. Musin, Y. Motohashi, Continuous dynamic recrystallization in an Al–Li–Mg–Sc alloy during equal-channel angular extrusion, Materials Science and Engineering A 396 (2005) 341–351

[96] R.D. Doherty, D.A. Hughes, F.J. Humphreys, J.J. Jonas, D.J. Jensen, M.E. Kassner, et al., Current issues in recrystallization: a review, Mater. Sci. Eng. A 238 (1997) 219-74, 45.

[97] H.J. Mcqueen, W. Blum, Dynamic recovery: sufficient mechanism in the hot deformation of Al, Mater. Sci. Eng. A 290 (2000) 95-107.

[98] T. Sakai, A. Belyakov, R. Kaibyshev, H. Miura, J.J. Jonas, Dynamic and post-dynamic recrystallization under hot, cold and severe plastic deformation conditions, Progress in Materials Science 60 (2014) 130–207.

[99] S. Lin, Z. Nie, H. Huang, B. Li, Annealing behavior of a modified 5083 aluminum alloy, Materials and Design 31 (2010) 1607–1612.

[100] Heat Treating of Aluminum Alloys, ASM Handbook, Volume 4, Heat Treating ASM Handbook Committee, 841-879.

[101] H.J. McQueen, S. Spigarelli, M.E. Kassner, and E. Evagelista, Hot deformation and processing of aluminum alloys, CRC, Bradenton, FL, (2011) 383-403

[102] D. Tsivoulas, P.B. Prangnell, The effect of Mn and Zr dispersoid-forming additionson recrystallization resistance in Al–Cu–Li AA2198 sheet, Acta Materialia 77 (2014) 1–16.

[103] O. Engler, M.Y. Huh, Evolution of the cube texture in high purity aluminum capacitor foils by continuous recrystallization and subsequent grain growth, Materials Science and Engineering A271 (1999) 371–381.

[104] Y. Birol, Impact of partial recrystallization on the performance of 6005A tube extrusions, Engineering Failure Analysis 17 (2010) 1110–1116.

[105] Z. Guo, G. Zhao, X.-G. Chen, Effects of two-step homogenization on precipitation behavior of Al_3Zr dispersoids and recrystallization resistance in 7150 aluminum alloy, Materials Characterization 102 (2015) 122-130.

[106] H. Li, Z. Gao, H. Yin, H.Jiang, X. Su and J. Bin, Effects of Er and Zr additions on precipitation and recrystallization of pure aluminum, Scripta Materialia 68 (2013) 59–62.

[107] Y. Birol, Effect of Cr and Zr on the grain structure of extruded EN AW 6082 alloy, Met. Mater. Int., Vol. 20, No. 4 (2014) 727-732

[108]. D. Tsivoulas, P.B. Prangnell, The effect of Mn and Zr dispersoid-forming additions on recrystallization resistance in Al–Cu–Li AA2198 sheet, Acta Materialia 77 (2014) 1–16

Chapter 3 Effect of homogenization treatment and micro-alloying with Mn on the microstructure and hot workability of AA6060 aluminum alloys

Abstract

The effects of a homogenization treatment and micro-alloying with Mn on the evolution of the microstructure and hot workability of AA6060 aluminum alloys were investigated. Various homogenization treatments with temperatures ranging from 520 to 610 ℃ and soaking times from 2 to 16 h were conducted. The results revealed that β-AlFeSi intermetallic was the dominant phase in the as-cast microstructure of the experimental alloys. During the homogenization, the fragmentation of intermetallics occurred and plate-like β-AlFeSi transformed into rod-like α-AlFeSi. In addition, a number of dispersoids precipitated in the 0.1Mn alloy in the temperature range of 520 to 580 ℃. The flow stress behavior of the homogenized AA6060 alloys was mainly determined by the solid solution level. Increasing homogenization temperatures resulted in higher flow stresses owing to the increase in solute atoms in the aluminum matrix. The incremental Mn addition from 0 to 0.1% moderately increased the flow stress by up to 3%. Grain growth occurred in the alloys with low Mn contents (<0.03Mn) during the high-temperature homogenization (580–610 ℃), which resulted in a sudden decrease in the flow stresses and an irregular sample shape after the deformation. Micro-alloying with Mn (>0.06%) can effectively prevent grain

growth at such temperatures. For an alloy with Mn (0.1%) micro-alloying, homogenization at 550–580 ℃ for 6 h could be the optimal condition to balance the flow stress and desirable microstructure.

3.1 Introduction

Over the last decades, the consumption and demand for aluminum alloys have rapidly grown owing to their light weight, high strength-to-weight ratio, and easy recyclability. AA6060 aluminum alloys are typically used for extrusion parts with complex cross sections in automobile and architectural applications because they possess a combination of medium strength, excellent formability, good corrosion resistance and anodizing properties. AA6060 extrusion billets are mostly produced via direct chill (DC) casting, during which the non-equilibrium solidification induces an inhomogeneous microstructure such as micro-segregations and a network of brittle Fe-bearing intermetallics, thereby causing a low formability [1, 2]. In general, the homogenization is conducted before the extrusion to eliminate such negative effects. During a homogenization, the micro-segregation of the alloying elements at dendrite boundaries can be diminished, and a more uniform element distribution can be achieved [3]. On the other hand, the interdendritic network of plate-like β-AlFeSi intermetallics is gradually replaced by more rounded and discrete α-AlFeSi intermetallic particles [4–6]. The precipitation of secondary particles (dispersoids) can occur in Mn- and Cr-containing alloys [7, 8]. A proper homogenization regime can significantly increase the extrusion productivity and benefit the surface finish [9, 10].

It is well known that the addition of Mn to 6xxx aluminum alloys can modify the

microstructure of as-cast and heat-treated samples and thus improve the alloy properties [11–13]. In AA6xxx alloys, Mn is present in constituent particles, fine dispersoids, and solid solutions. Kuijpers et al. [14] reported that during the homogenization of Al–Mg–Si alloys, β-AlFeSi transformed into α-$Al_{12}(FeMn)_3Si$ intermetallics. Lodgaard and Ryum [8] reported that Mn-bearing dispersoids started to form at 400 ℃ during the homogenization of Al–Mg–Si alloys. Shakiba et al. [15] reported that Mn addition to dilute Al–Fe–Si alloys increased the high-temperature flow stress owing to the increased Mn solid solution level.

Several research works have been performed to investigate the impact of the homogenization treatment on the microstructure evolution and Fe-rich intermetallic transformation in Al-Mg-Si 6xxx alloys [16-20]. Bryantsev [16] performed a quantitative analysis of the transformation of Fe-containing intermetallics during homogenization as a function of temperature and soaking time in 6xxx alloys. Haidemenopoulos et al. [17] carried out a computational simulation of the β-AlFeSi to α-AlFeSi transformation via integrating the process steps from solidification to homogenization. Recently, Liu et al. [18] built a predictive model for the evolution of critical microstructural features on spatial distribution of solutes, constituent particles and dispersoids during homogenization of AA6082 alloy based on the experiment results. However, most of the researches focused on the microstructure changes during homogenization, but the corresponding effect on the downstream properties such as hot workability was rarely addressed. In addition, AA6060 alloys contain a relatively low alloying element content (0.3-0.6Mg, 0.3-0.6Si) among 6xxx alloys,

which makes them relatively soft after homogenization and can be extruded at a high speed. Therefore, even a small reduction in the flow stress can greatly increase the extrusion speed and improve the productivity. However, the effect of micro-alloying of Mn on the microstructure change during homogenization and its influence on the hot workability are still far being clear.

In the present study, the effects of the homogenization and micro-alloying with Mn on the evolution of the microstructure and hot workability of AA6060 were investigated systematically. The as-cast and homogenized microstructures were examined, and the true stress–strain response was obtained by conducting hot-compression tests. The focus of this study is the relation between the microstructure, solid solution levels, and hot workability.

3.2 Experiments

Four AA6060 alloy samples with micro-alloying additions of 0–0.1 wt.% Mn were used. The chemical compositions are shown in Table 3.1. All alloy compositions are in wt.% unless otherwise indicated. The sample materials were taken from DC cast billets with a diameter of 101 mm, provided by the Arvida Research and Development Center of Rio Tinto based in Saguenay, Quebec. The billets were homogenized at 520, 550, 580, and 610 ℃ for 2, 6, and 16 h and finally water-quenched. Afterward, the samples were prepared with standard metallographic procedure for the microstructure observation. To reveal more details of the microstructure, some of the polished samples were etched with a 0.5% HF solution for 40 s. An optical microscope (Nikon, Eclipse ME600), a scanning electron

microscope (SEM, JEOL-6480LV), and transmission electron microscope (TEM, JEM−2100) were used to examine the microstructures. Moreover, a quantitative analysis of the dispersoid particle distributions was performed based on the SEM images of the etched surfaces. The electrical conductivity was measured with a Sigmascope SMP10 eddy-current device at room temperature to estimate the solid solution levels. Six measurements were performed for each sample to provide an average value. Further, cylindrical specimens of 10 mm diameter and 15 mm height were machined for the hot-compression tests. The uniaxial hot-compression tests were performed using a Gleeble 3800 thermo-mechanical testing unit. The specimens were heated at 2 ℃/s and held to 500 °C for 180 s to ensure a homogeneous temperature distribution. Next, the specimens were deformed to a total true strain of 0.8 at a strain rate of 1 s^{-1}.

Table 3.1 Chemical composition of investigated alloys (wt.%)

Alloys	Mg	Si	Fe	Mn	Al
Base alloy	0.37	0.50	0.17	-	Bal.
0.03Mn	0.37	0.50	0.17	**0.03**	Bal.
0.06Mn	0.37	0.50	0.17	**0.06**	Bal.
0.1Mn	0.37	0.51	0.19	**0.09**	Bal.

3.3 Results and discussion

3.3.1 As-cast microstructure

The as-cast microstructure of the base alloy is shown in Fig. 3. 1. As indicated in Fig. 3. 1a, it was composed of aluminum dendrite cells, β-AlFeSi intermetallic distributed along the dendrite boundaries, a small amount of α-AlFeSi intermetallic located within the dendrite cells, and primary Mg_2Si particles. Figs. 1b and 1c show enlarged SEM images of the β-AlFeSi and α-AlFeSi intermetallics, which exhibited plate-like and blocky morphologies, respectively. Figs. 1c and 1d illustrate that the small primary Mg_2Si particles were mostly co-located with α- and β-AlFeSi intermetallics. In the as-cast microstructure, β-AlFeSi intermetallic was the predominant phase, whereas α-AlFeSi and Mg_2Si were the minor phases. Regarding the three Mn-containing alloys, the as-cast microstructures were similar to that of the base alloy, thereby indicating that the presence of minor Mn had approximately no effect on the as-cast microstructure. Therefore, only the typical microstructure of the base alloy is presented here.

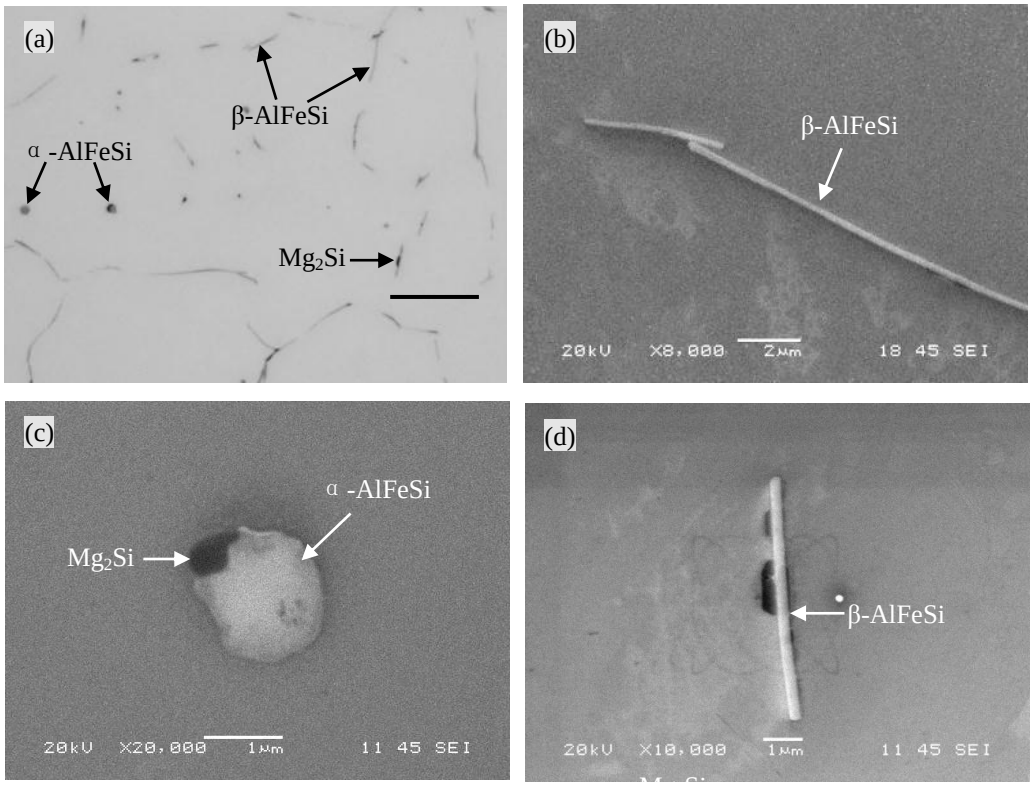

Fig. 3.1 As-cast microstructure of the base alloy, (a) optical image and (b) – (d) backscatter SEM images: (b) β-AlFeSi intermetallic, (c) α-AlFeSi intermetallic with co-located primary Mg_2Si particle and (d) Mg_2Si particles co-located with β-AlFeSi.

3.3.2 Microstructure after homogenization

The homogenized microstructures of the base and 0.1Mn alloys are shown in Figs. 2 and 3 for 520, 550, 580, and 610 ℃ and soaking times of 2, 6, and 16 h. In general, a fragmentation of β-AlFeSi intermetallics was observed in both alloys. Large plate-like β-AlFeSi particles were gradually replaced by separate particles. Increasing homogenization temperatures and longer soaking times promoted the fragmentation process. In addition, dispersoids precipitated in the 0.1Mn alloy at 520–580 ℃ and were visible after the HF etching (Fig. 3. 3).

During the homogenization, the phase transformation from plate-like β-AlFeSi to more rounded and discrete α-AlFeSi occurred in both base and 0.1Mn alloys. Both phases were confirmed via the SEM–EDX analyses. Regarding the homogenized base alloy at 550 ℃ and below, the Fe-bearing intermetallic remained in the form of β-AlFeSi. During the homogenization at 580 °C, β-AlFeSi began to transform into α-AlFeSi. By contrast, in the 0.1Mn alloy, the transformation of β-AlFeSi into α-Al(FeMn)Si already started at 520 ℃. The promotion of the transformation of β-AlFeSi into α-Al(FeMn)Si at lower temperatures by the addition of Mn is in line with the results from previous studies [19]. Fig. 3. 4 shows typical α-AlFeSi/α-Al(FeMn)Si particles in the base and 0.1Mn alloys after a homogenization at 580 ℃ for 6 h. They exhibit a rod-like morphology with rounded edges.

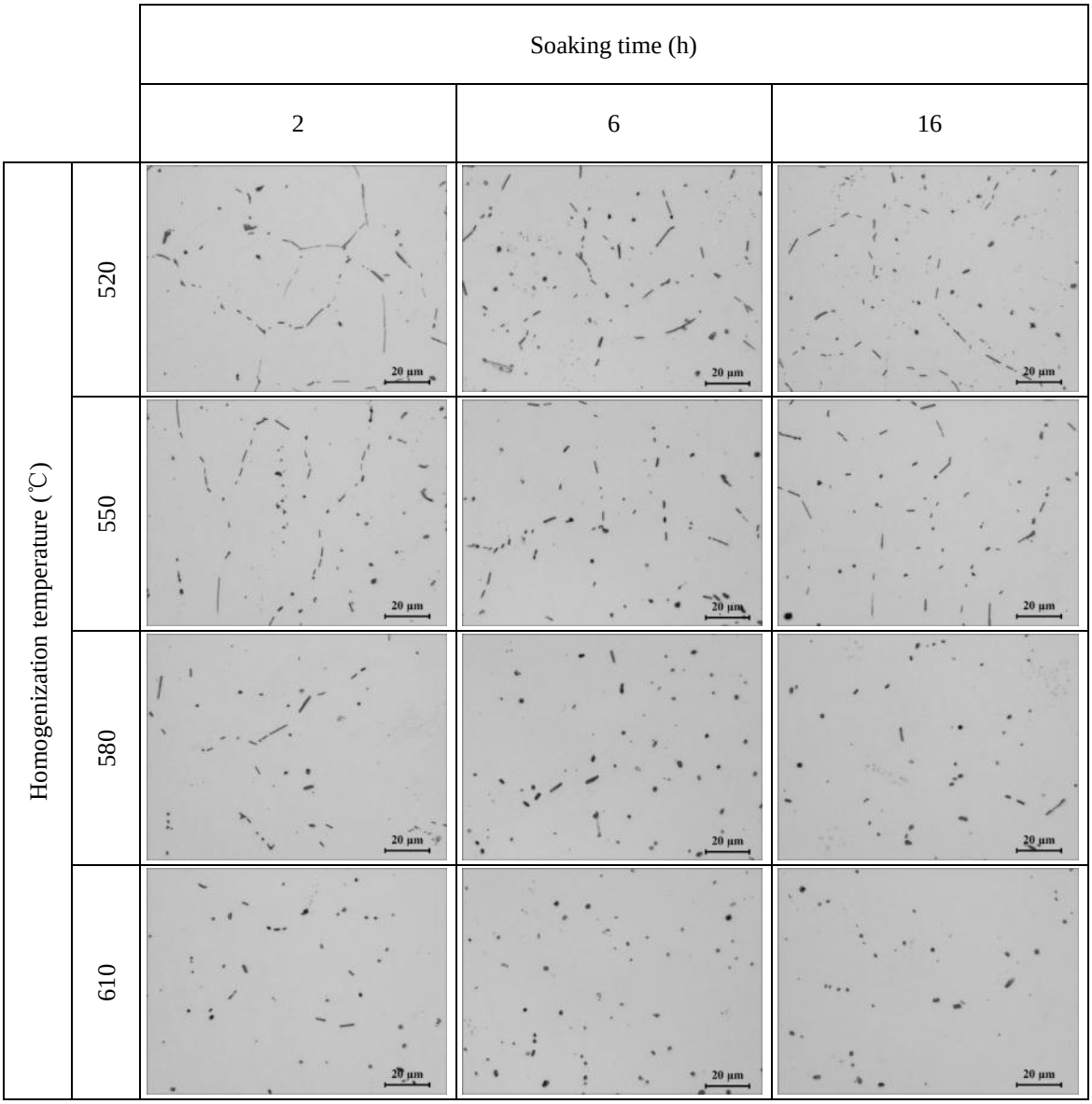

Fig. 3.2 Optical microstructure after homogenization of the base alloy under different conditions (0.5% HF/40 s etched)

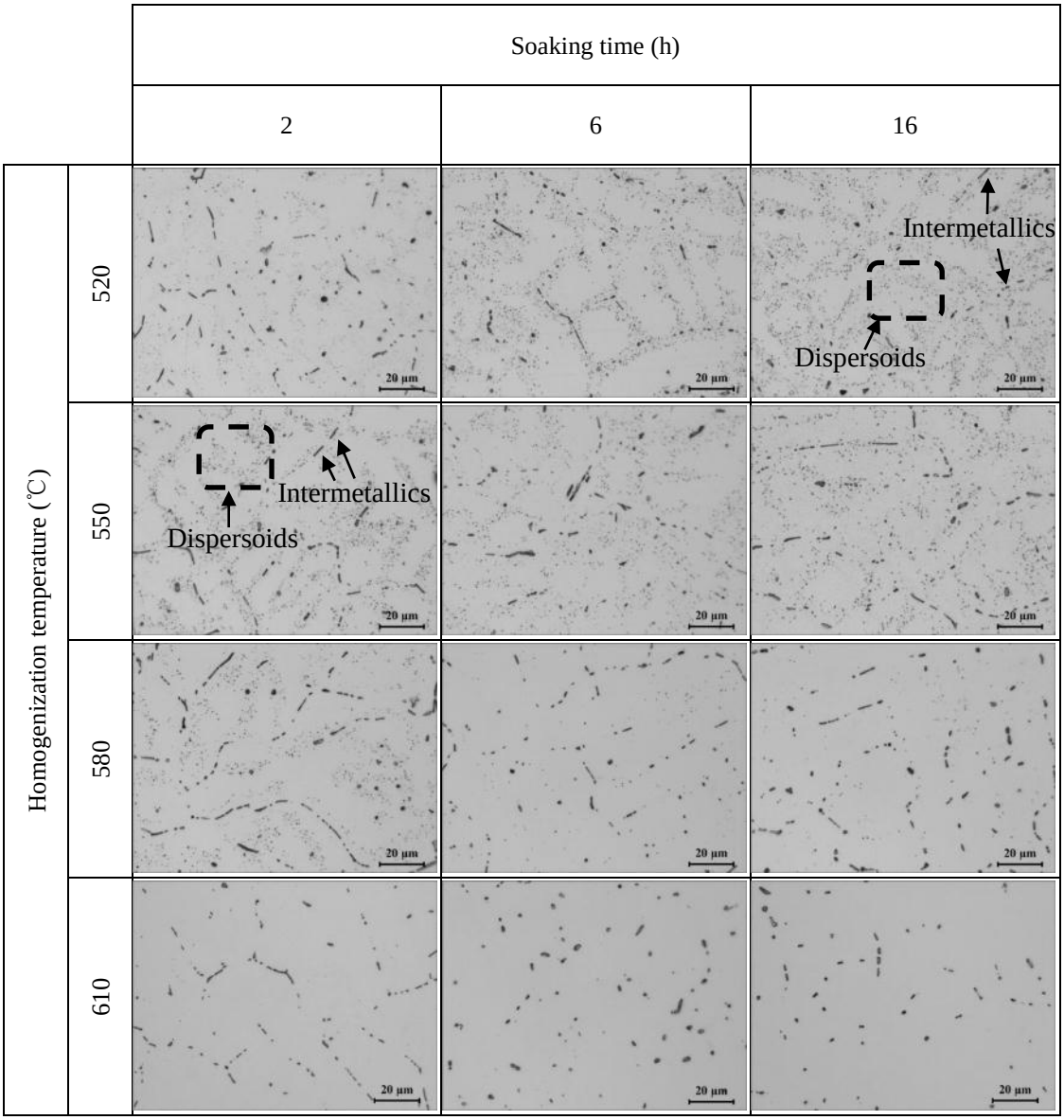

Fig. 3.3 Optical microstructure after homogenization of the 0.1Mn alloy under different conditions (0.5% HF/40 s etched)

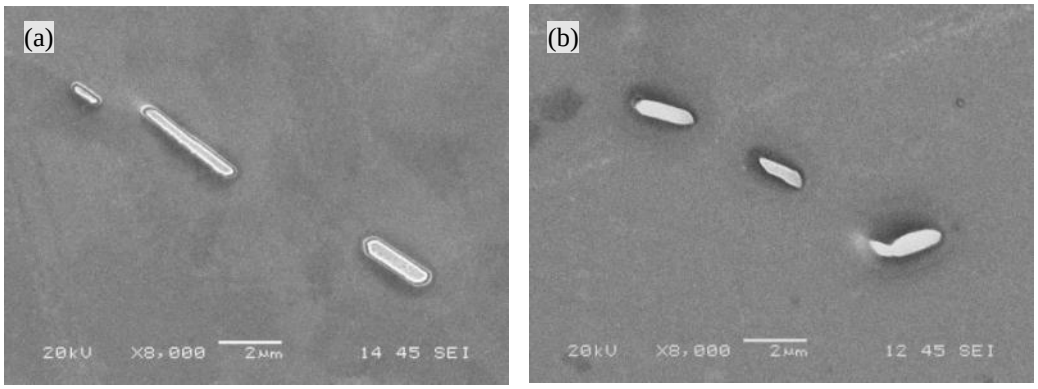

Fig. 3.4 SEM images (a) α-AlFeSi in the base alloy and (b) α-Al(FeMn)Si in the 0.1Mn alloy after homogenization at 580 ℃ for 6 h

The blocky α-AlFeSi intermetallics that pre-existed in the as-cast microstructure (Fig. 3. 1c) were not modified by the homogenization, whereas all primary Mg_2Si particles (Figs. 1c and d) were dissolved. Enlarged typical dispersoids are presented in Fig. 3. 5 for the 0.1Mn alloy after a homogenization at 520 ℃ for 6 h. According to the TEM–EDX analysis, the dispersoids were confirmed to be the an α-Al(FeMn)Si phase (Figs. 3. 5b and c), which agrees well with the results in [20].

Fig. 3. 6 shows the evolution of the number density and average equivalent diameter of the dispersoid particles after homogenizations under different conditions, measured via an image analysis of a series of SEM images of etched surfaces, an example of which is shown in Fig. 3. 5a. During the homogenization at 520 ℃, the dispersoid number density increased with increasing soaking time from 0.10/μm^2 after 2 h to 0.24/μm^2 after 16 h. The equivalent diameter increased from 0.50 μm after 2 h to 0.82 μm after 16 h. At 550 °C, the dispersoid number density started to decrease

with increasing soaking time. The equivalent diameter initially decreased slightly from 0.62 μm (2 h) to 0.52 μm (6 h) and then increased to 0.75 μm after 16 h, indicating a coarsening process at this temperature. At 580 ℃, only dispersoids with low number densities were observed after 2 h soaking. They nearly disappeared with increasing time, which indicates their dissolution. With a further increase in temperature to 610 ℃, no dispersoids were observed in the aluminum matrix.

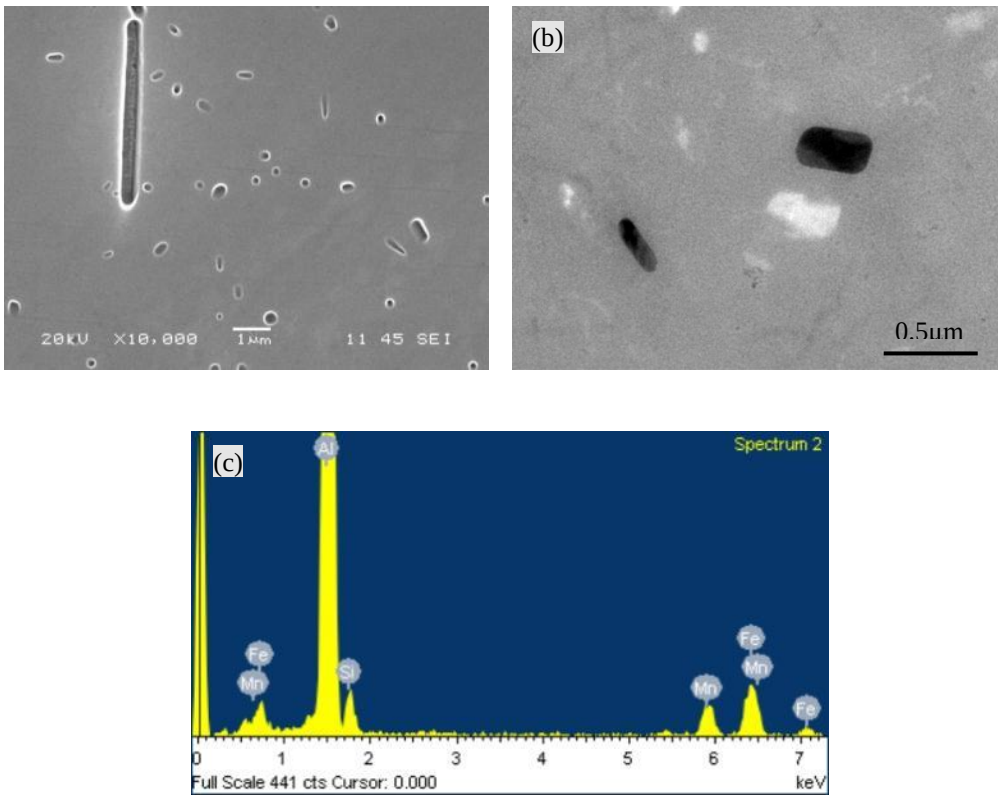

Fig. 3.5 Dispersoids in the 0.1Mn alloys homogenized at 520 ℃ for 6 h: (a) SEM image, (b) TEM bright field image and (c) TEM-EDX spectra image.

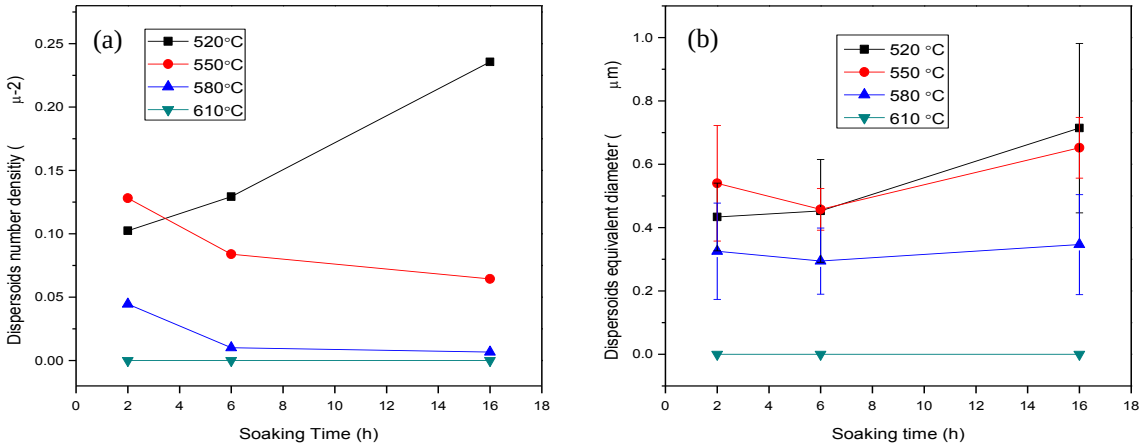

Fig. 3.6 Evolution of the number density (a) and average equivalent diameter (b) of dispersoids during homogenization for the 0.1Mn alloy

3.3.3 Solid solution levels

Solid solution levels can have a significant effect on the mechanical properties and high-temperature flow stress in aluminum alloys [21–23]. The change in the electrical conductivity was used as an indicator to investigate the solid solution level change during the homogenization. The effects of the homogenization treatment on the electrical conductivity are shown in Fig. 3. 7. Regarding the Mn-free base alloy (Fig. 3. 7a), the as-cast sample exhibited the highest electrical conductivity, which corresponds to the lowest solid solution level. This can be attributed to a portion of the main alloying elements (Mg, Si, and Fe) in the primary Mg_2Si and Fe-bearing intermetallics (Fig. 3. 1). After the homogenization, the electrical conductivity decreased with increasing homogenization temperature. For example, for a fixed

soaking time of 6 h, the electrical conductivity of the base alloy decreased from 50.89 to 50.7, 50.39, and 49.92 %IACS as the temperature increased from 520 to 550, 580, and 610 ℃, respectively. In addition, the electrical conductivity remained approximately constant with increasing soaking time. The decrease in the electrical conductivity reflects the increase in the solid solution levels at higher homogenization temperatures, which corresponds to more solute being released from the alloying elements (Mg, Si, and Fe) into the aluminum matrix owing to the dissolution of primary Mg_2Si and the fragmentation of Fe-bearing intermetallics.

Compared with the base alloy, the 0.1Mn alloy exhibited a significantly lower electrical conductivity, which corresponds to higher solid solution levels after the Mn addition. With a similar tendency as the base alloy, the electrical conductivity of the 0.1Mn alloy decreased with increasing homogenization temperature owing to the increased solid solubility limits. In contrast to that of the base alloy, the conductivity increased for longer soaking times. This indicates that the Mn level in the matrix decreased for longer soaking times.

Fig. 3. 8 presents the Mn/Fe ratio of the α-Al(FeMn)Si intermetallic in the 0.1Mn alloy for all experimental conditions measured via SEM–EDX. In as-cast condition, only β-AlFeSi intermetallic presented in the 0.1 Mn-containing alloy (Fig. 1). The Mn/Fe ratio of intermetallics was close to 0, because β-AlFeSi intermetallic was free of Mn. During transformation of β-AlFeSi to α-AlFeSi in the homogenization process, the Mn/Fe ratio of intermetallic at as-cast condition was close to 0, indicating nearly no Mn presented in the β-AlFeSi intermetallic.The Mn/Fe ratio increased with higher

homogenization temperature and longer soaking time, thereby indicating the loss of Mn solute from the aluminum matrix with prolonged soaking time. As discussed in section 3.2, during the homogenization, β-AlFeSi transformed into α-Al(FeMn)Si. The Mn atoms diffused from the matrix into Fe-bearing intermetallic during the transformation. However, in the 0.1Mn alloy, this transformation was completed relatively early. This suggests that the trends in Fig. 3. 8 are due to a continued long-range diffusion of Mn into the constituent particles with increasing time and temperature. Replacement of some Fe atoms by Mn in Fe-bearing intermetallics was reported in [19], when the transformation of β-AlFeSi to α-AlFeSi in aluminum alloys occurred. Similar effects were reported for AA6082 alloys with higher Mn contents [20, 24].

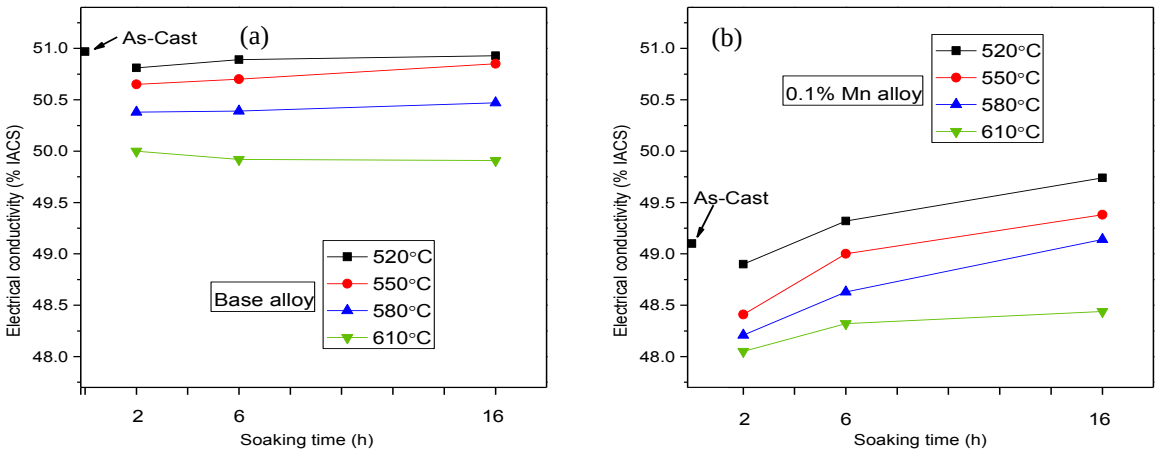

Fig. 3.7 Electrical conductivity of (a) base alloy and (b) 0.1Mn alloy after different homogenization conditions

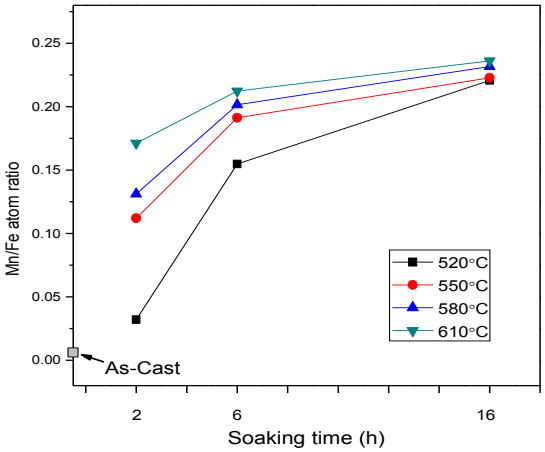

Fig. 3.8 Mn/Fe ratio of intermetallic in 0.1Mn alloy for different homogenization conditions

3.3.4 Flow stress behavior during hot deformation

The hot workability was assessed via compression tests performed at 500 ℃ and a strain rate of 1 s^{-1}. The test temperature was deliberately selected to be above the Mg_2Si solvus temperature (~ 472 ℃ for those alloys) to avoid any interactions with Mg_2Si precipitation/dissolution effects. Figs. 9 and 10 show the true stress–strain curves of the base and 0.1Mn alloys for the respective homogenization conditions. In most cases, the flow stress increased rapidly at the beginning of the deformation. Shortly afterward, the flow stress experienced a slow increase until the end of the deformation process, indicating that the dynamic work hardening was slightly stronger than the dynamic softening. In all compression tests for both alloys, the flow stress levels varied within a relatively narrow range of 27–32 MPa for a strain of 0.75.

However, this represents a difference of approximately 15%, which is significant in terms of commercial extrusion productivity.

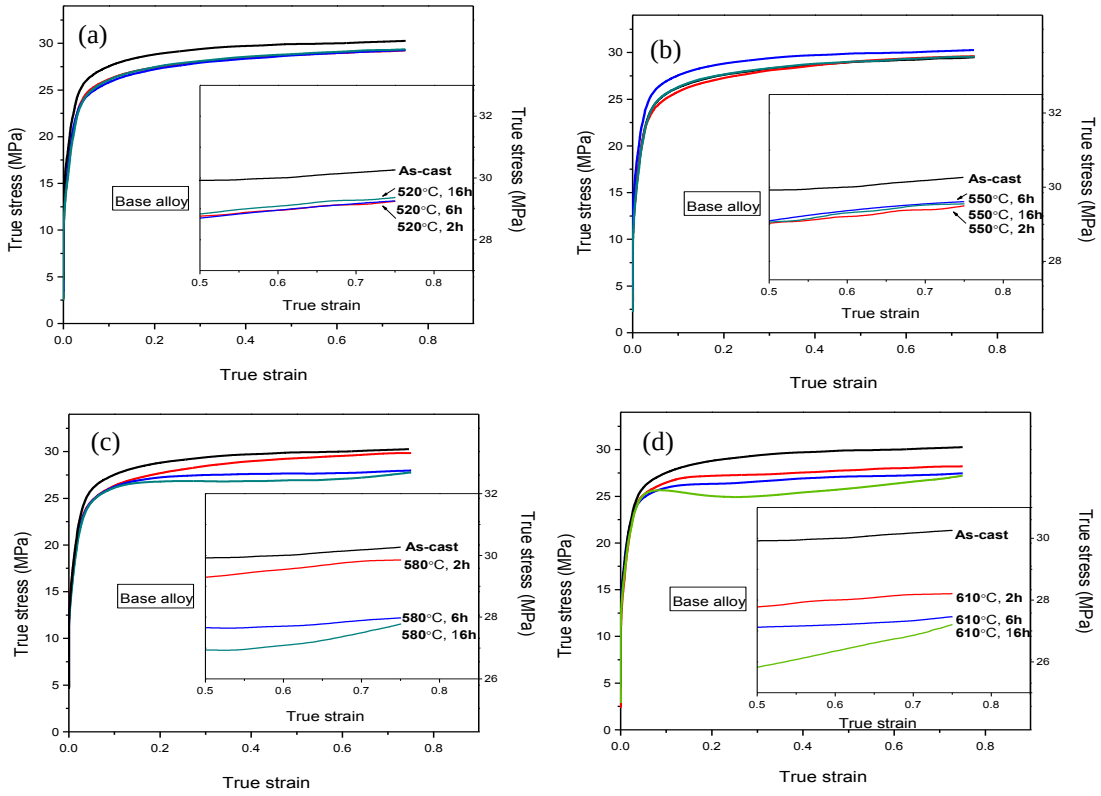

Fig. 3.9 True stress-strain curves of the base alloy at different homogenization conditions, (a) 520 ℃, (b) 550 ℃, (c) 580 ℃ and (d) 610 ℃

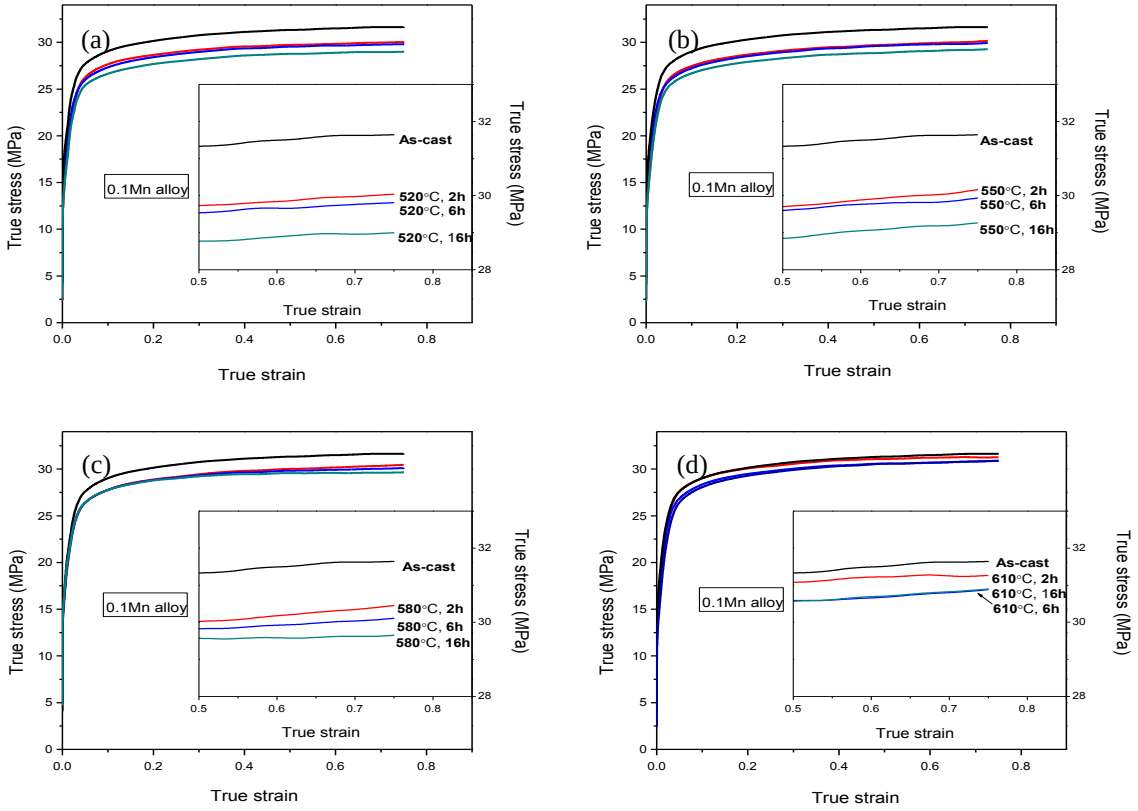

Fig. 3.10 True stress-strain curves of the 0.1Mn alloy at different homogenization conditions, (a) 520 ℃, (b) 550 ℃, 9c) 580 ℃ and (d) 610 ℃

To better compare the effect of the homogenization on the hot workability, the flow stress values at a strain of 0.75 are plotted in Fig. 3. 11 as a function of soaking temperature and time. In both alloys, the as-cast sample always exhibited the highest flow stress compared with the samples that experienced homogenization. This is probably due to the inter-connected network of Fe-bearing intermetallics surrounding the aluminum dendrite cell/grain boundaries (Fig. 3. 1a). Regarding the base alloy (Fig. 3. 11a), the flow stress increased when the soaking temperature increased from

520 to 550 ℃ but was independent of the soaking time. These trends are in line with the electrical-conductivity results in Fig. 3. 7a and indicate that the solute content in the aluminum matrix controlled the flow stress. Similarly, the flow stress increased when the temperature increased to 580 ℃ for a short soaking time. However, with increasing time, the flow stress decreased dramatically from 30 MPa (2 h) to 28 MPa (6 h) and 27.7 MPa (16 h). A further increase in temperature to 610 ℃ caused the flow stress to decrease even further. These results are not in line with the expected trends from the electrical-conductivity measurements for these high temperatures (Fig. 3. 7a).

The 0.1Mn alloy (Fig. 3. 11b) exhibited overall higher flow stresses than the base alloy for all homogenization conditions. The treatment at 520 ℃ resulted in the lowest flow stress. This result is consistent with the lowest solid solution level at this temperature (Fig. 3. 7b). The flow stress increased gradually with increasing homogenization temperature from 520 to 610 ℃. This is again attributed to the increase in solid solution content at higher temperatures. In addition, the flow stress decreased slightly with increasing soaking time for all temperatures, thereby matching the decrease in the Mn solute level (Fig. 3. 7b).

Fig. 3. 12 compares the flow stresses for the four tested Mn contents (the base, 0.03Mn, 0.06Mn, and 0.1Mn alloys) for a fixed soaking time of 6 h. The 0.1Mn alloy exhibited the highest flow stress among the four alloys. Overall, the flow stress increased with the Mn content. However, the range of the value changes was within 1 MPa. Although this effect appears quite small, it represents a flow-stress range of

approximately 3%. It is known in the industrial practice that even a difference of 1% can affect the commercial extrusion productivity. Similarly to the trends observed for the base alloy in Fig. 3. 11a, the alloys with low Mn contents (<=0.03Mn) exhibited a large decrease in the flow stress at high temperatures, namely the base alloy at >580 ℃ and the 0.03Mn alloy at 610 ℃.

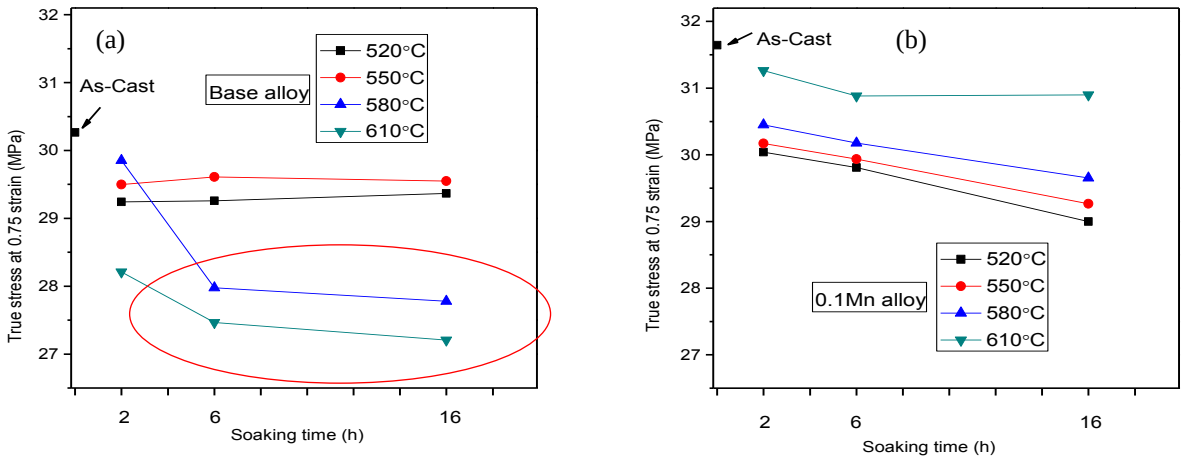

Fig. 3.11 Effect of homogenization conditions on the flow stress at strain of 0.75: (a) the base alloy and (b) 0.1Mn alloy

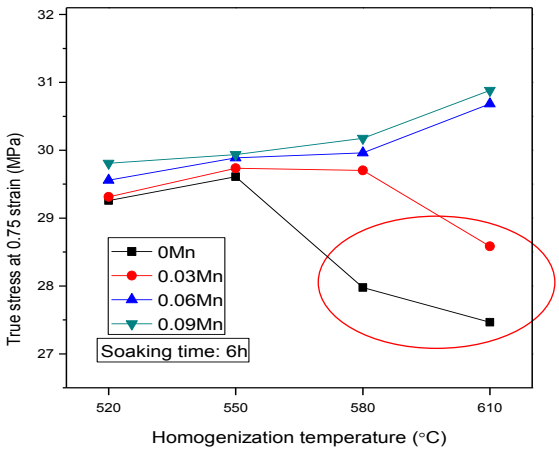

Fig. 3.12 Flow stress at a strain of 0.75 for different Mn contents

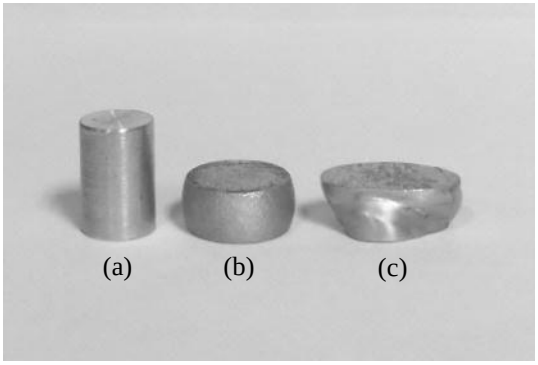

Fig. 3.13 Shape and appearance of compression samples: (a) cylindrical before deformation; (b) “drum” shape after deformation; (c) irregular” shape after deformation

It was observed that the deformed samples of these alloys under such treatment conditions possessed irregular shapes. Fig. 3. 13 shows the shape and appearance of the compression samples before and after the deformation. Regarding the “normal” condition, the cylindrical samples were compressed into a “drum” shape, indicating a uniform deformation along the entire sample. However, the homogenized alloys with low Mn contents exhibiting the unusual decrease in the flow stress described above, exhibited an “irregular” shape. The homogenization conditions and related sample shape after the deformation of the base alloy are listed in Table 3.2. At low homogenization temperatures (520 and 550 ℃), the deformed samples exhibited the drum shape. However, above 580 ℃ and for a soaking time of more than 6 h, the deformed samples became irregular. For 610 ℃, all deformed samples had an irregular shape. Regarding the 0.03Mn alloy, the samples homogenized at 610 ℃ for

longer than 6 h also exhibited an irregular shape (non-uniform deformation). For Mn levels >0.06 wt.%, all deformed samples exhibited a drum shape.

Table 3. 2 Effect of homogenization conditions on deformed sample shape – base alloy

	2 h	6 h	16 h
520 ℃	drum	drum	drum
550 ℃	drum	drum	drum
580 ℃	drum	irregular	irregular
610 ℃	irregular	irregular	irregular

The examination of the microstructure revealed that the irregular deformed sample was related to the abnormal grain growth during the high-temperature homogenization. Fig. 3. 14a shows the microstructure of the base alloy after the homogenization at 580 ℃/2 h. Its deformation is normal and it consists of equiaxed grains with a mean size of approximately 69 μm, which is typical for as-cast 6xxx billets. Under applied compressive stress, the deformation can distribute in many grains with different orientations, resulting in an overall uniform deformation. Fig. 3. 14b shows the microstructures of the base alloy homogenized at 610 ℃/2 h, which exhibited an irregular shape after the deformation. Evidently, only very few giant grains remained in the entire sample section owing to the abnormal grain growth during the homogenization. The size of giant grains reached up to several millimeters.

Under applied compressive stress, with this grain size, the deformation can only be directed to few grains with a limited number of slip directions. This leads to an uneven deformation in the macro scale and a decrease in the flow stress. Commercially, this condition is referred to as “giant grain” and shall be avoided because of its deleterious effect of the non-uniform deformation on the metal flow.

In addition, the grain sizes of four experiment alloys in as-cast and as-homogenized conditions were measured. The average grain sizes of the base alloy were 69 μm and 63-67 μm in the 0.03-0.1Mn alloys in the as-cast condition. After homogenization, the grain sizes remained nearly unchanged, except a few special cases mentioned above for the abnormal grain growth. Therefore, the influence of the grain sizes between different alloys on the electrical conductivity and high temperature flow stress, where no abnormal grain growth occurred, could be neglected. McQueen et al. [22] indicated that a change of the grain size had a relatively small effect on the flow stress during hot deformation, because the grain boundary sliding became pronounced above 300 ℃ in aluminum alloys and the effectiveness of grain boundary strengthening was remarkably reduced.

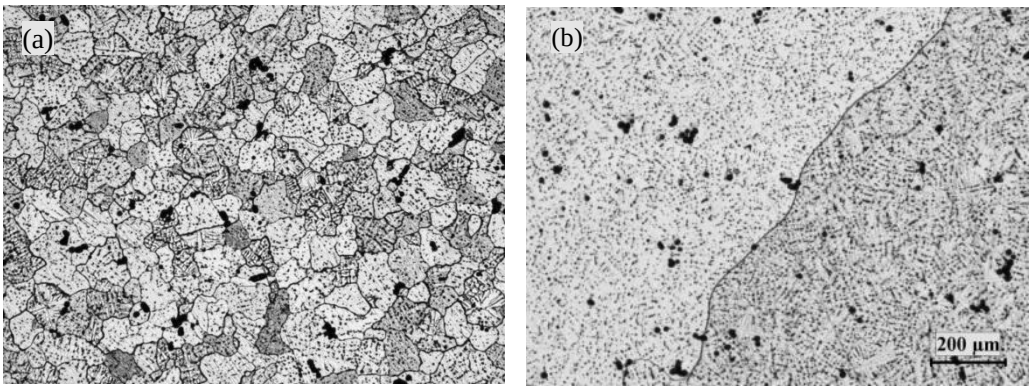

Fig. 3.14 Optical grain structures of the base alloy after homogenization (a) 580 ℃/2h, (b) 610 ℃/2h

3.3.5 Discussion

Homogenization is applied to 6xxx alloys to improve their extrusion performance in terms of extrusion pressure, speed, surface finish, and mechanical properties. In practice, these factors are interrelated. One of the key material parameters controlling the extrudability is the flow stress at the extrusion temperature. For dilute 6xxx alloys such as AA6060, which are often extruded into thin-walled profiles at high speeds, small flow stress differences of the order of 1% can have a measurable effect on the extrusion performance. In the present study, all homogenization treatments decreased the flow stress compared to the as cast condition (Fig. 3. 11). One of the goals of the study was to optimize the homogenization time and temperature. In general, it was found that:

- The flow stress generally increased with higher homogenization temperatures

for Mn contents of up to 0.10 wt.% (Fig. 3. 11).

- The flow stress moderately increased with increasing Mn level in the alloy (Fig. 3. 12) for a given homogenization condition.

During a hot deformation, several factors can contribute to the high-temperature flow stress. In the investigated alloys, three main microstructural features existed in the microstructures under as-cast and homogenized conditions (i.e., Fe-bearing intermetallic particles, α-Al(FeMn)Si dispersoids, and solid solution level), which influence the hot workability of the alloy.

Fe-bearing intermetallic particles can effectively pin dislocations, which in turn changes the flow stress during a hot deformation if their particle sizes are small (<0. 1 μm) and distributed uniformly in the matrix [22]. In the present study, the Fe-bearing intermetallic particles were mainly distributed in the interdendritic region, and the interparticle spacing was very large (in the range of tens of μm (Figs. 2 and 3)). In addition, their sizes were large and ranged from one to tens of μm. Therefore, the effect of the intermetallic particles on the high-temperature flow stress is probably insignificant. However, α-Al(FeMn)Si dispersoids could possibly have a strengthening mechanism during the high-temperature deformation. Li et al. [25] reported that a large number of dispersoids with small sizes (45–50 nm) significantly strengthened AA3004 at high temperatures. In this study, α-Al(FeMn)Si dispersoids were observed in the Mn-containing alloy (0.1Mn) after a homogenization at 520–580 ℃ (Fig. 3. 6). However, owing to the low Mn level, the number density was relatively low and the dispersoid size was relatively large (of the order of 0.5 m

(Figs. 3 and 6)). It is unlikely that such a distribution could remarkably influence the dislocation motion at high temperatures. For example, the number density of dispersoids in the 0.1Mn alloy homogenized at 520 ℃ increased significantly with the soaking time (Fig. 3. 6). However, the flow stress did not increase correspondingly but exhibited a decrease (Fig. 3. 11b).

The similarity in the trends between the electrical conductivity and flow stress in Figs. 7 and 11 suggests that the flow stress is closely related to the solid solution levels. It was reported that solute elements can have a significant influence on the high-temperature flow stress by interacting with the mobile dislocations and retarding softening processes [22, 26]. Regarding the base alloy, with increasing homogenization temperature from 520 to 580 ℃, the fragmentation of the Fe-bearing intermetallic, dissolution of primary Mg_2Si, and solubility of the alloying elements including Fe increased with temperature, resulting in a higher level of solute atoms in the aluminum matrix and lower electrical conductivity (Fig. 3. 7a). Correspondingly, the flow stress increased with increasing homogenization temperature (Fig. 3. 11a). This tendency was interrupted for the homogenization at 580 and 610 ℃, in which the flow stress exhibited a sudden decrease owing to the grain growth (Table. 3. 2 and Fig. 3. 14). However, regarding the 0.1Mn alloy (where no grain growth occurred), the solid solution level and flow stress followed the same trend for the tested homogenization conditions. Increasing the homogenization temperature from 520 to 610 ℃ significantly increased the solid solution level in the matrix (Fig. 3. 7b). The flow stress exhibited a corresponding increase (Fig. 3. 11b). In addition, the solid

solution level decreased with extended soaking time for all homogenization temperatures, indicating a reduced Mn solute level in the matrix. In line with this trend, the flow stress at all homogenization temperatures also decreased slightly with increasing soaking time (Fig. 3. 11b). The decrease in the Mn solid solution level in the matrix with extended treatment time matches the increase in the Mn/Fe ratio in the constituent particles. The same trend was reported for AA6082 [21]. Owing to these changes in the solute level and ignoring the effects of the growth of giant grains, the results of the current study suggest that the flow stress of a typical AA6060 alloy containing up to 0.10 wt.% Mn can be changed by 6% via variations in the homogenization conditions.

The incremental Mn addition from 0 to 0.1% moderately increased the flow stress at all four homogenization temperatures by approximately 1 MPa (Fig. 3. 11c). This represents an increase in the flow stress of 3%, which is still significant in terms of commercial extrusion. Hence, micro-alloying additions of Mn can negatively impact the flow stress of an alloy. However, in commercial alloys, the micro-alloying effect of Mn is typically employed to contribute to the hot workability by facilitating the β-α intermetallic transformation. Additionally, as presented in this paper, a small Mn addition (>0.06%) effectively suppresses undesirable grain growth and enables high-temperature homogenization (above 550 ℃). The precise role of the small Mn addition in preventing grain growth was not completely investigated in this work. It is probably due to the increased constituent volume fraction and number density, which result in an increase in grain boundary pinning.

The experimental results demonstrate that the homogenization treatment can reduce the flow stress and improve the hot workability. Obtaining a minimal flow stress is desirable, which directly control the extrusion speed. However, other features such as the fragmentation and transformation of Fe constituents and the removal of micro-segregations also need to be realized. Consequently, the selection of the homogenization conditions is often a trade-off. Regarding the investigated AA6060 alloys, the homogenization at a low temperature (520 ℃) can reduce the flow stress owing to a low solid solution level. High-temperature homogenization (>550 ℃) raises the flow stress by increasing the solid solution level. Nevertheless, it can effectively promote the fragmentation of intermetallics. Regarding the base alloy (free of Mn), the optimal homogenization treatment could be at 550 ℃ for 6 h, in which the flow stress is still relatively low and the Fe-bearing intermetallics become partially fragmented, whereas the growth of giant grains is suppressed. Regarding the alloy with 0.1 wt.% Mn, a homogenization at 550–580 ℃ for 6 h could be the best trade-off choice to balance the flow stress and achieve the desired microstructure. Under such conditions, β-AlFeSi particles completely transform into α-AlFeSi, and the fragmentation level of the intermetallics is considerably high (Fig. 3. 3).

3.4 Conclusions

(1) The β-AlFeSi intermetallic was the dominant phase in the as-cast microstructure of AA6060 alloys containing up to 0.10 wt.% Mn. During the homogenization, intermetallic fragmentation occurred, and plate-like β-AlFeSi transformed into rod-like α-AlFeSi. The micro-alloying with Mn promoted the transformation of

β-AlFeSi into α-AlFeSi at lower temperatures.

(2) α-Al(FeMn)Si dispersoids were precipitated during the homogenization of the 0.1 wt.% Mn variant. The highest number density was observed at 520 ℃, and coarsening and dissolution occurred above 550 ℃. Owing to their low number density and relatively large size, the effect of dispersoids on the flow stress was determined to be negligible.

(3) The flow stress behavior of homogenized AA6060 alloys was mainly determined by the solid solution level. The increase in the homogenization temperature resulted in higher flow stresses owing to the increase in Fe, Si solute levels released from intermetallics in the aluminum matrix.

(4) The incremental Mn addition from 0 to 0.1% moderately increased the flow stress by up to 3%. In Mn-containing alloys, the flow stress decreased with increasing soaking time owing to the long-range diffusion of Mn to the constituent particles, which exhibited a corresponding increase in the Mn/Fe ratio.

(5) The abnormal grain growth occurred in alloys with low Mn contents (<0.03Mn) during the high-temperature homogenization (580–610 ℃), which resulted in a reduced flow stress and non-uniform deformation. Higher additions of Mn (>0.06%) effectively prevented this effect.

References

[1] J. Li, A. Wimmer, G. Dehm, and P. Schumacher, Intermetallic Phase Selection During Homogenization for AA6082 Alloy, Philosophical Magazine, 94(8),

(2014) 830-846.

[2] S. Kumar, K.A.Q. O'Reilly, Influence of Al Grain Structure on Fe Bearing Intermetallics During DC Casting of an Al-Mg-Si Alloy, Materials Characterization, 120 (2016) 311-322.

[3] S. Samaras, G. Haidemenopoulos, Modelling of Microsegregation and Homogenization of 6061 Extrudable Al-alloy, Journal of Materials Processing Technology, 194 (2007) 63–73.

[4] A. Dons, The Alstruc Homogenization Model for Industrial Aluminum Alloys, J. Light Met., 1 (2001) 133–149.

[5] C. Niels, W. Kuijpers, F. Vermolen, K. Vuik, and S. Zwaag, A Model of the β-AlFeSi to α-Al(FeMn)Si Transformation in Al-Mg-Si Alloys, Materials Transactions, 44(7) (2003) 1448-1456.

[6] N. Bayat, T. Carlberg, and M. Cieslar, In-situ Study of Phase Transformations During Homogenization of 6005 and 6082 Al Alloys, Journal of Alloys and Compounds, 725 (2017) 504-509.

[7] R. Hu, T. Ogura, H. Tezuka, T. Sato and Q. Liu, Dispersoid Formation and Recrystallization Behavior in an Al-Mg-Si-Mn Alloy, J. Mater. Sci. Technol., , 26(3) (2010) 237-243.

[8] L. Lodgaard, N. Ryum, Precipitation of Dispersoids Containing Mn and/or Cr in Al–Mg–Si alloys, Materials Science & Engineering A, 283 (2000) 144-152.

[9] O. Reiso, Extrusion of AlMgSi Alloys, The 9th International Conference on Aluminium Alloys (2004) 32-46.

[10] Y. Totik, M. Gavgali, The Effect of Homogenization Treatment on the Hot Workability Between the Surface and the Center of AA 2014 Ingots, Materials Characterization, 49 (2003) 261–268.

[11] Y. Han, K. Ma, L. Li, and W. Chen, H. Nagaumi, Study on Microstructure and Mechanical Properties of Al–Mg–Si–Cu Alloy With High Manganese Content, Materials and Design, 39 (2012) 418–424.

[12] A. Muggerud, E. Mortsell, Y. Li, R. Holmestad, Dispersoid Strengthening in AA3xxx Alloys with Varying Mn and Si Content During Annealing at Low Temperatures, Materials Science & Engineering A, 567 (2013) 21-28.

[13] Z. Li, Z. Zhang, X.-G. Chen, Effect of Magnesium on Dispersoid Strengthening of Al−Mn−Mg−Si (3xxx) Alloys, Trans. Nonferrous Met. Soc. China, 26 (2016) 2793-2799.

[14] N. Kuijpers, F. Vermolenb, C. Vuikb, P. Koenisc, The Dependence of the β-AlFeSi to α-Al(FeMn)Si Transformation Kinetics in Al–Mg–Si Alloys on the Alloying Elements, Materials Science & Engineering A, 394 (2005) 9-19.

[15] M. Shakiba, N. Parson, X.-G.Chen, Hot Deformation Behavior and Rate-controlling Mechanism in Dilute Al–Fe–Si Alloys with Minor Additions of Mn and Cu, Materials Science & Engineering A, 636 (2015) 572-581.

[16] P. Yu. Bryantsev, Quantitative Estimation of the Transformation of Ferrous Phases during Homogenizing Annealing of Alloys of the 6XXX Series, Russian Journal of Non-Ferrous Metals, 48, 6 (2007) 433–437

[17] G. N. Haidemenopoulos, H. Kamoutsi, A. D. Zervaki, Simulation of the

Transformation of Iron Intermetallics during Homogenization of 6xxx Series Extrudable Aluminum Alloys, Journal of Materials Processing Technology, 212 (2012) 2255–2260

[18] C. L. Liu, H. Azizi-alizamini, N. C. Parson, W. J. Poole, Q. Du, Microstructure Evolution during Homogenization of Al−Mg−Si−Mn−Fe Alloys: Modelling and Experimental Results, Trans. Nonferrous Met. Soc. China 27 (2017) 747−753

[19] N. Kuijpers, Kinetics of the β-AlFeSi to α-Al(FeMn)Si transformation in Al-Mg-Si Alloys, PhD thesis, Delft University of Technology (2004) 8-10, 41-48, 49-58, 105–125 .

[20] Y. Wu, J. Xiong, R. Lai, X. Zhang, Z. Guo, The Microstructure Evolution of an Al–Mg–Si–Mn–Cu–Ce Alloy During Homogenization, Journal of Alloys and Compounds 475 (2009) 332–338

[21] M. Shakiba, N. Parson, X.-G. Chen, Effect of Homogenization Treatment and Silicon Content on the Microstructure and Hot Workability of Dilute Al–Fe–Si Alloys, Materials Science & Engineering A619 (2014) 180–189

[22] H. McQueen, S. Spigarelli, M. Kassner, E. Evagelista, Hot Deformation and Processing of Aluminum Alloys, CRC Press, Florida (2011) 14-16, 87-233.

[23] J. Zhang, F. Pan, R. Zuo, C. Bai, The Low Temperature Precipitation in Commercial-purity Aluminium Sheets for Foils, Journal of Materials Processing Technology 206 (1-3) (2008) 382-387

[24] C. Liu, Q. Du, N. Parson, W. Poole, The Interaction Between Mn and Fe on the Precipitation of Mn/Fe Dispersoids in Al-Mg-Si-Mn-Fe Alloys. Scripta Materialia

152 (2018) 59-63

[25] Z. Li, Z. Zhang, X.-G. Chen, Microstructure, Elevated-temperature Mechanical Properties and Creep Resistance of Dispersoid-strengthened Al-Mn-Mg 3xxx Alloys with Varying Mg and Si Contents, Materials Science & Engineering A, 708 (2017) 383-394

[26] Q. Zhao, M. Slagsvold and B. Holmedal, Comparison of the Influence of Si and Fe in 99.999% Purity Aluminum and in Commercial-purity Aluminum, Scripta Materialia, 67 (2017) 217-220

Chapter 4 Effect of post homogenization cooling rate and Mn contenton Mg_2Si precipitation and hot workability of AA6060 alloys

Abstract

Three post homogenization cooling rates and three homogenization temperatures were applied to direct chill cast AA6060 alloys. The microstructure evolution for different homogenization conditions and the flow stress behavior during hot deformation were systematically studied. During post homogenization cooling, Mg_2Si precipitated in the aluminum matrix, which had an important influence on the solid solution level and the high temperature flow stress. Results revealed that decreasing cooling rates reduced the flow stress significantly due to the precipitation of Mg_2Si and the reduction of the solid solution level. Micro-alloying with 0.1wt% Mn generated a distribution of α-Al(FeMn)Si dispersoids during homogenization with the size and number density decreasing and the Mn in solid solution increasing at higher homogenization temperatures. TEM studies confirmed that α-Al(FeMn)Si dispersoids acted as favorable nucleation sites of Mg_2Si and thus greatly promoted the precipitation of Mg_2Si during subsequent cooling. As a result the high temperature flow stress was controlled by the residual solid solution levels of Mg, Si and Mn resulting from the interactions between dispersoid formation and Mg_2Si precipitation. The combination of the Mn addition, a low cooling rate and a low homogenization temperature provided the lowest flow stress and a high number density of fine Mg_2Si. This combination improved the hot workability and should promote ready dissolution

of Mg_2Si during extrusion.

Keywords

6060 aluminum alloys, Cooling during homogenization, Mn addition, Mg_2Si precipitation, High temperature flow stress

4.1 Introduction

Al-Mg-Si 6xxx alloys possess an attractive combination of strength, excellent formability and corrosion resistance as well as superior anodizing properties [1, 2]. AA6060 aluminum alloys are widely used for the parts with complex cross sections in automobile and architecture industries, which are usually produced from the extrusion process. In the industrial practice, the direct chill cast billets are first homogenized and are then extruded. The objective of the homogenization is to modify the as-cast microstructure and to improve the hot workability and mechanical properties of extruded products. The homogenization consists of the heating, soaking and cooling stages. During heating and soaking, fragmentation of constituent particles and precipitation of dispersoids can occur, while during the cooling stage Mg_2Si precipitation takes place. These microstructure changes during homogenization can have an important impact on the hot workability and downstream properties.

Extrusion under T5 condition is often used in the aluminum extrusion industry due to the economic benefit of low cost production. T5 extrusion condition refers to the in situ solution treatment and press quenching of extruded profiles in the extrusion press followed by a subsequent artificial aging [3]. During this process, the

supersaturated solid solution of Mg and Si is created, and thus no specific solution treatment after extrusion is required. Extrusion under T5 condition provides not only an economic advantage but also can avoid the negative influence of the high temperature solution treatment on the distortion of the complex shapes of extruded profiles [4]. Rapid post homogenization cooling tends to trap the Mg and Si in the solid solution and prevent Mg_2Si precipitation, resulting in an increase in the flow stress, while a slow cooling may promote the precipitation of Mg_2Si particles, leading to the low flow stress and the improvement of hot workability [4, 5, 6]. However, if the precipitated Mg_2Si particles are too coarse, it is very difficult to achieve fully dissolution during extrusion, which results in a partial loss of potential strengthening in subsequent ageing step. For these considerations, the amount of Mg_2Si particles precipitated during cooling of homogenization should be high to reduce the flow stress [7], but the particle size should be small for an easy dissolution during extrusion [8].

A small addtion of Mn is normally made to 6xxx aluminum alloys in order to modify the microstructure and control the recrystallization and grain structure. During homogenization, Mn-containing dispersoids (α-Al(FeMn)Si) are often formed[9]. The α-Al(FeMn)Si dispersoids can influence the deformation process and act as obstacles to grain boundary migration and dislocation movement [10, 11]. Mn also has a significant influence o4n the strength of aluminum alloys when present in solid solution. Li et al. [12] found that the increase of Mn solutes in Al matrix increased the microhardness in the Al−Mn−Mg−Si alloy. Liu [13] reported that with increasing

addition of Mn, the flow stress increases significantly in the AA6082 alloy. It is also reported that the dispersoids formed during homogenization may act as heterogeneous nucleation sites for the precipitation of Mg_2Si phases [14, 15].

Several research works have been performed on various effects of the cooling during homogenization in 6xxx alloys. It was reported that during the cooling stage in an AA6063 alloy, Mg_2Si precipitation was promoted by decreasing the cooling rate from 2000 to 100 ℃/h [16]. However, a further decrease in the cooling rate below 100 ℃/h led to coarser Mg_2Si particles. It was confirmed that the equilibrium β-Mg_2Si was the predominant phase precipitated during 1000-250 ℃/h cooling after homogenization at 580 ℃ for 8h in an AA6082 alloy [17]. Birol [18] reported that a low quenching temperature during cooling led to more Mg_2Si precipitation and resulted in the decrease of the room temperature hardness in 6082 alloy. In our previous work [19], the influence of the homogenization treatment (temperature and soaking time) on the hot workability of AA6060 alloys was investigated. It was found that the flow stress behavior of the homogenized AA6060 alloys was mainly determined by the solid solution level. However, few studies have been focused on the effect of the cooling practice of homogenization on the hot deformation behavior. In addition, the interaction of heterogeneous nucleation between dispersoids and Mg_2Si during homogenization is not well understood.

In the present study, the microstructure changes in AA6060 alloys with and without a Mn addition were examined during homogenization as a function of soak temperature and cooling rate with particular emphasis on the role of dispersoid and

Mg_2Si particles. The effects of microstructure on high temperature flow stress behavior during hot deformation were then investigated by hot compression testing.

4.2 Experimental

Experiments were conducted on two AA6060 alloys with and without a 0.1wt% Mn addition. All samples were taken from direct chill (DC) cast billets with a diameter of 101 mm, provided by the Arvida Research and Development Center, Rio Tinto Aluminium in Saguenay, Quebec. The chemical compositions of two experimental alloys are listed in Table 4. 1. All samples for microstructural analysis and hot deformation were taken 15 mm away from the cast surface of billets to avoid possible microstructural and compositional variations. The samples were homogenized at 515, 545 and 575^{o}C for 6 hours and cooled at three cooling rates, e.g. water quenching, 500^{o}C/h and 100^{o}C/h. The samples were mounted and polished for microstructure observation. To reveal the microstructure details, the polished samples were etched with a 0.5% HF solution for 40 seconds. The microstructure examination was performed using optical microscopy, scanning electron microscopy (SEM, JEOL-6480LV) and transmission electron microscopy (TEM, JEM−2100). Quantitative image analysis for Mg_2Si and dispersoid distributions was performed based on SEM images on the etched surfaces. When quantify the dispersoids size, at least 40 dispersoids were measured, equivalent diameter of the particles was used as the dispersoids size. Electrical conductivity (EC) after homogenization was measured at room temperature using a Sigmascope SMP10 eddy current device. The

average value of each sample was taken from 5 measurements.

For hot deformation testing, cylindrical specimens of 10 mm diameter and 15 mm in height were machined out from the DC cast billets after homogenization. Uniaxial hot compression tests were performed at 400 and 500 ℃ with strain rates of 1 s^{-1} using a Gleeble 3800 thermo-mechanical testing unit. Specimens were heated at a rate of 2 ℃/s to the desired temperature and held for 180 s to ensure a uniform temperature distribution. The specimens were deformed to a total true strain of 0.75 followed by water quench.

Table 4. 1 Chemical composition of two experimental alloys (wt.%)

Alloys	Mg	Si	Fe	Mn	Al
Base alloy	0.37	0.50	0.17	-	Bal.
0.1Mn alloy	0.37	0.51	0.19	0.10	Bal.

4.3 Results

4.3.1 Microstructures

4.3.1.1 As-cast Microstructures

The as-cast microstructures for the base and 0.1Mn alloys are shown in Fig. 4. 1. As indicated, the as-cast microstructure of the base alloy (Fig. 4. 1a) was composed of aluminum dendrite cells (Al matrix) and large plate-like β-AlFeSi intermetallic (gray) and primary Mg_2Si particles (dark) distributed along the dendrite boundaries. For the 0.1Mn alloy (Fig. 4. 1b), the microstructure was similar to the base alloy, indicating the presence of 0.1% Mn had almost no influence on the as-cast microstructure.

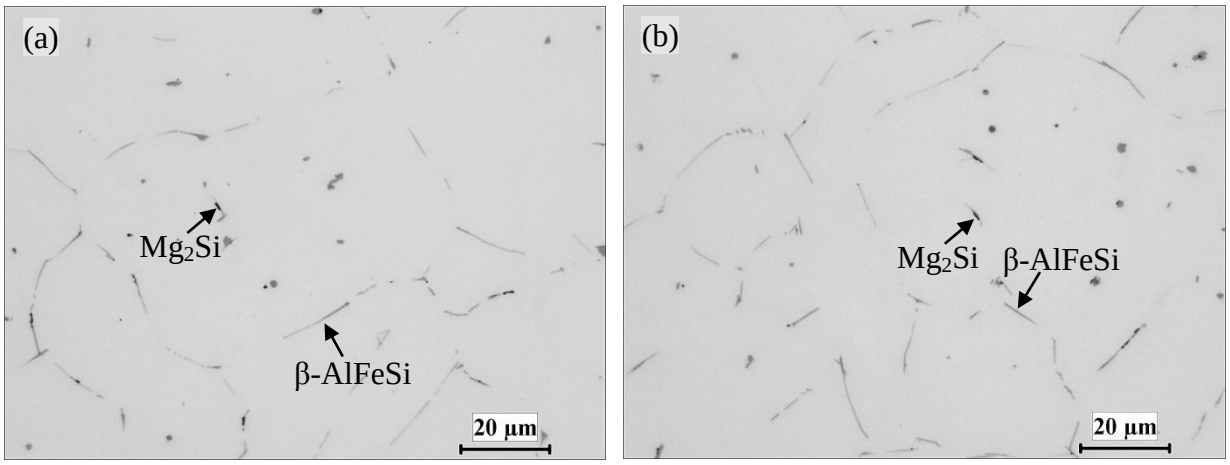

Fig.4. 1 Microstructures of as-cast (a) base alloy and (b) 0.1Mn alloy

4.3.1.2 Microstructures after homogenization with water quench

The homogenized microstructures of the base and 0.1Mn alloys with the fastest cooling rate (water quench) are shown in Fig. 4. 2. To reveal more details, the samples were etched with a 0.5% HF solution for 40 seconds. In general, fragmentation of intermetallics was observed in both alloys. Large plate-like β-AlFeSi particles were replaced by more rounded and separate particles, which were α-AlFeSi in the base alloy (Fig. 4. 2a) and α-Al(FeMn)Si in the 0.1Mn alloy (Fig. 4. 2b, c, d) respectively. In the base alloy, there was no phase precipitation in the aluminum matrix (Fig. 4. 2a). In contrast, a number of dispersoids were evident in the 0.1Mn alloy (Fig. 4. 2b, c and d). The apparent number density of the dispersoids became smaller with increasing homogenization temperature. In addition, a non-uniform distribution of dispersoids was observed with preferential precipitation near the interdendritic region. This was closely related to the concentration gradient of solution elements formed during solidification. The interdendritic region presented higher level of alloying elements

and provided larger driving force for the precipitation of dispersoids. The dispersoids were closely observed by SEM, the images are inserted in Fig. 4. 2b and c.

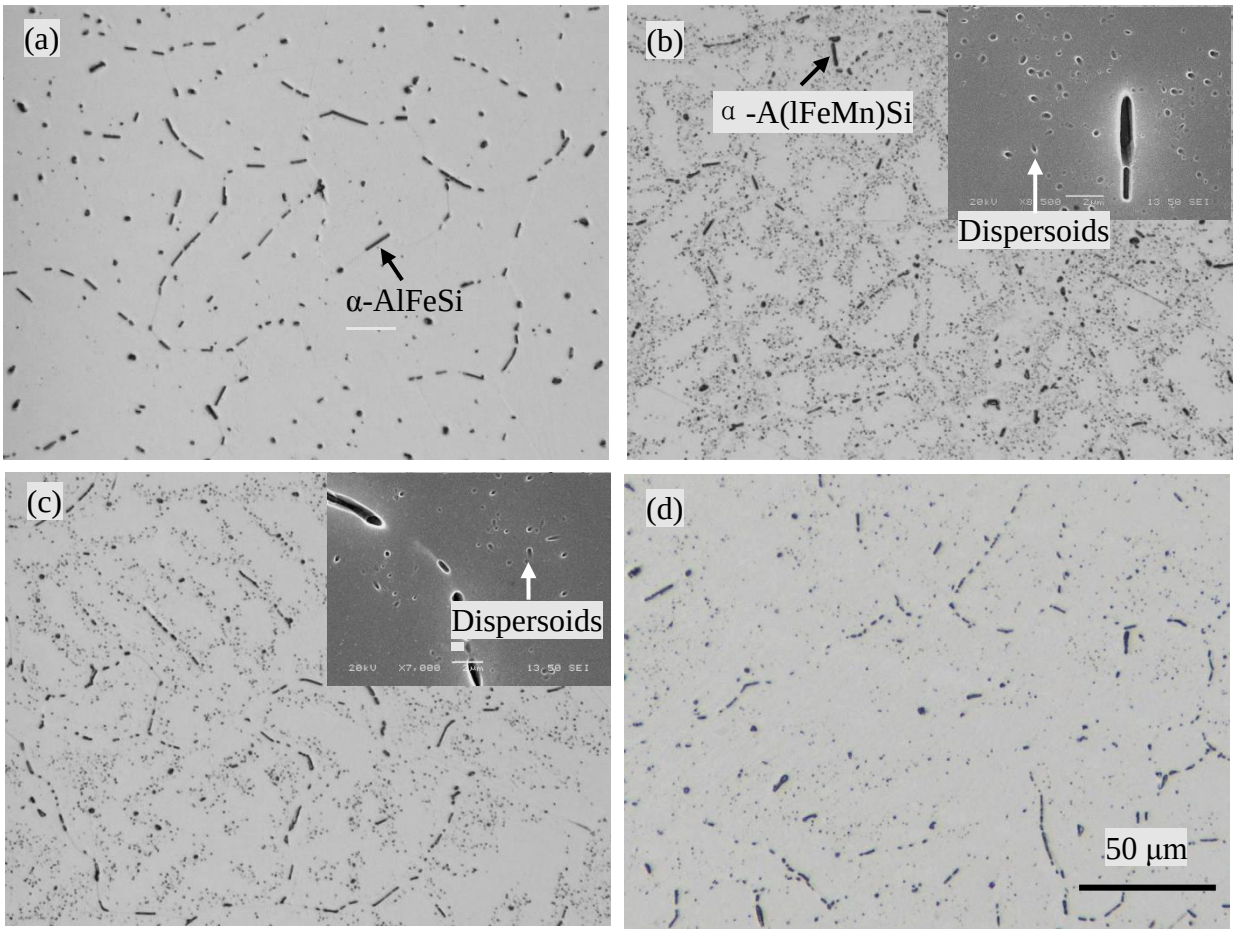

Fig.4. 2 Microstructures of homogenized sample with water quench: (a) the base alloy homogenized at 545 ^{o}C, the 0.1Mn alloy homogenized at 515 ^{o}C (b), 545 ^{o}C (c) and 575 ^{o}C (d). SEM images are inserted in Fig.4.2 b and c.

Fig. 4. 3a shows a bright field TEM image of typical dispersoids in the 0.1Mn alloy after homogenization at 545 ^{o}C for 6h with water quench. The dispersoids are present with short plate and rod forms, which can be attributed to the projection of plate-like morphology in a 2D image. According to the TEM–EDX analysis (Fig. 4.

3b), the dispersoids were identified as α-Al(FeMn)Si, which corresponds with earlier work [10, 13]. Fig. 4. 4 shows the evolution of the number density and equivalent diameter of the dispersoid particles, measured by image analysis on a series of SEM images. With increasing homogenization temperature from 515 to 575^{o}C, both the number density and size of dispersoids decreased, consistent with a dissolution process.

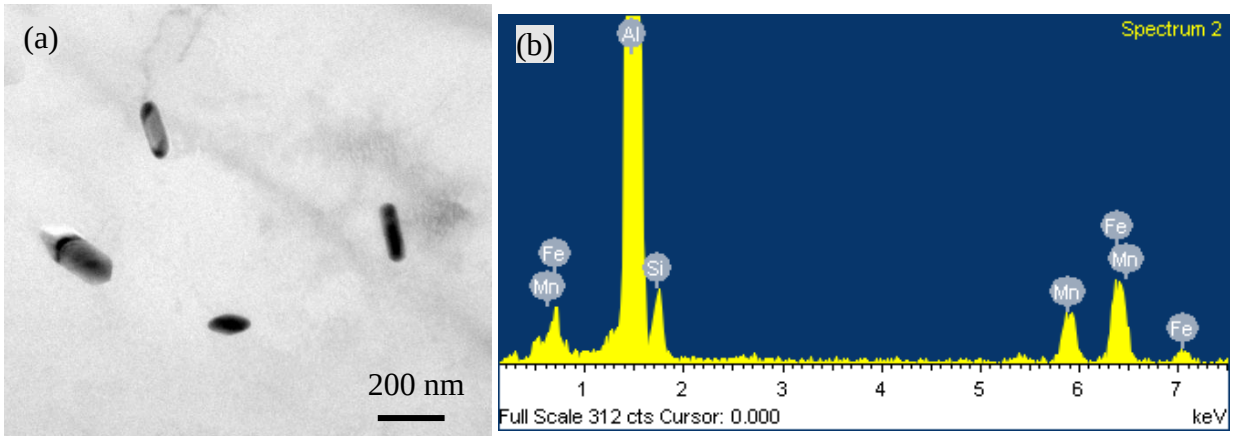

Fig.4. 3 (a) TEM bright field image and (b) TEM-EDX results of dispersoids in the 0.1Mn alloy after 545 ^{o}C of homogenization for 6h with water quench.

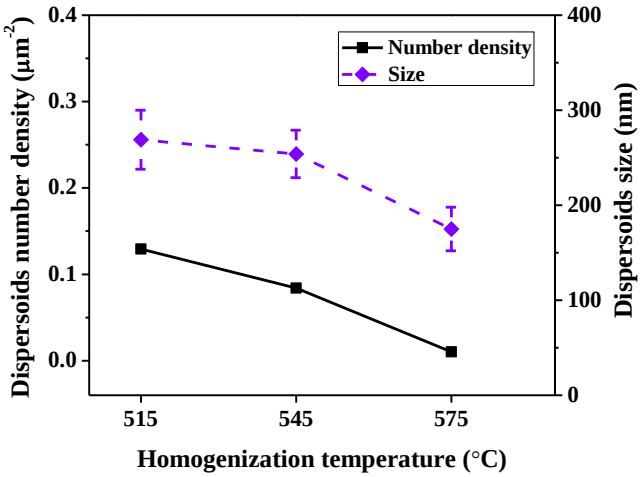

Fig.4. 4 Dispersoids number density and size in the 0.1Mn alloy after homogenization at different temperatures with water quench

4.3.1.3 Microstructures after homogenization with 500 ^{o}C/h and 100 ^{o}C/h cooling rates

The microstructures of the base and 1Mn alloys after homogenization at 545 ^{o}C and cooling at 100 ^{o}C/h are shown in Fig. 4. 5. The precipitation of Mg_2Si was observed in the aluminum matrix of both alloys. For the base alloy (Fig. 4. 5a), when compared to the water quenched samples (Fig. 4. 2a), it is evident that a high number of Mg_2Si particles precipitated inside the matrix. In the 0.1Mn alloy (Fig. 4. 5b), the precipitation of Mg_2Si was mixed with the pre-existing dispersoids. Compared to the base alloy, an overall higher number density and finer size of Mg_2Si particles was observed.

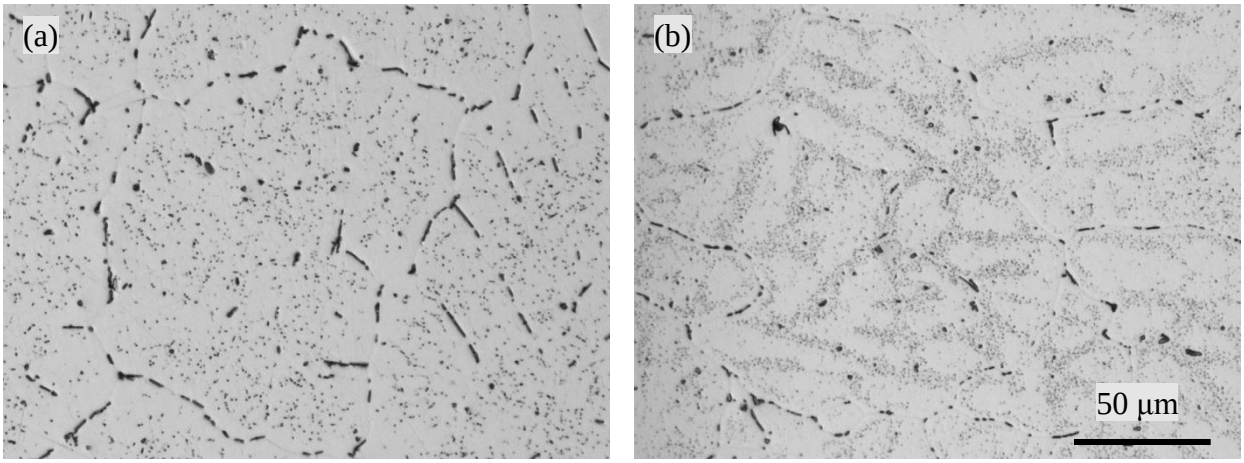

Fig.4. 5 Microstructures of (a) the base alloy and (b) the 0.1Mn alloy homogenized at 545^{o}C for 6h with 100 ^{o}C/h cooling

Fig. 4. 6 displays a series of typical SEM images showing the precipitation of Mg_2Si at high magnification in the base and 0.1Mn alloy after different homogenization conditions. In general, the Mg_2Si particles exhibited a rod-like morphology and clear changes in size and number density as a function of the Mn content and homogenization conditions. A higher number density and finer Mg_2Si particle size were observed in the 0.1Mn alloy compared to the base alloy. Quantitative analysis of Mg_2Si particles in term of the number density and size was performed based on SEM images. The Mg_2Si number density was calculated as the amount of Mg_2Si particles in a unit area including the region having less particle distribution. The size of Mg_2Si was defined as the length of rod-like Mg_2Si particles. Fig. 4. 7 shows the evolution of the number density and size of the Mg_2Si particles. In general for both alloys, the 100 ^{o}C/h cooling rate resulted in a higher number density

and larger size than a faster rate of 500^{o}C/h. In addition, the 0.1Mn alloy produced a higher Mg_2Si particle number density and smaller size than the base alloy for the same homogenization condition. In the base alloy (Fig. 4. 7a), the Mg_2Si number density and size remained nearly unchanged with the increasing homogenization temperature. However, in the 0.1Mn alloy (Fig. 4. 7b), the Mg_2Si number density decreased while the size increased slightly with increasing homogenization temperatures.

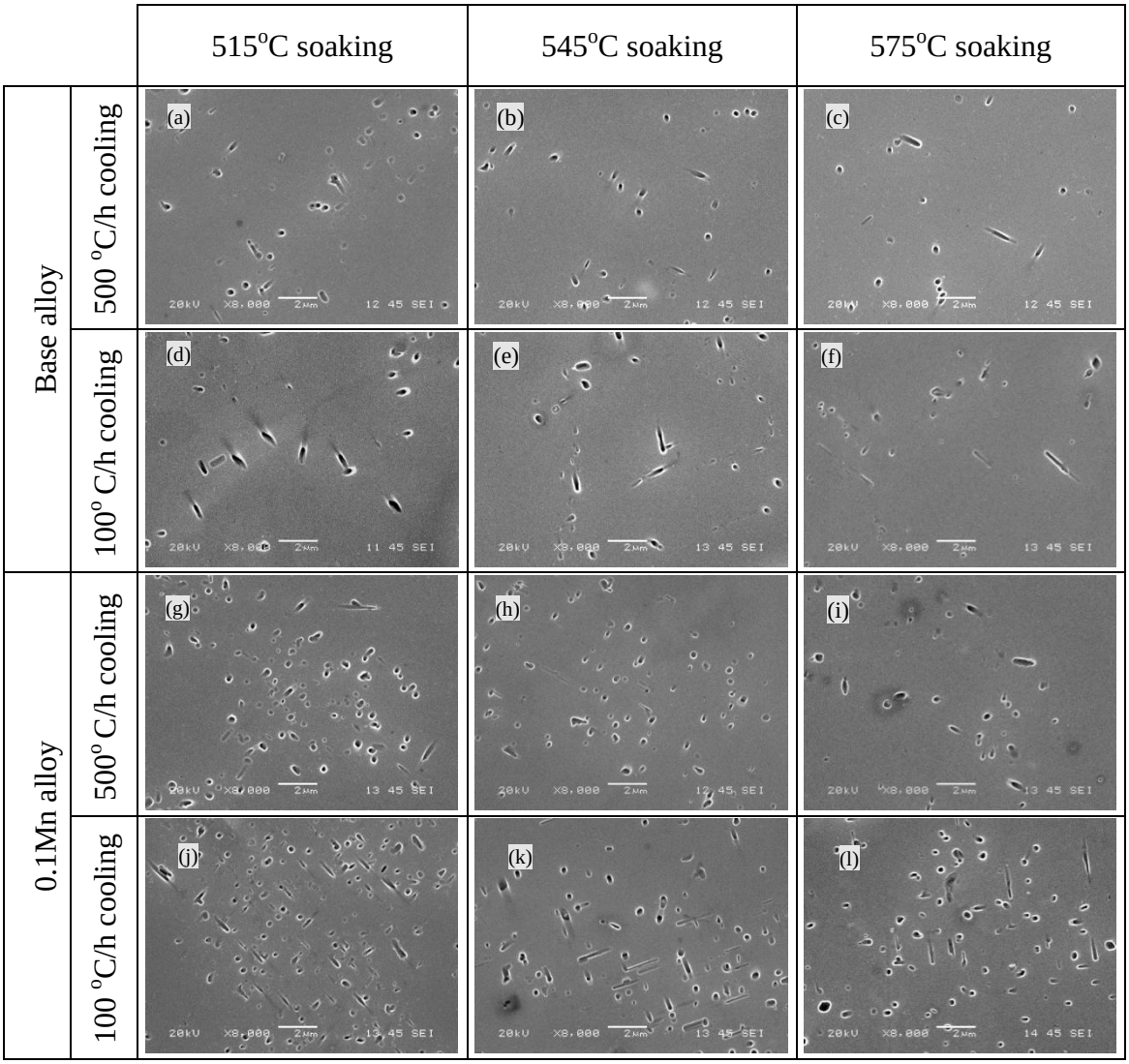

Fig. 4. 6 Mg_2Si precipitation in the base and 0.1Mn alloy after different homogenization conditions

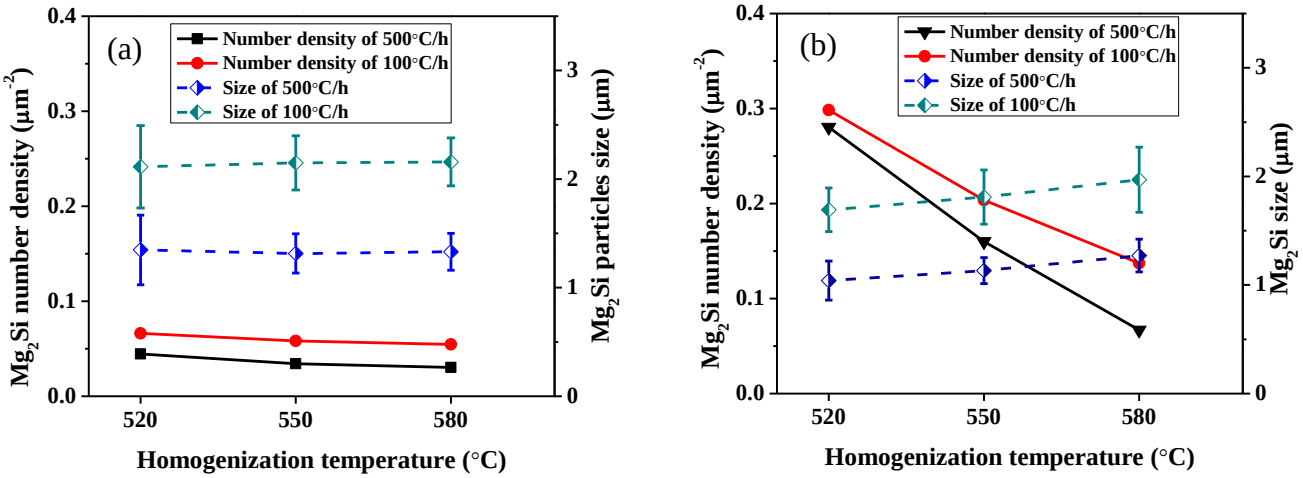

Fig. 4. 7 The number density and size of Mg_2Si in (a) the base alloy and (b) 0.1Mn alloy after homogenized with different cooling rates at different temperatures.

4.3.2 Electrical conductivity and elements in the solution

Electrical conductivity after homogenization was used to monitor the solid solution level in the aluminum matrix. Fig. 4. 8 illustrates the impact of the cooling rate and homogenization temperature on the electrical conductivity of the experimental alloys. In both cases, the electrical conductivity increased with decreasing cooling rates due to the precipitation of Mg_2Si and hence the reduced solid solution level. However, the changes in electrical conductivity with cooling rate for the 0.1Mn alloy were greater than those in the base alloy. For example, at a fixed homogenization temperature of 545 ℃, the electrical conductivity decreased by 2.55 %IACS in the base alloy as the cooling rate shifted from the water quench to the 100 ℃/h cooling rate, while the change in electrical conductivity of the 0.1Mn alloy was 3.67 %IACS, which is 30.5% larger than that of the base alloy. The greater

change in the electrical conductivity in the 0.1Mn containing alloy reflects a larger amount of Mg_2Si precipitation at the same cooling condition due to nucleation on the AlMnFeSi dispersoids (Fig. 4. 6). In the base alloy, electrical conductivity remained nearly unchanged with increasing homogenization temperature, indicating the limited influence of homogenization temperature on the solid solution level, which is associated with a constant number density and size of Mg_2Si (Fig. 4. 7a). However, the electrical conductivity in the 0.1Mn alloy decreased with the increasing homogenization temperature. This was believed to be related to the dissolution of dispersoids at high temperatures and the increased level of Mn in solid solution (Fig. 4. 2b, c, d and Fig. 4. 4).

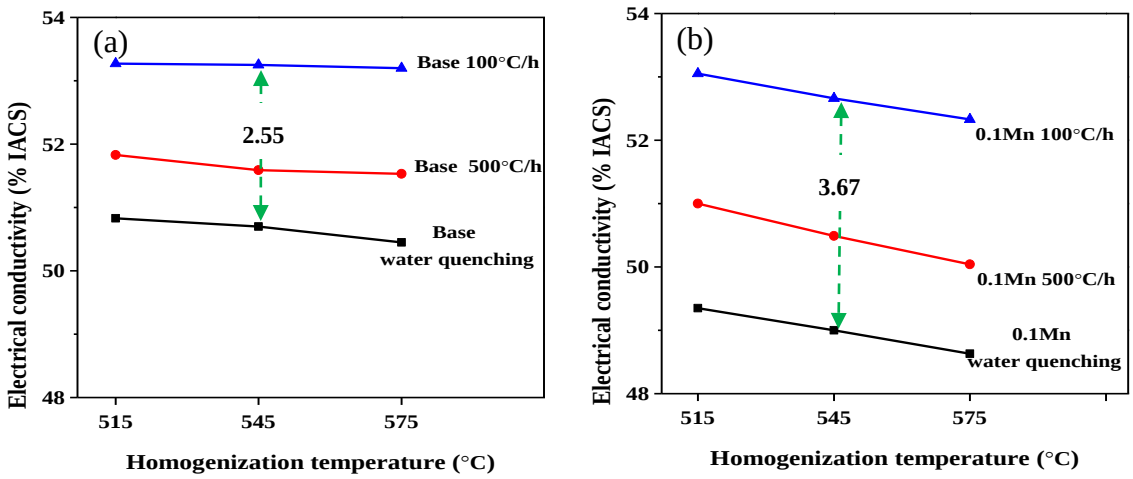

Fig.4. 8 Electrical conductivity of (a) base alloy and (b) 0.1Mn alloy as a function of the cooling rate and homogenization temperature

4.3.3 High temperature flow stress

To study the hot workability of the experimental alloys, compression tests were

performed at the temperatures of 400 ℃ and 500 ℃ with a strain rate of 1 s^{-1}. Samples homogenized at 575 ℃ were chosen to illustrate typical true stress-true strain curves and these are shown in Fig. 4. 9.

In the most cases, the flow stress increased sharply at the beginning of deformation, due to the dislocation multiplication and the high rate of work hardening [20, 21]. Shortly afterwards, the flow stress experienced a slow increase until the end of the deformation process, indicating the balance between dynamic work hardening and dynamic softening. It was evident that the flow stress was temperature dependent, and the deformation at 400 ^{o}C showed higher flow stress levels than at 500 ^{o}C. The higher flow stress at lower deformation temperature was due to a stronger dynamic work hardening, which was a general trend in hot deformation [22].

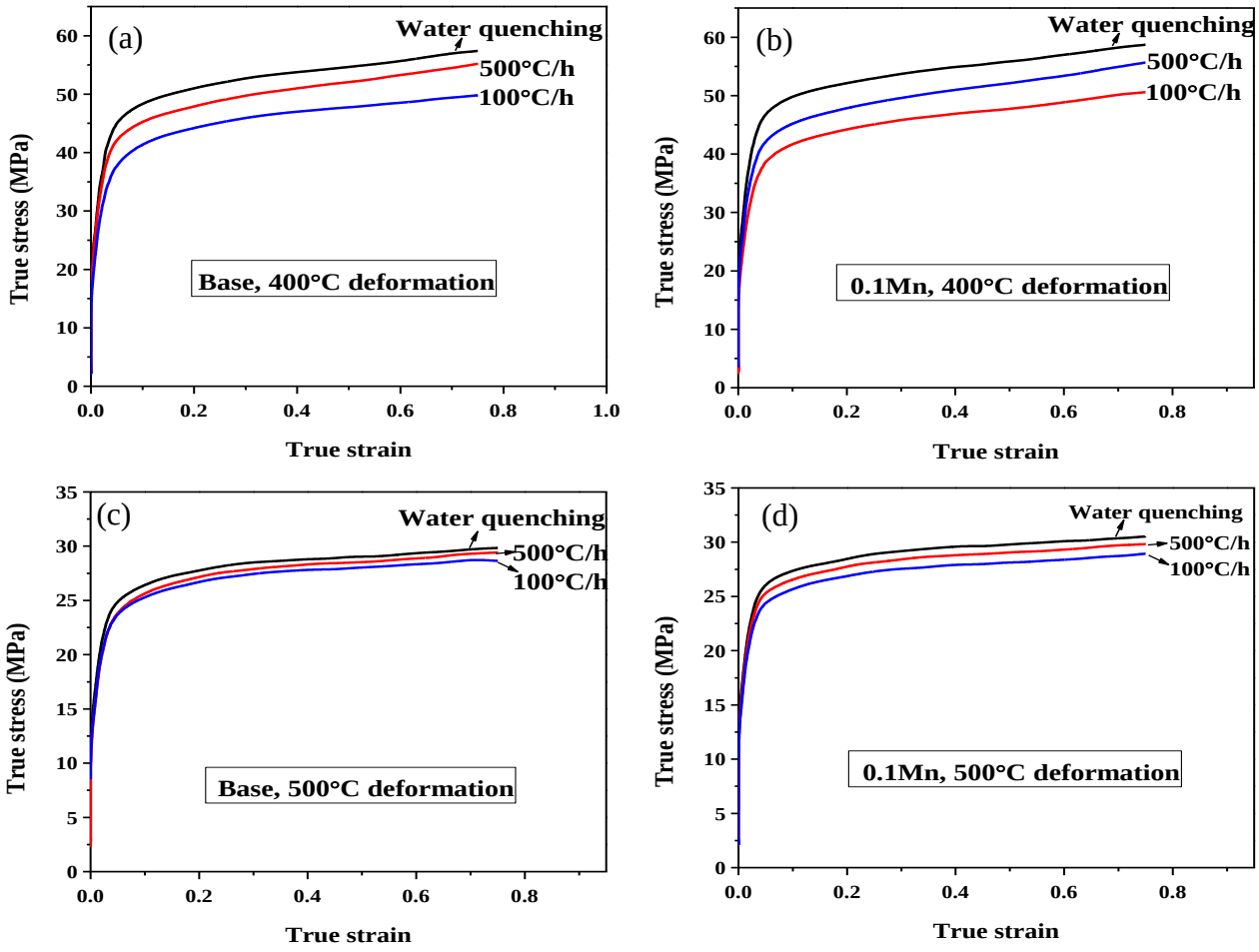

Fig.4. 9 True stress-true strain curves of the samples after 575 ℃ homogenization with 1 s^{-1} strain rate

To better compare the effect of the cooling rate and homogenization temperature on hot workability, the flow stress values at a strain of 0.75 are plotted in Fig. 4. 10. It is evident that the flow stress decreased with reduced cooling rate at deformation temperatures of 400 and 500 ℃. The trends with homogenization temperature and cooling rate are very similar for the two deformation temperatures. This suggests that although the higher temperature of 500 ℃ was above the Mg_2Si solvus of ~ 470 ℃,

the rapid heat to the test temperature and short soak before deformation was insufficient to dissolve the Mg_2Si particle distribution produced by homogenization. The water quenched samples gave the highest flow stress, while the samples with the lowest cooling rate of 100 ℃/h exhibited the lowest flow stress for both alloys. In addition, the flow stress of the base alloy showed low sensitivity to homogenization temperature (Figs. 4. 10a and 4. 10c), whereas in the case of the 0.1Mn alloy (Fig. 4. 10b, d) the flow stress increased moderately with increasing homogenization temperature. Changes in cooling rate resulted in different flow stress responses for the two alloys. For example, with an homogenization temperature of 545^{o}C and deformation at 400^{o}C, the increment in flow stress between water quenching and 100 ℃/h cooling was 6.9 MPa for the base alloy (Fig. 4. 10a), while for the 0.1Mn alloy, a larger decrease of 8.4MPa was observed (Fig. 4. 10b). The wider variation for the Mn containing alloy was probably due to enhanced Mg_2Si precipitation on Mn dispersoids at low cooling rates and increased Mn in solid solution for the water quenched condition. It is clear that overall the flow stress behavior showed a similar but reversed tendency with the electrical conductivity when the results between Fig. 4. 10 and Fig. 4. 8 are compared, suggesting that the high temperature flow stress was closely related to the solid solution levels [19].

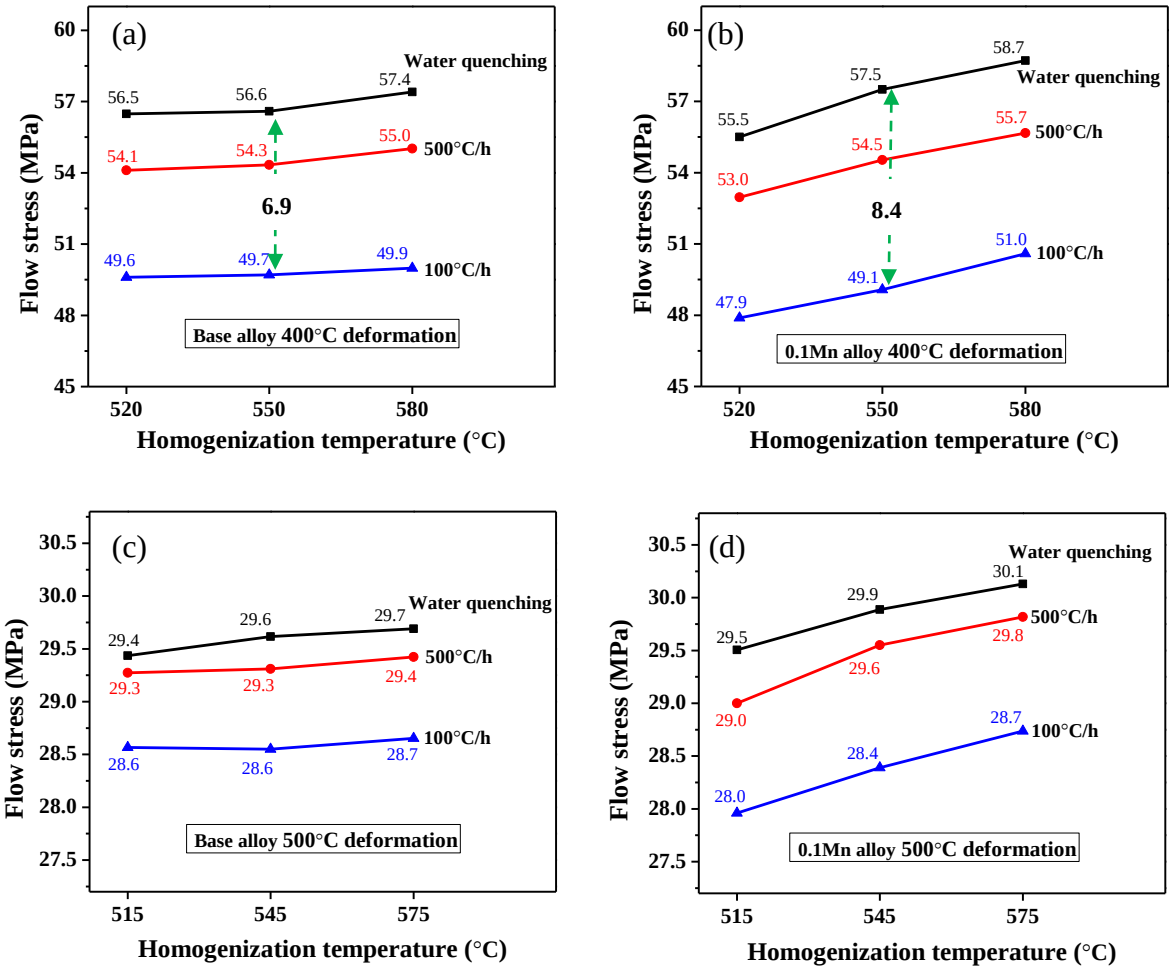

Fig.4. 10 Flow stresses at 0.75 strain of experimental alloys as a function of the cooling rate and homogenization temperature

4.4 Discussion

Two AA6060 aluminum alloys (base and 0.1Mn) were studied and the results revealed that the water quench samples retained nearly all of Mg and Si in solution, while the samples with post homogenization cooling rates of 500 and 100°C/h contained Mg_2Si precipitates formed during cooling. The extent of Mg_2Si precipitation varied with cooling rate resulting in changes to the Mg and Si solid

solution levels. In the case of the Mn containing alloy, the Mn solid solution level also varied with the homogenization temperature. It is reported that solute elements can significantly influence hot deformation behavior of aluminum alloys by hindering dislocation movement and creation of pile-ups [23, 24], which in turn leads a significant hardening and contributes to an increase in flow stress.[25, 26]. The flow stress behavior of the two alloys studied here is therefore related to variations in Mg and Si solid solution levels with cooling rate, variations in Mn in solid solution caused by changes in homogenization temperature and also interactions between Mn dispersoids and Mg_2Si precipitation.

4.1 Effect of the cooling rate and dispersoids on Mg_2Si precipitation and flow stress

In the present study, the cooling rate played a predominant role controlling the Mg and Si solid solution levels in the aluminum matrix and hence the flow stress. For both alloys water quenching after homogenization suppressed any Mg_2Si precipitation and resulted in the highest level of Mg and Si in solution and hence the highest flow stress. Cooling at the intermediate rate of 500 ℃/h promoted Mg_2Si precipitation (Fig. 4. 7), the solid solution level in the matrix decreased and the flow stress also correspondingly decreased (Fig. 4. 10). Decreasing the cooling rate to 100 ℃/h, resulted in increased Mg_2Si precipitation and a corresponding further decrease in flow stress (Fig. 4. 10) due to the even lower solid solution level in the matrix (Fig. 4. 7).

In the 0.1Mn alloy, α-Al(MnFe)Si dispersoids precipitated during homogenization (Fig. 4. 2b, c, d) and acted as nucleation sites for Mg_2Si formation during cooling. For the same cooling conditions (500 ℃/h or 100 ℃/h), the 0.1Mn alloy always produced a higher Mg_2Si particle number density and finer size compared to the base alloy free of dispersoids. The enhanced Mg_2Si precipitation in turn reduced the Mg and Si solid solution levels and further decreased the flow stress (Fig. 4. 10). However, with increasing homogenization temperature, the dispersoid number density decreased due to coarsening and dissolution (Fig. 4. 4), resulting in a corresponding decrease in the Mg_2Si number density and an increase in particle size (Fig. 4. 7b). This contributed to the flow stress increase with homogenization temperature for the Mn containing alloy (Fig. 4. 10b and d).

Comparison of the flow stress values for the Mn free and Mn containing alloys for both deformation temperatures in Fig. 4. 10 reveals a difference in behavior dependent on the homogenization temperature. At the lowest temperature (515 ℃) the Mn containing alloy gave a lower flow stress for all cooling rates whereas for homogenization at the highest temperature of 575 ℃ the Mn containing alloy always gave the highest flow stress. This can be rationalized in terms of the Mn dispersoid formation. At 515 ℃ a high density of dispersoids was produced giving a low level of Mn in solid solution and additionally the dispersoids promoted increased Mg_2Si precipitation compared to the base alloy giving low levels of Mg and Si in solution resulting in a lower flow stress. Conversely at 575 ℃ the Mn solid solution level

was higher resulting in a lower density of dispersoids such that for cooling rates of 500 and 100 ℃/hr the Mg_2Si particle density was only slightly higher than for the base alloy. In this situation the Mg and Si levels in solution were quite similar such that the Mn solid solution level dominated the flow stress behavior. This is reflected in the fact that after water quenching, where all the Mg and Si were held in solution, the flow stress of the Mn containing alloy was higher than the base alloy. For a homogenization temperature of 545 ℃ the comparative behavior of the two alloys was between these two extremes; after water quenching the flow stress was higher for the 0.1Mn alloy due to higher Mn in solution whereas after 100 ℃/h cooling the flow stress was lower for the Mn containing alloy indicating the decreased Mg and Si in solution due to heterogeneous precipitation on dispersoids reduced the flow stress compared to the base alloy. These results clearly indicate that the presence of the dispersoids resulting from a Mn addition to AA6060 can promote Mg_2Si precipitation during the cooling, and reduce the high temperature flow stress which is beneficial for extrudability. However, care has to be taken in selection of the homogenization temperature to prevent the Mn solid solution level dominating the flow stress response.

TEM investigation revealed a close nucleation and growth relationship between dispersoids and Mg_2Si during homogenization cooling (Fig. 4. 11). In the 0.1Mn alloy as indicated with the arrows, the Mg_2Si particles always precipitated on the pre-existing dispersoids. This phenomenon was observed at both cooling rates (Fig. 4. 11a and b for 100 ^{o}C/h and Fig. 4. 11c and d for 500 ^{o}C/h). During the

homogenization cooling, the driving force for the Mg_2Si precipitation is the supersaturation of Mg and Si in aluminum solid solution. Although the nature of the crystallographic relation between this type of dispersoid and Mg_2Si is still not well understood, the TEM finding provided the strong evidence that the pre-existing dispersoids could act as favorable nucleation sites for the subsequent precipitation of Mg_2Si. The greater the dispersoid density, for example from low temperature homogenization, the more Mg_2Si particles precipitated and the more uniform the distribution.

The multiple benefits of the nucleation effects between dispersoids and Mg_2Si have been known for many years, but the mechanisms are still not completely understood. The earlier literature [14] indicates that when Mg_2Si particles first form in the aluminum matrix during the heating stage of homogenization, the dispersoids can nucleate on the metastable Mg_2Si phase or its transition phase in Al-Si-Mg 6xxx alloys. It was also reported in Al-Mg-Si alloys that Mg_2Si provided an essential condition for the formation of α-Al(MnFe)Si dispersoids during heat treatment [27]. Recently, Li et al. [28] reported that α-Al(MnFe)Si dispersoids preferentially nucleated and grew in the original orientation of pre-existing β'-Mg_2Si during heating of 3xxx alloys. On other hand, Reiso [15] investigated the Mg_2Si precipitation in Al-Mg-Si alloy after extrusion with force air cooling. It was found that Mg_2Si precipitated preferentially on pre-existing AlFeSi dispersoids, and the amount of Mg_2Si increased with increasing number density of AlFeSi dispersoids.

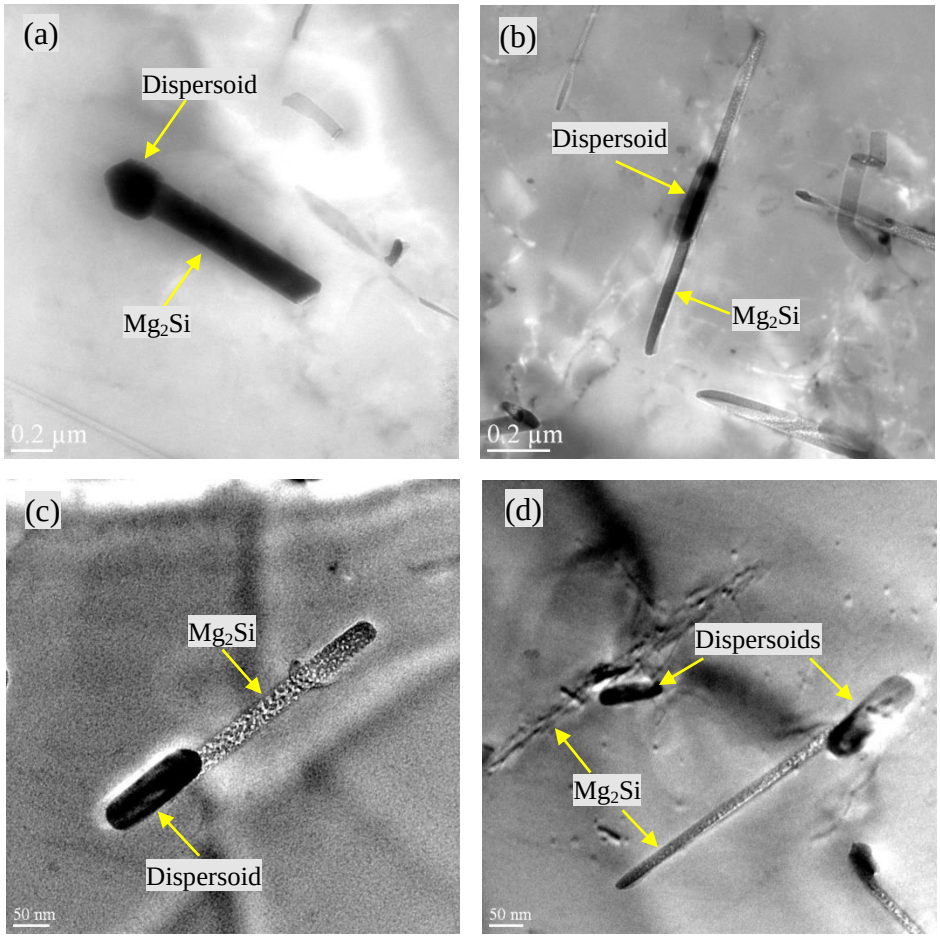

Fig.4. 11 TEM bright field images showing that Mg_2Si precipitated and grew on the pre-exiting dispersoids in the 0.1Mn alloy after homogenization at 515 ^{o}C with 100 ^{o}C/h cooling rate (a and b) and 500 ^{o}C/h cooling rate (c and d).

It should be mentioned that the presence of dispersoids and Mg_2Si particles under certain conditions could effectively pin dislocations, which in turn increases the flow stress during hot deformation if their number density is enough high and particle size is fine [23]. However, in the present work, the amount of both dispersoids and Mg_2Si was fairly low and the interparticle spacing of the dispersoids and Mg_2Si particles was too large (Figs. 4. 4 and 4. 7). Therefore, the effect of dispersoids and Mg_2Si particles

on high temperature flow stress can be almost neglected. For example, at the 400 ^{o}C deformation condition, the flow stress of the base alloy with 100 ^{o}C/h cooling rate was 49 MPa, while the flow stress of the 0.1Mn alloy that exhibited a reasonable amount of dispersoids and Mg_2Si was actually slightly lower(48 MPa).

4.5 Industrial aspect

In the direct hot extrusion process for aluminum alloys, DC cast and homogenized billets are preheated to a selected temperature and then loaded into the press and extruded to obtain the desired profile. Fig. 4. 12 shows the schematic extrusion pressure and temperature curves as the billet passes through the extrusion process [15]. The press force at extrusion breakthrough is a limiting factor for the process in terms of productivity as a given press can only provide a certain press force. The breakthrough force results from a combination of the billet container friction and the force required to push the billet through the die. As a result the press force is highest at the very start of extrusion when the billet length is the greatest. The lower the breakthrough pressure the higher the extrusion speed a given press can achieve and this also allows lower billet temperatures to be used with further gains in press productivity. Furthermore a lower flow stress results in a lower temperature rise during in extrusion which can effectively increase the extrusion speed at which surface defects are encountered. The work done during extrusion is mainly converted to heat which results in a temperature rise as the metal passes through the die as shown in Fig. 4. 12. Typically this is controlled such that the product reaches

a temperature above the Mg_2Si solvus. With the rapid diffusion rates encountered during hot deformation, the Mg_2Si particles in the billet can be dissolved and the extrusion process is used as a solution treatment step for the majority of 6XXX extrusion.

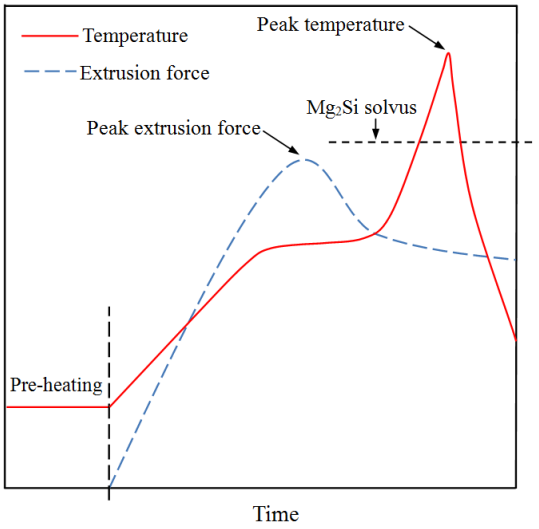

Fig.4. 12 A schematic of extrusion force and temperature curves during extrusion

The material flow stress clearly has a direct effect on the extrusion force, the force at breakthrough and corresponding extrusion productivity. Small differences of 1-2% can translate into significant improvements in extrusion speed. The present work has shown that the flow stress can be significantly reduced by slower post homogenization cooling rates to enhance Mg_2Si precipitation and reduce Mg and Si solid solution levels. This can be further enhanced with an addition of Mn combined with the correct choice of homogenization temperature. However, care has to be taken to avoid excessive Mn levels in solution which can counteract the effect. Although Mg_2Si particles are normally dissolved during extrusion due to the

temperature rise, the controlling breakthrough pressure occurs at the beginning of the cycle when the post homogenized Mg_2Si distribution is still substantially present. Obviously, care has to be taken not to produce a billet where the Mg_2Si particles are too coarse to be dissolved during the extrusion thermal cycle as this could result in a loss of mechanical properties.

The current study has also shown that the addition of 0.10wt% Mn can reduce the Mg_2Si particle size compared to a Mn free alloy over a wide range of homogenization temperatures (Fig. 4. 7). In combination with 100 ℃/hr cooling and homogenization at 515 ℃, the 0.1Mn addition produced a higher Mg_2Si particle number density and lower size (Fig. 4. 7b) than the base alloy resulting in a significantly lower flow stress (Fig. 4. 10). Using a homogenization temperature of 545^{o}C, and commercially achievable cooling rates of 100-500 ℃/hr, the flow stress for the 0.1Mn alloy was similar to that of the base alloy, but the Mg_2Si particle number density was higher and the particle was size finer than that for the base alloy. This should still be advantageous for Mg_2Si dissolution during extrusion. At the highest homogenization temperature (575^{o}C), the Mg_2Si number density in the 0.10Mn alloy decreased and the particle size increased due to coarsening and partial dissolution of dispersoids. Although the particles were still finer than in the base alloy, which is beneficial for Mg_2Si dissolution during extrusion, the flow stress was higher than the base alloy, due to the increased Mn in solid solution, which would be detrimental to extrudability.

4.6 Conclusions

(1) During post homogenization cooling of AA6060 alloys at commercially relevant rates, Mg_2Si particles precipitated in the aluminum matrix, and their number density and size had a significant effect on the solid solution level and high temperature flow stress.

(2) At lower post homogenization cooling rates, the flow stress decreased due to the precipitation of Mg_2Si and the reduction of solid solution levels. The lowest cooling rate tested (100 ^{o}C/h), produced the lowest flow stress corresponding to the maximum precipitation of Mg_2Si.

(3) Micro-alloying of 0.1% Mn in AA6060 alloys generated a reasonable number of α-Al(FeMn)Si dispersoids during homogenization. These acted as favorable nucleation sites for Mg_2Si and promoted the precipitation of Mg_2Si during post homogenization cooling, resulting in a higher number density and smaller size of Mg_2Si compared to the base alloy free of Mn.

(4) The benefits of the 0.10wt%Mn addition varied with the homogenization temperature applied, reflecting the relative effects on Mg, Si and Mn solid solution levels:

   a) At 515 ℃ the flow stress was reduced compared to the base alloy and the Mg_2Si particle size was reduced

   b) At 545 ℃ the flow stress was similar to the base alloy but the Mg_2Si particles size was still reduced

   c) At 575 ℃ the flow stress was increased due to the Mn solid solution level but

the Mg_2Si particle size was still finer than the base alloy.

References

[1] J.R. Davis, Aluminum and Aluminum Alloys, ASM International, Materials Park, OH (1993)59-87.

[2] J.G. Kaufman, Introduction to Aluminum Alloys and Tempers, ASM International, Materials Park, OH (2000) 87-118.

[3] L. Aydi, M. Khlif, C. Bradai, S. Spigarelli, M. Cabibbo, M. El Mehtedi, Mechanical properties and microstructure of primary and secondary AA6063 aluminum alloy after extrusion and T5 heat treatment, Materials Today, Proceedings 2 (2015) 4890 – 4897

[4] E.B. Bjornbakk, The influence of homogenization cooling rate, billet preheating temperature and die geometry on the T5-properties for three 6xxx alloys extruded under industrial conditions, Materials Science Forum 396-402 (2002) 405-410

[5] N. Dahl, T. Johnsen, B.R. Henriksen, E.K. Jensen. Precipitation of Mg_2Si in Al–Mg–Si-alloys during cooling from homogenization temperature, Proceedings of 6th International Aluminum Extrusion Technology Seminar 1 (1996) 529-535.

[6] J. Langerweger, Effect of metallurgical factors on productivity in the extrusion of aluminum–magnesium–silicon (AlMgSi) alloys, Aluminum 58 (1982) 107-109.

[7] J. van de Langkruis, The effect of thermal treatments on the extrusion behaviour of AlMgSi alloys, Ph.D. Thesis, Delft University of Technology (2000) 61-84.

[8] Y. Birol, The effect of homogenization practice on the microstructure of AA6063

billets, J. Mater. Process. Technol. 148 (2004) 250-258.

[9] N.C.W. Kuijpers, F.J. Vermolen, K.Vuik and S. van der Zwaag, A Model of the β-AlFeSi to α-Al(FeMn)Si Transformation in Al-Mg-Si Alloys, Materials Transactions, 44, 7 (2003) 1448-1456

[10] K.C. Prince, J.W. Martin, The effects of dispersoids upon the micromechanisms of crack propagation in AlMgSi alloys, Acta Metall. 27 (1979) 1401-1408.

[11] D.H. Lee, J.H. Park, S.W. Nam, Enhancement mechanical properties of Al-Mg-Si alloys by means of manganese dispersoids, Mater. Sci. Technol 15 (1999) 450-455.

[12] Z. Li, Z. Zhang, X-G. Chen, Effect of magnesium on dispersoid strengthening of Al−Mn−Mg−Si (3xxx) alloys, Trans. Nonferrous Met. Soc. China 26 (2016) 2793-2799.

[13] C. liu, Microstructure evolution during homogenization and its effect on the high temperature deformation behaviour in AA6082 based alloys, Phd thesis, The university of British Columbia (2017) 93.

[14] L. Lodgaard, Nils Ryum, Precipitation of dispersoids containing Mn and/or Cr in Al–Mg–Si alloys, Materials Science and Engineering A283 (2000) 144–152

[15] O. Reiso, Extrusion of AlMgSi alloys, Mater. Forum 28 (2004) 32-46.

[16] Y. Birol, The effect of homogenization practice on the microstructure of AA6063 billets, Journal of Materials Processing Technology 148 (2004) 250–258

[17] Y. Birol, Effect of homogenisation cooling rate and press exit temperature on extrudability and T5 hardness of EN AW 6082 alloy, Materials Science and Technology, 29,12 (2013) 1518-1521

[18] Y. Birol, Effect of cooling rate on precipitation during homogenization cooling in an excess silicon AlMgSi alloy, Materials Characterization 73 (2012) 37–42

[19] M. V. Kral, H.R. McIntyre, M.J. Smillie, Identification of intermetallic phases in a eutectic Al-Si casting alloy using electron backscatter diffraction pattern analysis, Scripta Materialia 51 (2004) 215-219.

[20] H. Tezuka, A. Kamio, L. Arnberg (Ed.), Aluminum Alloys: Their Physical and Mechanical Properties, Proceedings of the 3rd International conference (1992) 117-122.

[21] C. Shi, X.-G. Chen, Effect of vanadium on hot deformation and microstructural evolution of 7150 aluminum alloy, Materials Science and Engineering A 613 (2014) 91–102

[22] H.J. Mc Queen, S. Spigarelli, M. E. Kassner, E. Evagelista, Hot deformation and processing of aluminum alloys, CRC Press, Florida, (2011) 14-16,143-190.

[23] Q. hao, M. lagsvold and B. olmedal, Comparison of the influence of Si and Fe in 99.999% purity aluminum and in commercial-purity aluminum, Scripta Materialia, 67 (2012) 217-220.

[24] O. D. Sherby, A. Goldberg, O.A. Ruano, Solute-diffusion-controlled dislocation creep in pure aluminium containing 0.026 at.% Fe, Philosophical Magazine, 84, 23, (2004) 2417–2434

[25] O.D. Sherby, O.A. Ruano, Rate-controlling processes in creep of subgrain containing aluminum materials, Materials Science and Engineering A 410–411 (2005) 8–11

[26] Z. Li, Z. Zhang, X.-G. Chen, Microstructure, elevated-temperature mechanical properties and creep resistance of dispersoid-strengthened Al-Mn-Mg 3xxx alloys with varying Mg and Si contents, Materials Science & Engineering A 708 (2017) 383–394

[27] R. Hu, T. Ogura, H. Tezuka, T. Sato and Q. Liu, Dispersoid Formation and Recrystallization Behavior in an Al-Mg-Si-Mn Alloy, J. Mater. Sci. 26, 3, (2010) 237-243

[28] Z. Li, Z. Zhang, X.-G. Chen, Microstructure, elevated-temperature mechanical properties and creep resistance of dispersoid-strengthened Al-Mn-Mg 3xxx alloys with varying Mg and Si contents, Materials Science & Engineering A 708 (2017) 383–394

Chapter 5 Effect of Mn addition and its related Mn-containing dispersoids on the hot deformation behavior of 6082 aluminum alloys

Abstract

The hot deformation behaviors of 6082 aluminum alloys containing different Mn contents (0.05–1.0 wt%) were systematically investigated by uniaxial compression tests in a temperature range of 400–550 ℃ and strain rate range of 0.001–1 s^{-1}. Prior to the hot deformation, a low-temperature homogenization (450 ℃ for 6 h) was carried out on direct-chill cast billets to promote the precipitation of Mn-containing dispersoids. The large numbers of dispersoids in the Mn-containing alloys yielded significantly increased high-temperature flow stresses, compared to that of the base alloy without dispersoids. The material constants and activation energies for hot deformation were determined using the hyperbolic-sine constitutive equation and experimental peak flow stress data. The activation energy increased from 191 kJ/mol for the base alloy to 286 kJ/mol for the alloy with 0.5% of Mn. With further increase in Mn content, the activation energy increased only moderately to 315 kJ/mol for the alloy with 1.0% of Mn. The influences of the Mn content and deformation conditions on the dynamic recovery and recrystallization were quantitatively analyzed. The precipitation of dispersoids in the Mn-containing alloys promoted the retardation of the dynamic recovery and inhibition of the recrystallization owing to their strong pinning effect on the dislocation movement and subgrain migration.

Keywords: 6082 aluminum alloy, Mn addition, Dispersoids, Hot deformation, Activation energy, Dynamic recovery and recrystallization

5.1. Introduction

In recent years, driven by the automotive and aerospace industries, the demand for aluminum alloys operating at elevated temperatures has increased. Dispersoid strengthening is one of the most important hardening mechanisms in aluminum alloys for elevated temperature applications, which has led to an increasing academic and industrial interest for the development of dispersoid-strengthened aluminum alloys [1–4]. Recent studies have demonstrated that the addition of Mn or its combinations with other transition elements can introduce a high number of thermally stable nano-sized dispersoids, such as α-Al(MnFe)Si in 3xxx alloys [2,5,6], Al_6(MnFe) in 5xxx [7,8], and α-Al(MnFe)Si in Al–Si foundry alloys [3,9,10], providing remarkable increases in strengths at room temperature and particularly at elevated temperatures. For Al–Mg–Si 6xxx alloys, Mn is an important alloying element to increase the strength and control the grain structure [11]. Among the other 6xxx alloys, the 6082 alloys have a high potential for the formation of dispersoids owing to their high contents of Mn and Si, which are supersaturated in the as-cast state and follow the decomposition of the supersaturated solid solution during the heat treatment to precipitate a considerable number of dispersoids [12,13]. The addition of Mn in 6082 alloys could significantly enhance the precipitation of α-Al(MnFe)Si dispersoids

during the homogenization [13,14]. In a recent study by Li [15], it is found that α-Al(FeMn)Si dispersoids in 6082 alloys started to precipitate at 350 ℃ and reached the highest number density at 400–450 ℃. At temperatures higher than 500 ℃, the dispersoids coarsened and the number density sharply decreased with time.

The production of aluminum wrought alloys involves many steps, starting mainly with direct chill (DC) casting of billets/ingots and processing with a homogenization heat treatment, followed by hot deformation processes, such as extrusion, rolling, or forging. The high-temperature flow stress is one of the most significant factors for the hot deformation regime owing to its substantial impacts on the required deformation load and kinetics of the metallurgical transformation [16]. The high-temperature flow stress was closely related to the alloy chemistry, homogenization heat treatment history, and microstructure [14,16,17]. In general, Al–Mg–Si 6082 alloys prior to the hot deformation are subjected to a high-temperature homogenization treatment (550–580 ℃) [14], where dispersoids could precipitate during the heating. The sizes and number density of the dispersoids have an important role in determining the high-temperature flow stress, retardation of the dynamic recovery (DRV), and inhibition of the recrystallization. However, after such high-temperature homogenization treatments, the Mn-containing dispersoids in the 6082 alloys were coarsened and dissolved, leaving a limited number of dispersoids in the aluminum matrix [12–14]. Several studies have been carried out to investigate the effects of Zr and V and related dispersoids on the flow stress behavior and inhibition of the dynamic recrystallization (DRX) in 7xxx alloys [18–20]. However, a systematic

investigation of the effects of Mn and related Mn-containing dispersoids on the hot deformation behaviors and deformed microstructures of Al–Mg–Si 6xxx alloys has not been carried out.

Different types of constitutive equations have been applied to analyze and predict the hot deformation behaviors of aluminum alloys. Among the many equations and models, the hyperbolic-sine Arrhenius-type equation proposed by Sellars and McTegart [21] is widely used for the constitutive analysis over wide ranges of temperature and strain rate. Using this constitutive equation, the activation energy, *Q*, for hot deformation could be derived based on a series of flow stress data. The *Q* values were often used to compare the difficulty degrees of plastic deformation of different aluminum alloys [19,20,22]. Recent studies demonstrated that *Q* of an alloy was not constant, but might vary with deformation conditions (mainly temperature and strain rate) [23–25]. The changes in hot deformation flow stress and activation energy are closely related to the balance between the dynamic work hardening and dynamic softening under a specific hot deformation condition [19]. DRV and DRX are the main softening mechanisms during the deformation at a high temperature [26–28]. The DRV is associated with changes in density and distribution of line defects, while DRX occurs through a progressive transformation of subgrains to newly formed grains as well as grain boundary migration [19,20]. The effects of Zr-containing dispersoids (Al_3Zr) and V-containing dispersoids ($Al_{11}V$) on the DRV and DRX in 7xxx alloys have been thoroughly studied [18–20]. The softening mechanism of 7050 alloys shifted from DRV to DRX with a decrease in Zener–Hollomon parameter (*Z*)

[19,29]. However, the influences of Mn-containing dispersoids (α-Al(MnFe)Si) on the deformed microstructures of 6xxx alloys owing to the DRV and DRX are still not well understood.

In this study, we focused on the effects of Mn and related Mn-containing dispersoids on the hot deformation behavior of 6082 aluminum alloy. In contrast to the usual high-temperature homogenization, a low-temperature homogenization at 450 ℃ for 6 h was applied to DC cast billets to promote the maximum precipitation of Mn-containing dispersoids prior to the hot deformation. The influences of different Mn contents (0.05–1.0 wt%) on the high-temperature flow stresses as a function of the deformation temperature and strain rate were studied. Using the hyperbolic-sine constitutive equation, the material constants and activation energies for hot deformation were calculated based on flow stress data. The microstructural evolution of the alloy during the hot deformation was investigated to understand the effects of the dispersoids on the DRV and DRX.

5.2. Experimental

Experiments were carried out on four 6082 alloys without and with different Mn contents of 0.5–1.0% (denoted as the base, 0.5Mn, 0.75Mn, and 1Mn alloys). The materials were obtained from DC cast billets with diameters of 101 mm, provided by the Arvida Research and Development Center of Rio Tinto in Saguenay, Quebec. The chemical compositions of the alloys analyzed by optical emission spectroscopy are presented in Table 5. 1. To promote the precipitation of a large number of dispersoids,

homogenization at a relatively low temperature of 450 ℃ for 6 h at a heating rate of 100 ℃/h, followed by water quenching at room temperature, were applied to the DC cast billets prior to the hot deformation, aiming to evaluate mainly the dispersoid effects on the hot deformation behaviors of the 6082 alloys.

Table 5.1 Chemical compositions (wt.%) of the experimental alloys.

Alloy	Mg	Si	Fe	Mn	Al
Base	0.79	1	0.18	**0.05**	Bal.
0.5Mn	0.83	1.01	0.22	**0.50**	Bal.
0.75Mn	0.84	1.02	0.23	**0.72**	Bal.
1Mn	0.81	1.02	0.24	**0.99**	Bal.

After the homogenization, cylindrical specimens having diameters of 10 mm and lengths of 15 mm were machined for uniaxial hot compression tests, performed in a Gleeble 3800 thermomechanical testing unit. The specimens were heated at a rate of 2 ℃/s to the desired temperature and held for 180 s to ensure a homogeneous temperature distribution. The deformation temperatures were 400, 450, 500, and 550 ℃, while the strain rates were 1, 0.1, 0.01, and 0.001 s^{-1}. The specimens were deformed to a total true strain of 0.75 and then immediately water-quenched to retain the deformed microstructures at the specific temperature and strain rate.

To analyze the microstructures of the as-homogenized materials, the polished samples were etched with a 0.5% HF solution for 40 s and investigated using optical microscopy (Nikon, Eclipse ME600) and scanning electron microscopy (SEM,

JEOL-6480LV). All deformed samples were sectioned parallel to the compression axis along the centerline and metallographically prepared. An electron back-scattered diffraction (EBSD) analysis was carried out in the SEM to investigate the grain structures under different deformation conditions. In the EBSD image analysis, the boundaries of grains and subgrains were defined as low-, medium-, and high-angle boundaries with misorientation angles of 2–5°, 6–15°, and larger than 15°, respectively. Misorientation angles below 2° were not considered to avoid the noises caused by the sample surface and polishing conditions. The step size of the EBSD analysis was set to 0.5 μm. Bisides, the subgrain size of the deformed samples was measured using the line intercept method [20, 22], the subgrian was defined as the grians separated by the low- and medium-angle boundaries. To ensure the statical reliability, more than 100 subgrains were measured in each deformed sample, EBSD step size was set to 0.2 μm. To observe the Mn-containing dispersoids in detail, transmission electron microscopy (TEM, JEM−2100) operated at 200 kV was employed. TEM thin foils were prepared by a twin-jet polishing unit using a solution of 30% nitric acid and 70% methanol at 15 V and - 20 ℃.

5.3. Results

5.3.1. Microstructure after heat treatment

The microstructures of the base and 0.75Mn alloys after the heat treatment at 450 ℃ for 6 h are shown in Fig. 5. 1. The microstructures were composed of aluminum dendrite cells (Al matrix), Fe-rich intermetallics (white) distributed along

the dendrite boundaries, and primary Mg_2Si particles (black) mostly colocated with the Fe-rich intermetallics. The intermetallics exhibited a plate-like morphology (β-AlFeSi, Fig. 5. 1a) in the base alloy and Chinese-script-like morphology (α-Al(FeMn)Si, Fig. 5. 1b) in the 0.75Mn alloy. As the microstructures of the three Mn-containing alloys (0.5Mn, 0.75Mn, and 1Mn) after the heat treatment were similar, only the typical microstructure of the 0.75Mn alloy is presented.

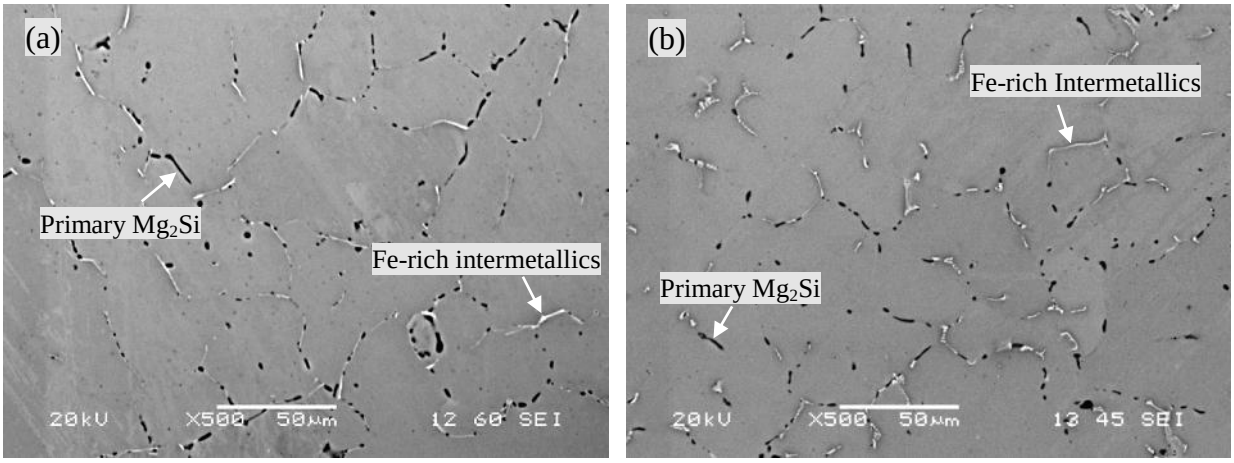

Fig. 5.1 Microstructures of the base (a) and 0.75Mn (b) alloys after heat treatment of 450 ℃ for 6h.

After the etching with the 0.5% HF, the dispersoids can be clearly revealed in the three Mn-containing alloys (Fig. 5. 2). In the base alloy, no change in the aluminum matrix was observed, indicating the absence of dispersoid formation (Fig. 5. 2a). On the contrary, dispersoid zones emerged inside the aluminum dendrite cells and large numbers of dispersoids precipitated in the three Mn-containing alloys (as an example, the 0.75Mn alloy is shown in Fig. 5. 2b and c). However, in the interdendritic regions containing the Fe-rich intermetallics and primary Mg_2Si, almost no dispersoids were

observed (Fig. 5. 2c), which are thus defined as particle-free zones (PFZs).

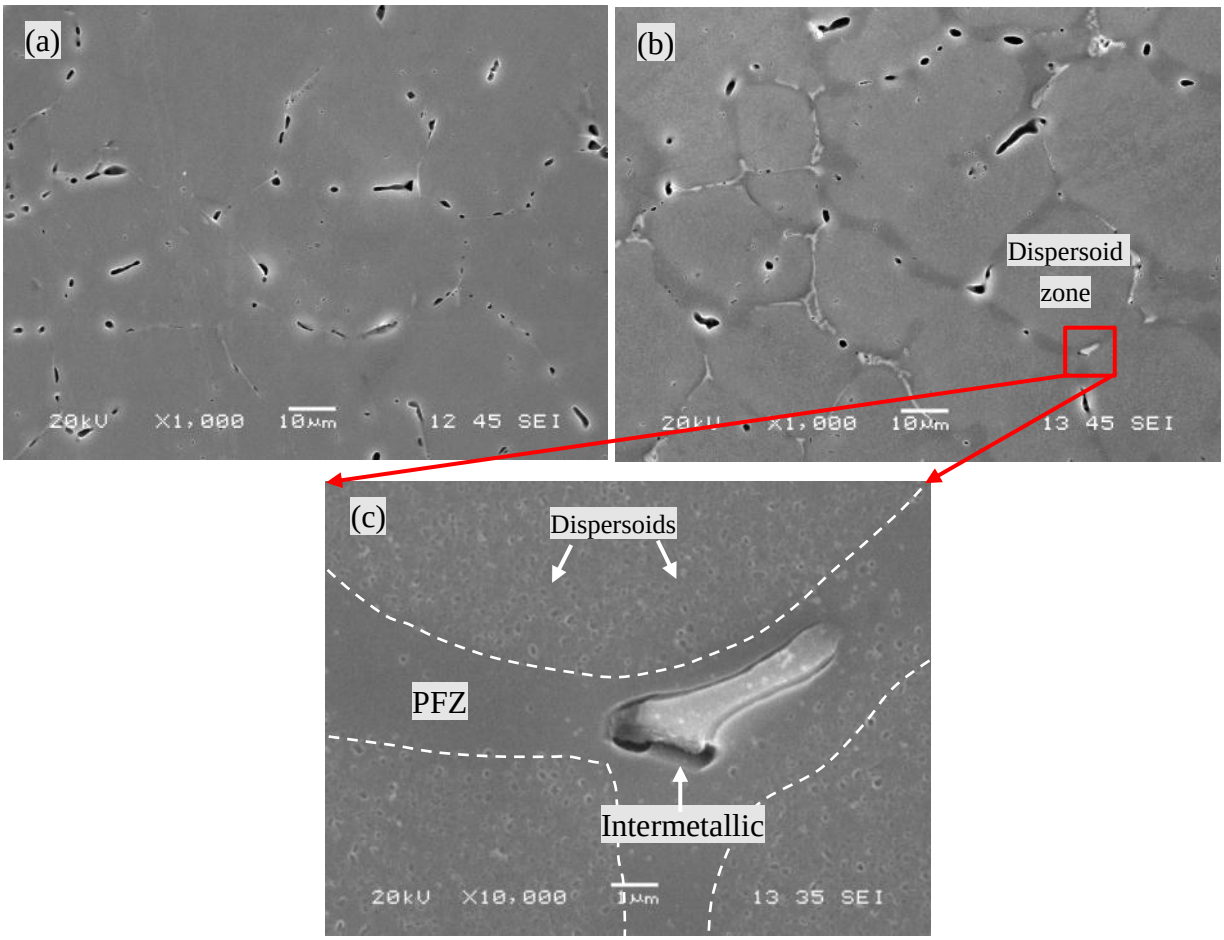

Fig. 5.2 Microstructures after heat treatment and etched with 0.5% HF for 40 s: the base alloy showing no evidence of dispersoids (a), the 0.75Mn alloy with large dispersoid zones (b) and the enlarged image from Fig. 5.2b showing dispersoids and PFZ (c).

The dispersoids in the dispersoid zones in the three Mn-containing alloys were analyzed in detail using SEM at a high magnification (Fig. 5. 3). Large numbers of fine dispersoids were uniformly distributed in the aluminum matrices of 0.5Mn,

0.75Mn, and 1Mn (Fig. 5. 3a–c, respectively). Fig. 5. 3d shows a TEM image of typical dispersoids in the 0.75Mn alloy. The dispersoids appeared in various shapes, mostly short plates and rods, which can be attributed to the projection of the plate-like morphology into the two-dimensional image. The dispersoids were confirmed to be α-Al(MnFe)Si, according to the TEM–energy dispersive X-ray spectroscopy (EDXS) results (Fig. 5. 3e) and previously reported data [12,15,30]. Fig. 5. 4 shows the evolution of the number density and equivalent diameter of the dispersoid particles, obtained by the image analysis on a series of SEM images. The number density of the dispersoids increased with the Mn content from 9.7 μm^{-2} in the 0.5Mn alloy to 11.5 and 17.2 μm^{-2} in the 0.75Mn and 1Mn alloys, respectively. The mean equivalent diameters of the dispersoids in the three alloys were almost equal (~85 nm).

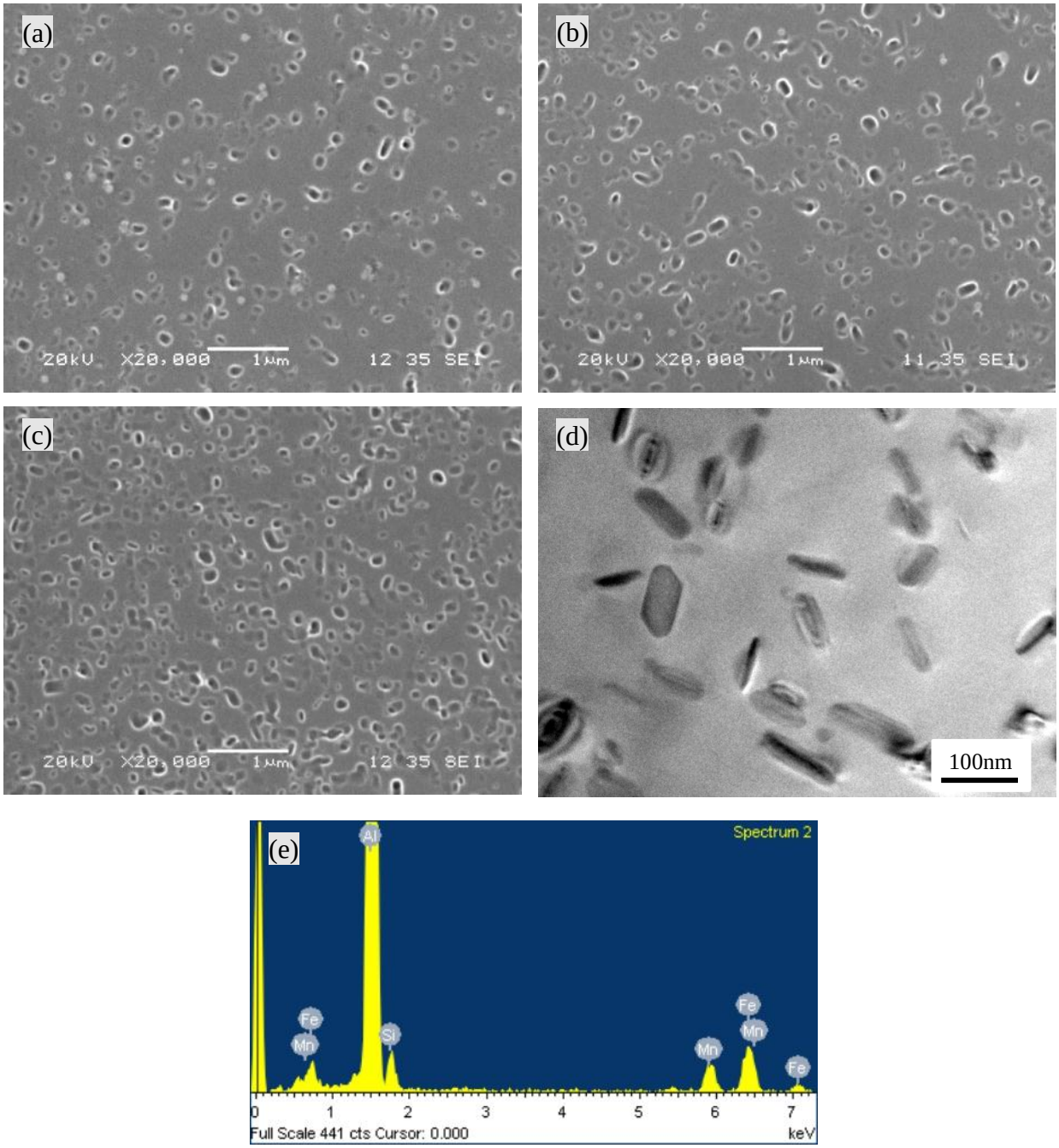

Fig. 5.3 SEM micrographs of etched samples of the 0.5Mn alloy (a), 0.75Mn alloy (b) and 1Mn alloy (c), TEM micrograph of the 0.75Mn alloy (d) and TEM-EDX results of dispersoids in the 0.75Mn alloy (e).

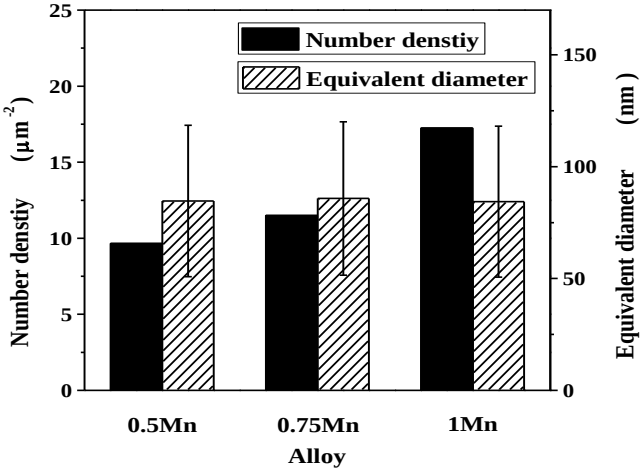

Fig. 5.4 Number density and equivalent diameter of dispersoids in the different alloys after heat treatment of 450 ^{o}C for 6 h.

5.3.2. High temperature flow stress behavior

High-temperature compression tests were performed at various deformation temperatures (400 to 550 ℃) and strain rates (1 to 0.001 s^{-1}). Fig. 5. 5 shows a series of typical true stress–true strain curves obtained under various hot deformation conditions for the four alloys. In general, the flow stress increased sharply at the beginning of the hot deformation reaching the peak value. Depending on the deformation conditions, the flow stress after the peak exhibited three types of trend, a) continuous but slow increase mostly under a high-*Z* (*Z* is the Zener–Hollomon parameter [21]) deformation condition (e.g., at 400 ℃ and 1 s^{-1}), b) fairly stable (e.g., at 450 ℃ and 0.1 s^{-1}), and c) continuous decrease until the end of the deformation at a relatively low *Z* deformation condition, which is more evident starting from 500 ℃ and 0.01 s^{-1} toward the high deformation temperature and low strain rate in the three

Mn-containing alloys (Fig. 5. 5b–d). The different trends of the flow stress curves indicated the various balances of the work hardening and dynamic softening during the hot deformation [16,31].

As shown in Fig. 5. 5, a general tendency was observed, i.e., the flow stress increased with the decrease in deformation temperature and increase in strain rate for all four alloys. On the other hand, the Mn addition led to a significant increase in flow stress.

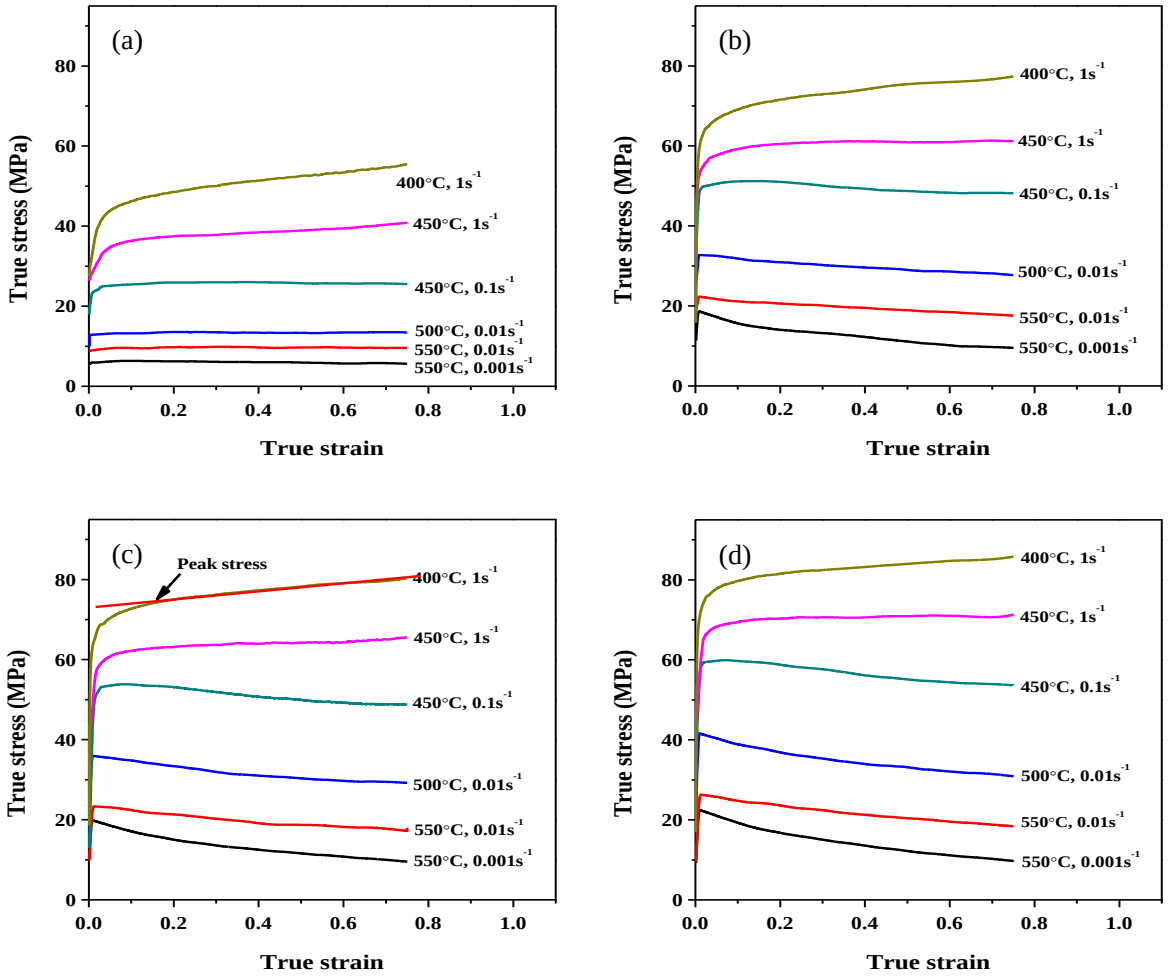

Fig. 5.5 Typical true stress–true strain curves during hot compression deformation, the base alloy (a); 0.5Mn alloy (b), 0.75Mn alloy (c) and 1Mn alloy (d).

For comparison of the flow stresses of the four alloys, the peak flow stresses were chosen to demonstrate the relationship between the Mn addition and flow stress. For the flow stress, which continuously increased during the hot deformation (e.g., at 400 ℃ and 1 s^{-1}), the peak stress was identified as the tangent point on the flow curve by the extension of the line along the steady-state flow stress (outlined by the arrow and line in Fig. 5. 5c) [24]. The peak flow stresses of the four alloys are plotted in Fig. 5. 6 as functions of the deformation temperature and strain rate. Under given deformation condition, the flow stress significantly increased with the increase in Mn content to 0.5%. With the further increase in Mn content to 0.75 and 1%, the flow stress exhibited a moderate increase. For example, under identical deformation conditions (400 ℃ and 0.01 s^{-1}, Fig. 5. 6a), the flow stress increased from 26 MPa for the base alloy to 51 MPa for the 0.5Mn alloy, an increase almost by a factor of two. With the further increase in Mn content, the flow stress moderately increased to 55 MPa for 0.75Mn and 63 MPa for 1Mn. Compared to that of the base alloy, the flow stresses of the three Mn-containing alloys are considerably higher, indicating the enhanced deformation resistance after the dispersoid formation. The increased flow stress with the increase in Mn content is consistent with the increased number density of the dispersoids in the alloy (Fig. 5. 4).

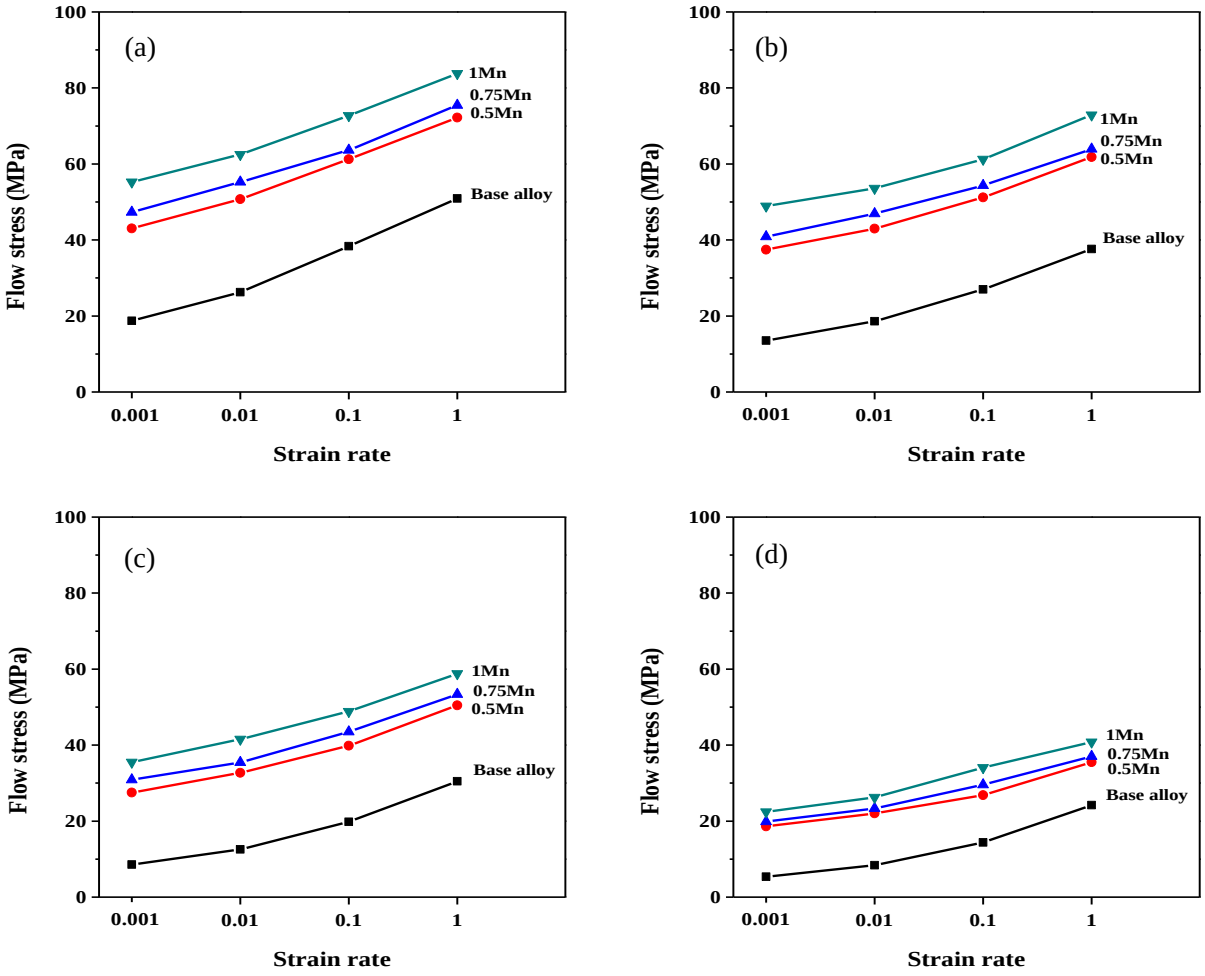

Fig. 5.6 Typical flow stresses of four experimental alloys at the hot deformation temperature of 400 ℃ (a), 450 ℃ (b), 500 ℃ (c) and 550 ℃ (d) as a function of the strain rate.

5.3.3. Constitutive analyses

The hyperbolic-sine equation, proposed by Sellars and Mc Tegart [21], is widely used to demonstrate the relationship between the strain rate, deformation temperature, and flow stress, particularly over a wide range of stresses:

$$Z = \dot{\varepsilon}\exp\left(\frac{Q}{RT}\right) = A[\sinh(\alpha\sigma)]^n \quad (1)$$

where Z is the Zener–Hollomon parameter, $\dot{\varepsilon}$ is the deformation strain rate, n and A are material constants, α is the stress multiplier, σ is the flow stress (MPa), Q is the activation energy for hot deformation (kJ/mol), R is the universal gas constant (8.314 J/mol K), and T is the deformation temperature (K). The experimental flow stress data for the 0.75Mn alloy were used as an example to derive the activation energy Q and material constants. The flow stress, σ, was obtained using the peak stress. The stress multiplier, α, was defined as $\alpha = \beta/n_1$, where β and n_1 were evaluated using the mean slopes of the plots of $\ln\dot{\varepsilon}$–σ and $\ln\dot{\varepsilon}$–$\ln\sigma$, respectively, for the range of experimental deformation temperatures. The mean values of β and n_1 were determined using the results in Fig. 5. 7, while α of 0.75Mn was calculated to be 0.023 MPa^{-1}.

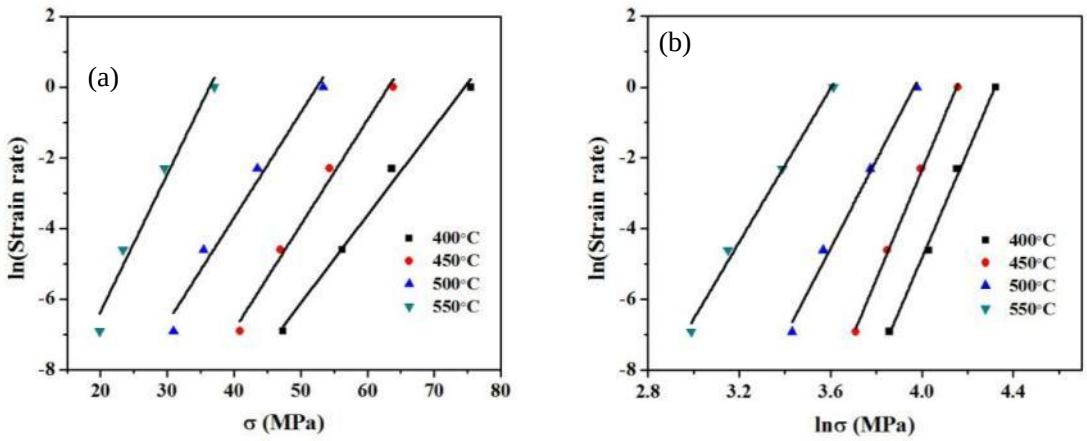

Fig. 5.7 Relationships between (a) lnε and σ and (b) lnε and lnσ.

Differentiating Eq. (1) yields the following:

$$Q = R\left[\frac{\partial \ln \dot{\varepsilon}}{\partial \ln[\sinh \alpha\sigma_p]}\right]_T \left[\frac{\partial \ln[\sinh \alpha\sigma]}{\partial(1/T)}\right]_{\dot{\varepsilon}} = RnS, \quad (2)$$

where n is the mean slope of the plots of $\ln\dot{\varepsilon}$–$\ln[\sinh(\alpha\sigma)]$ at various temperatures and S is the mean slope of the plots of $\ln[\sinh(\alpha\sigma)]$–$1/T$ at different strain rates. The

relationship between ln$\dot{\varepsilon}$ and ln[sinh($\alpha\sigma$)], derived using the measured flow stresses (Fig. 5. 6), was calculated (Fig. 5. 8a). The mean value of the slopes at the four different deformation temperatures, *n*, was then calculated to be 9.85. In addition, the relationship of ln[sinh($\alpha\sigma$)]–1/*T* is plotted in Fig. 5. 8b. The mean slope *S* at various strain rates was 3.77. The activation energy *Q* could be then calculated by Eq. (2), yielding a value of 308.7 kJ/mol for 0.75Mn alloy.

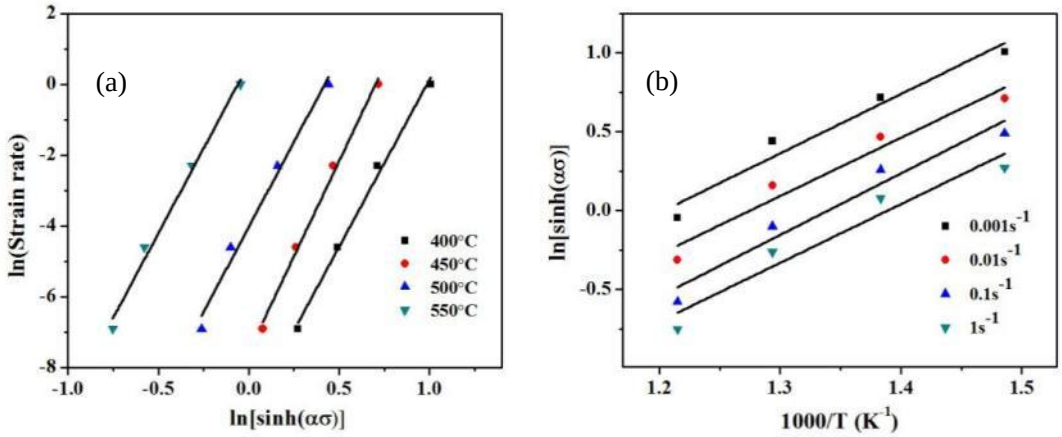

Fig. 5.8 Relationships between (a) lnε̇ and ln[sinh(ασ)] and (b) ln[sinh(ασ)] and 1000/T.

The application of natural logarithm on both sides of Eq. (1) yields,

$$\ln Z = \ln A + n \ln[\sinh(\alpha\sigma)] \quad (3)$$

where ln(A) is obtained as the intercept of the plot of lnZ-ln[sinh(ασ)], as shown in Fig. 5. 9.

In a similar manner, the material constants *A*, *n*, and α and activation energies *Q* were calculated according to Eqs. 1–3 for all studied alloys, as shown in Table 5. 2.

With the increase in Mn content, α decreased whereas n, A, and Q increased. Compared to that of the base alloy (191.2 kJ/mol), the 0.5Mn alloy exhibited a significantly increased Q (285.6 kJ/mol) value. With the further increase in Mn content, the 0.75Mn and 1Mn alloys exhibited moderately increased Q values of 301.2 and 315.4 kJ/mol, respectively.

Among the material constants, the activation energy for hot deformation Q is an important indicator of the difficulty degree of plastic deformation. Q of the base alloy (191 kJ/mol) is generally in agreement with the value reported for a similar alloy (185 kJ/mol) [32]. However, it is considerably higher than those of pure aluminum (145 kJ/mol) [16] and dilute Al–Fe–Si alloy (161 kJ/mol) [21], owing to the pinning effect of the high amount of intermetallics and high solute alloying element contents in the aluminum matrix on dislocation glides. Q of a 6082 alloy having a similar chemistry to that of the base alloy but under the full-solution-treated condition was 269 kJ/mol [33]. The large difference is most likely attributed to the high solid solution levels of alloying elements (particularly Mg and Si) in the aluminum matrix provided by the full solution treatment, while most Mg and Si were still bonded in the primary Mg_2Si in the base alloy in this study because of the low homogenization temperature of 450 ℃. The three Mn-containing alloys (0.5Mn, 0.75Mn, and 1Mn) exhibited significant increases in activation energy, indicating a very strong effect of the large number of dispersoids on the dislocation movement and hence on the deformation resistance during the hot working. Distinct increases in Q and corresponding resistance of hot deformation owing to the Zr- and V-containing dispersoids in 7150

aluminum alloys were also reported in [19,20].

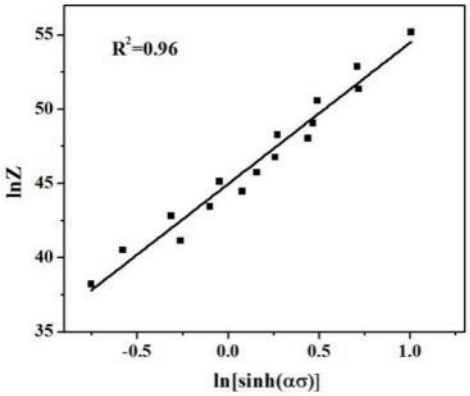

Fig. 5.9 Relationship between lnZ and ln[sinh(ασ)].

Table 5.2 Values of material constants and activation energies of four alloys studied.

Alloy	α (MPa^{-1})	n	A (s^{-1})	Q (kJ/mol)
Base alloy	0.054	4.27	2.54E+11	191.2
0.5Mn alloy	0.025	8.98	8.72E+17	285.6
0.75Mn alloy	0.023	10.04	9.34E+18	301.2
1Mn alloy	0.021	10.40	7.29E+19	315.4

5.3.4. Microstructural evolution during hot deformation

The EBSD technique was used to investigate the grain and subgrain structures after the hot deformation. Three typical deformation conditions, 400 ℃/0.1 s^{-1}, 500 ℃/0.01 s^{-1}, and 550 ℃/0.001 s^{-1}, were selected representing the high-, medium-, and low-*Z* conditions, respectively. Fig. 5. 10 shows all Euler orientation maps of the deformed samples of the four alloys under the three deformation conditions. In addition, the misorientation angle distributions of the boundaries for the four alloys

were quantified to provide a more detailed information on the microstructural evolution under the same *Z* deformation conditions; the results are presented in Fig. 5. 11.

Mainly elongated grains perpendicular to the compression direction were observed in all deformed samples (Fig. 5. 10). At the high *Z* (400 ℃, 0.1 s^{-1}), large numbers of low- and medium-angle boundaries in the deformed microstructures were observed (Fig. 5. 10a, d, g, and j), indicating the high densities of dislocation cells and subgrains. These microstructures were typically characterized by DRV. It should be noted that in the Gleeble compression tests when the samples were deformed to a true strain of 0.75, they were subjected to an immediate water quenching. Therefore, all deformed microstructures in Fig. 5. 10 exhibited DRV or DRX. The level of DRV varied with the Mn content, which can be demonstrated by the misorientation angle distributions in Fig. 5. 11a. Compared to those of the base alloy, the three Mn-containing alloys (0.5Mn, 0.75Mn, and 0.75Mn), overall, have higher fractions of low-angle boundaries (2–5 °) and lower fractions of high-angle boundaries (>15 °), suggesting the larger restriction effect on the DRV owing to the large number of dispersions. The 1Mn alloy has the lowest fraction of high-angle boundaries, yielding the largest restriction effect on the DRV.

For the deformation at the medium *Z* (500 ℃, 0.01 s^{-1}), the substructures were better organized with lower substructure densities (Fig. 5. 10b, e, h, and k). Correspondingly, the fraction of low-angle boundaries (1–5 °) was reduced, while that of high-angle boundaries was increased (Fig. 5. 11b), which implies an increase in

DRV level as *Z* was reduced. In the deformed microstructure of the base alloy, an uneven distribution of low-angle boundaries (white line) was observed in the different grains, as indicated in Fig. 5. 10b. For example, in grain 1, the high density of low-angle boundaries was still observed, while in grain 2, the low-angle boundaries were almost removed, leaving only few well-ranged low- and medium-angle boundaries. This result indicates that, in some grains, low-angle boundaries were progressively combined or converted into medium-angle boundaries, which in turn led to new grains, without low-angle or even medium-angle boundaries. This evolution can be considered as the occurrence of DRX [28,34], which also corresponds to the remarkable increase in fraction of high-angle boundaries compared to that in the sample deformed at the high *Z* (Fig. 5. 11a and b). However, in 0.5Mn, 0.75Mn, and 1Mn alloys, no such phenomenon was observed and thus the DRV was still the predominant mechanism (Fig. 5. 10e, h, and k), which is consistent with the relatively low content of high-angle boundaries, shown in Fig. 5. 11b.

Under the low-*Z* deformation condition (550 ℃, 0.001 s^{-1}), large reductions in substructure density were observed for all alloys (Fig. 5. 10c, f, i, and l), characterized with the overall lower fractions of low-angle boundaries and higher fractions of high-angle boundaries (Fig. 5. 11c). In the base alloy (Fig. 5. 10c), the low- and medium-angle boundaries almost disappeared and the grains almost did not exhibit internal substructures. In general, the disappearance of low- and medium-angle boundaries could be attributed to both DRV and DRX [16]. However, in this case, a series of high-angle boundaries parallel to the compression direction appeared (see

arrows in Fig. 5. 10c), the original deformed and elongated grains had been broken up and replaced by newly recrystallized grains via the migration of high-angle boundaries. In addition, the results of the boundary angle distribution (Fig. 5. 11c) revealed that the fraction of the low- and medium-angle boundaries was as low as 20%, while that of the high-angle boundaries was larger than 70%. Therefore, the grain structure of the base alloy is almost full DRX. In the 0.5Mn, 0.75Mn and 1Mn alloys, considerable numbers of low- and medium-angle boundaries were still observed in the deformed grains (Fig. 5. 10f, i, and l). However, newly formed grains could be observed near the original grain boundaries. These new grains were small and equiaxed without internal substructures and their sizes were in the range of 5 to 20 μm, indicating a partial DRX during the hot deformation. Compared to those of the base alloy, the fraction of the high-angle boundaries significantly decreased, while the fractions of the low- and medium-angle boundaries increased (Fig. 5. 11c). Therefore, the large numbers of dispersoids in the three Mn-containing alloys could effectively inhibit the DRX.

The small recrystallized grains were located mostly near the original grain boundaries in the Mn-containing alloys, which were considered to be closely related to the PFZs (Fig. 5. 2b and c). During the hot deformation, the DRX occurred preferentially in the regions where the dislocation movement and subgrain boundary migration easily occurred [16]. Therefore, the PFZs without dispersoids were the preferred locations of DRX. However, once the dislocation movement and subgrain boundary migration encountered the dispersoid zone, the ongoing DRX was limited.

Therefore, the recrystallized grains were restricted in the PFZs and the growth of such grains was limited.

Based on the EBSD data, a quantitative analysis of the mean misorientation angle of the boundaries and subgrain size was performed for the four alloys. Fig. 5. 12 shows the mean misorientation angles of the boundaries in the alloys under the three *Z* deformation conditions. With the shift in deformation from the high to the low *Z*, with the increased temperature and decreased strain rate, the mean misorientation angles of the boundaries of the four alloys were generally increased, suggesting the increased DRV/DRX levels with the decrease in *Z*. For the base alloy, the mean misorientation angle of the boundaries significantly increased. This is consistent with the transition of the deformed microstructure from the recovered microstructure at the high *Z* through the partially recrystallized microstructure to the fully recrystallized microstructure at the low *Z*. For the three Mn-containing alloys, the mean misorientation angles of the boundaries were relatively low (below 15 °) at both high and medium *Z* values. Toward low *Z* values, they increased slightly to values above 15 °, indicating a partially recrystallized microstructure. At any given Z, there is a sharp drop in the mean misorientation anglesfrom the base alloy to the 0.5Mn alloy, while the differences in mean misorientation angle between the three Mn-containing alloys were small.

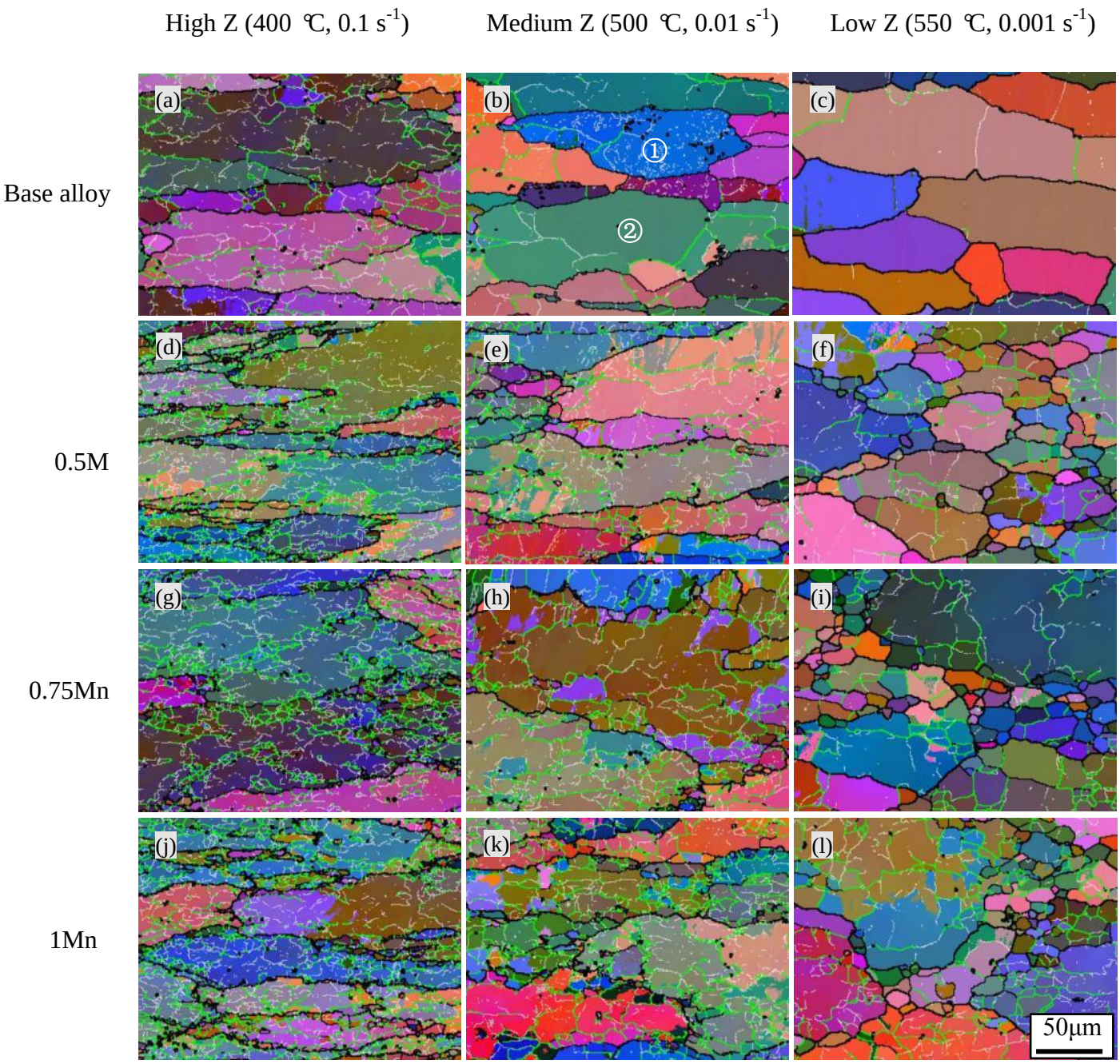

Fig. 5.10 All Euler orientation maps of four experimental alloys under various deformation conditions. The boundary misorientation angles are marked by white lines 2-5 °, green lines 5-15 °and black lines＞15 °.

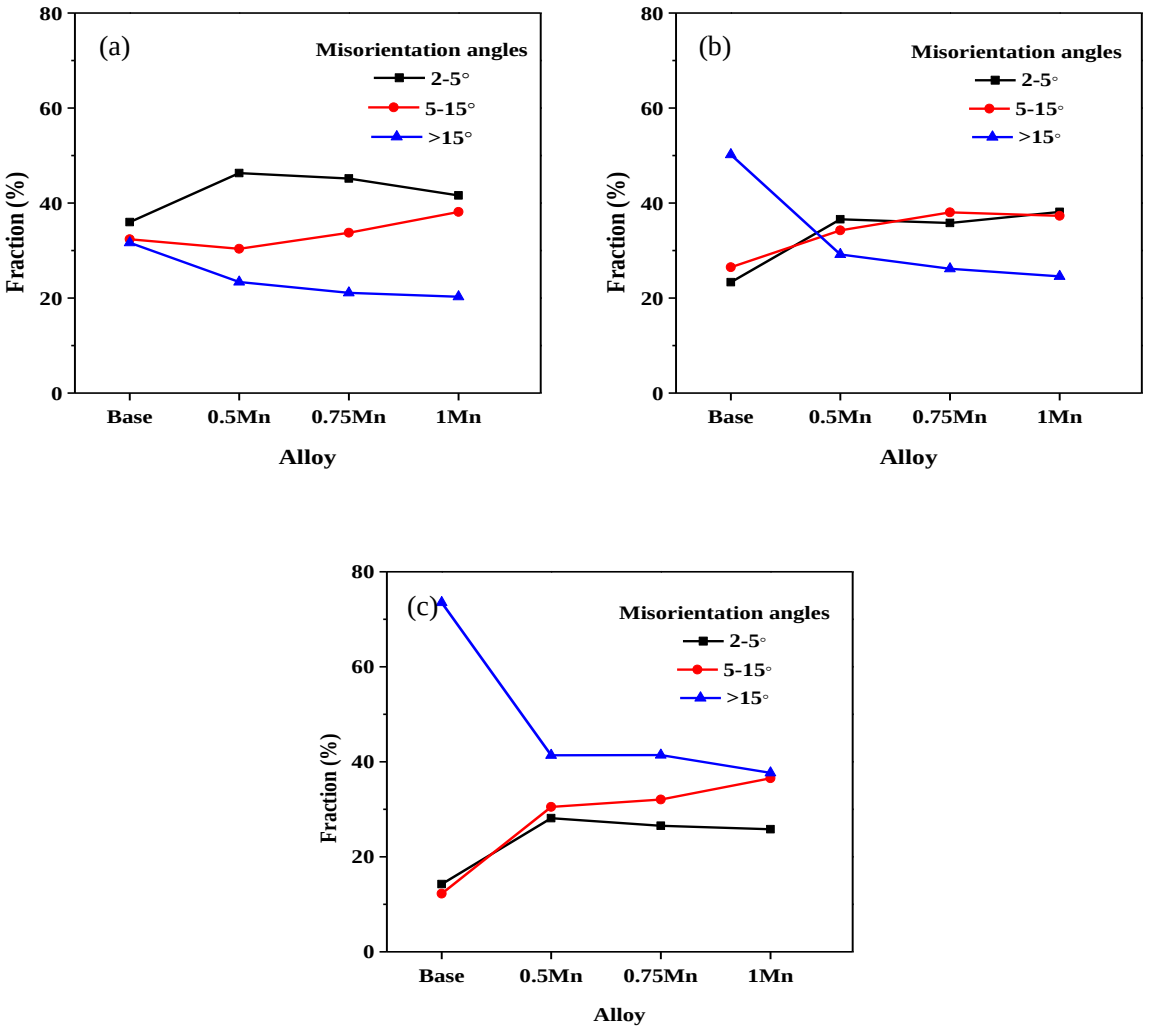

Fig. 5.11 Evolution of misorientation angle distribution of boundaries as a function of Mn content under different deformation conditions: (a) High Z (400 ℃, 0.1 s^{-1}); (b) Medium Z (500 ℃, 0.01 s^{-1}) and (c) Low Z (550 ℃, 0.001 s^{-1}).

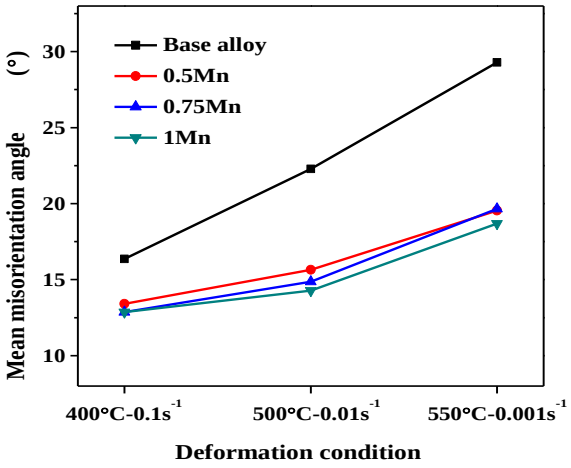

Fig. 5.12 Mean misorientation angles of boundaries in four experimental alloys under different deformation conditions.

Fig. 5. 13a shows the influences of the deformation conditions on the subgrain sizes of the alloys. The general tendency of the subgrain size change is very similar with the mean misorientation angle change. It increased with the decrease in *Z* and decreased with the increase in Mn content. At the high *Z*, the subgrain sizes of the four alloys were quite low (in the range of 2.8–7.6 μm), indicating strong restrictions on the DRVs during the deformation [35]. At the medium and low *Z* values, the subgrain sizes of the base alloy significantly increased, reaching values as large as 17 and 39 μm, respectively, while the subgrain sizes of the 0.5Mn, 0.75Mn and 1Mn alloys increased only moderately (mostly below 10 μm). This also reveals the strong effects of the Mn addition and dispersoids on the retardation of the DRV/DRX during the hot deformation. Fig. 5. 13b shows the relationship between the flow stress σ and subgrain size *d*. The flow stress increased with the decrease in subgrain size. A good linear relationship between the flow stress and subgrain size can be established based

on Eq. 4, proposed by McQueen et al. [36] and Jonas et al. [37].

$$\sigma = 212.99d^{-1} - 3.26 \quad (4)$$

This relationship is in good agreement with the results reported for aluminum alloys under hot compression, torsion, and extrusion [37–39]. It shows that both deformation conditions and Mn content influence the subgrain size (Fig. 5. 13a), which in turn determines the flow stress (Fig. 5. 13b) [16].

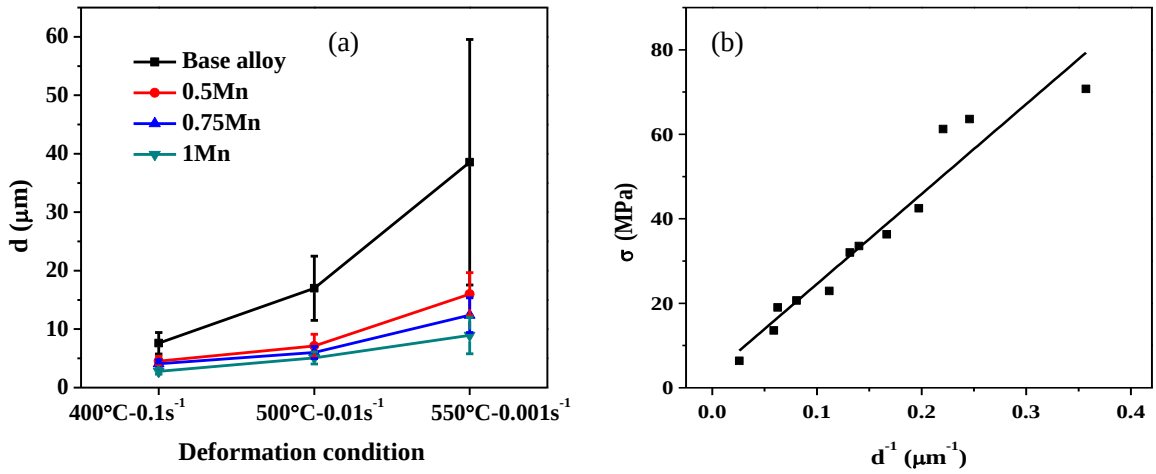

Fig. 5.13 (a) Subgrain size under different deformation conditions and (b) Relationship between flow stress and reciprocal subgrain size in the experimental alloys.

5.4. Discussion

The hot deformation behaviors of 6082 aluminum alloys with different Mn contents were systematically studied. With the addition of Mn (0.5 to 1%), a large number of α-Al(MnFe)Si dispersoids were formed by the low-temperature

homogenization treatment at 450 ℃ for 6 h. The number density of the dispersoids increased with the Mn content, whereas the dispersoid size was almost unchanged. The dispersoids increased the high-temperature flow stress and hence the activation energy. They also promoted the retardation of DRV and inhibition of DRX in the deformed microstructure.

5.4.1 Effect of dispersoids on DRV/DRX

In general, the levels of DRV and DRX decreased after the alloying with Mn (Fig. 5. 10–12). When Mn was added, the precipitation of the large number of dispersoids had an important role in the dynamic softening. Fig. 5. 14a shows the interaction of the α-Al(MnFe)Si dispersoids with dislocations in the 0.75Mn alloy under the deformation conditions of 450 ℃/0.01 s^{-1}. The dislocations were retarded at the points where they encountered the dispersoids, and thus the dispersoids acted as stronger barriers to deformation. Fig. 5. 14b shows the interaction of the dispersoids with subgrain boundaries of the same alloy under the same deformation conditions. The subgrain boundaries, formed through piled-up dislocations during the deformation, were strongly pinned by the dispersoids, restricting the subgrain migration and rotation [16,35,40]. In this manner, the DRV and DRX were restrained owing to the high number of dispersoids [3,41]. On the other hand, the strong pinning effect of the dispersoids on dislocation slips and subgrain rotations yielded significant increases in flow stress and activation energy *Q* compared to the case of the base alloy without dispersoids.

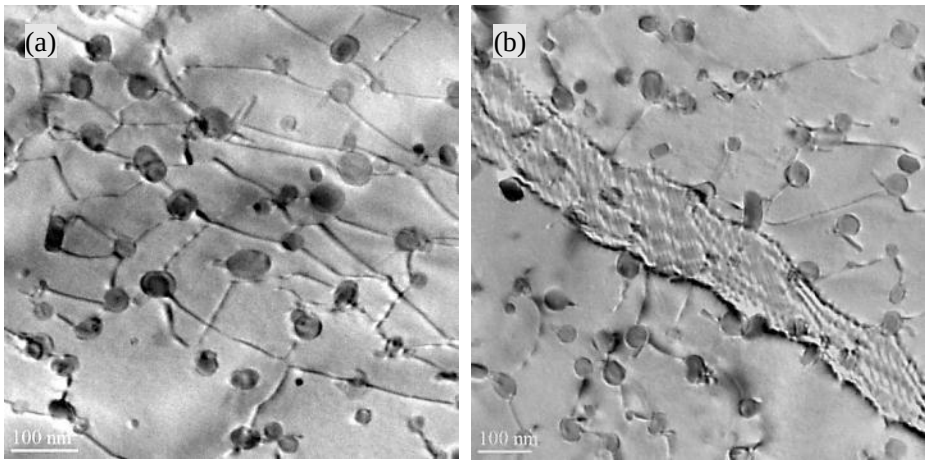

Fig. 5.14 Interactions of α-Al(MnFe)Si dispersoids with dislocations (a) and with subgrain boundaries (b) in the 0.75Mn alloy at the deformation condition of 450 ℃ and 0.01 s^{-1}.

In addition to those under the three typical deformation conditions presented above, the microstructure changes after hot deformation under other deformation conditions were also analyzed by the EBSD technique. Table 3 shows a comparison of the DRV/DRX in the base and Mn-containing alloys. Although the DRV and DRX levels of the three Mn-containing alloys were slightly different, the occurrence conditions of DRX in 0.5Mn, 0.75Mn, and 1Mn alloys were almost identical and thus were regrouped into one group (Table 5. 3b). In the base alloy (Table 5. 3a), DRV was the main softening mechanism at the deformation temperatures lower than 450 ℃ and strain rates higher than 0.01 s^{-1}. The DRX occurred at 500 ℃ and strain rates of 0.01 and 0.001 s^{-1}, yielding a partial DRX microstructure. With the increase in deformation temperature to 550 ℃, full DRX occurred. For the Mn-containing alloys, it seems that when a sufficient number of dispersoids existed in the matrix (starting

from 0.5Mn alloy), the further increase in number density of dispersoids (0.75Mn and 1Mn) had smaller effects on the DRV and DRX. The DRX in these three alloys started at 500 ℃/0.001 s^{-1} with a small number of recrystallized grains. At 550 ℃ and 0.01 and 0.001 s^{-1}, a partial DRX microstructure was formed with a moderate number of recrystallized grains. The results indicated the onsets of DRX of the Mn-containing alloys requiring higher deformation temperatures and lower strain rates than those of the base alloy, which is attributed to the strong inhibition effect of the dispersoids on the DRX.

Table **5.3** DRV/DRX in (a) the base alloy and (b) the Mn-containing alloys at various deformation conditions

(a)

$\dot{\varepsilon}$ (s^{-1}) / T	1	0.1	0.01	0.001
400 °C	DRV	DRV	DRV	
450 °C	DRV	DRV	DRV	
500 °C		DRV	DRV DRX	DRV DRX
550 °C			DRX	DRX

(b)

$\dot{\varepsilon}$ (s^{-1}) / T	1	0.1	0.01	0.001
400 °C	DRV	DRV	DRV	
450 °C	DRV	DRV	DRV	
500 °C		DRV	DRV	DRV DRX
550 °C			DRV DRX	DRV DRX

5.4.2 Variation of the active energy with different deformation strains

The calculation of the activation energy *Q* and material constants presented above (Table 5. 2) was based on the peak flow stresses obtained in the true stress–strain curves (Fig. 5. 5). However, in the three Mn-containing alloys (0.5Mn, 0.75Mn,

and 1Mn), the flow stresses largely decreased with the increase in strain at a relatively low *Z* after reaching the peak flow stress at the early stage of the deformation. This could be observed at 500 ℃ and 0.01–0.001 s^{-1} and became more obvious under the high-temperature deformation conditions (550 ℃ at 0.01–0.001 s^{-1}, Fig. 5b and c). For example, for the deformation at 550 ℃ and 0.001 s^{-1}, the flow stress of the 0.75Mn alloy decreased from 19.9 MPa at the peak value to 9.5 MPa at a strain of 0.75, i.e., a decrease of 52%. Under low Z deformation conditions, high deformation temperature and low strain rate provided higher mobility of boundaries and longer time for the energy accumulation, which results in enhanced dislocation annihilation and occurrence of DRV and DRX [37, 38] (Fig. 5. 10, Table 5. 3). In this case, the dynamic softening greatly overcame the working and contributed to the decline of flow stress. Besides of the softening mechanisms, a rapid coarsening and dissolution of dispersoids was found during low Z deformation conditions. For example, after deformation at 550 ℃/0.001 s^{-1} condition, the dispersoids number density in 0.75Mn alloy dropped by 49%, which was believed to be another factor contributing to flow stress decline." Additionally, the large variation in flow stress with the progress of the deformation can affect the calculated *Q*.

Different approaches were employed for the calculation of *Q*. Although the peak flow stresses were commonly used [19,20,24,33], the flow stresses at certain strains in the steady stage of deformation, e.g., 0.3 [32], 0.5 [42], and 0.8 [43], were also used as typical values to derive the *Q* values in the literature. It is recognized that a complex microstructure evolution is involved during the hot deformation [44], which

could strongly influence the flow stresses and thus the derived *Q*. In this study, the *Q* values of the four alloys were also calculated using the flow stresses at different strains, as shown in Fig. 5. 15. The *Q* values were the highest when were derived using the peak flow stresses. With the increase in strain from 0.3 to 0.75, the *Q* values significantly decreased, particularly for the three Mn-containing alloys. The decrease in *Q* was smaller for the base alloy because the decrease in flow stress with the increase in strain under the low-*Z* deformation conditions was not considerable (Fig. 5. 5a). Fig. 5. 15 shows that under all conditions, the differences in *Q* between the base alloy (without dispersoids) and three dispersoid-containing alloys were considerable, indicating the strong effect of the dispersoids on the hot deformation resistance. However, with the increase in strain, the difference decreased and the differences in *Q* between the three dispersoid-containing alloys vanished.

According to the constitutive analyses (section 3.3), it could be expected that a unique index *Q* could be used to compare the difficulty levels of hot deformation of different chemical compositions or different microstructures. However, the results reveal that *Q* is not constant and that considerably depends on the hot deformation conditions, because the flow stress often changes with the progress of the deformation. Therefore, it is not always simple to assess the hot workabilities of different aluminum materials using only *Q*. Shi et al. [24] reported that *Q* mainly reflected the free-energy barrier to dislocation movement, which was affected by the deformation temperature and strain. In recent years, the concept of activation energy mapping was explored instead of treating *Q* as a constant to study the hot workabilities of aluminum

alloys [25,45,46].

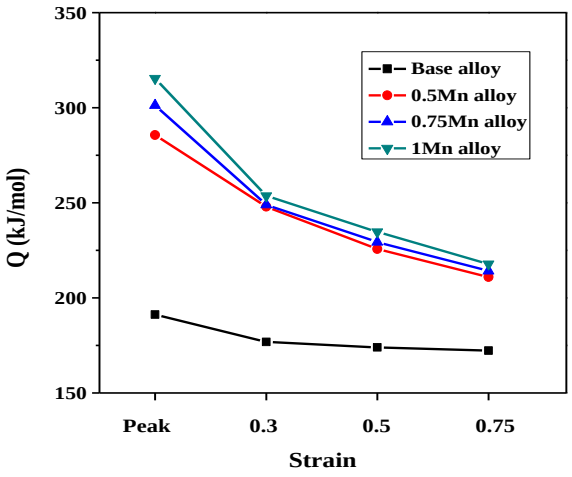

Fig. 5.15 Variation of the activation energy Q of experimental alloys with deformation strain.

5.5 Conclusions

(1) Upon treatment at the low homogenization temperature of 450 ℃ for 6 h, large numbers of α-Al(FeMn)Si dispersoids precipitated and were retained in the microstructures of the Mn-containing 6082 aluminum alloys. With an increase in Mn content, the number density of dispersoids increased, whereas the equivalent diameter was almost unchanged.

(2) With the addition of 0.5% of Mn, the peak flow stress significantly increased owing to the strong strengthening effect of the dispersoids, compared to the case of the base alloy without dispersoids. With a further increase in the Mn content from 0.5 to 1%, the peak flow stress increased moderately.

(3) The material constants and activation energies for hot deformation were calculated

using the hyperbolic-sine constitutive equation and experimental peak flow stress data. The activation energies for hot deformation of the 6082 alloys considerably increased from 191.2 kJ/mol for the base alloy to 285.6 kJ/mol for the alloy containing 0.5% of Mn. With a further increase in the Mn content, the activation energy increased moderately to 301.2 and 315.4 kJ/mol for 0.75Mn and 1Mn alloys respectively.

(4) The addition of Mn in the 6082 alloy promoted the retardation of DRV and inhibition of DRX during the hot deformation owing to the strong pinning effect of the Mn-containing dispersoids on the dislocation slips and subgrain rotations.

(5) In the Mn-containing alloys, the flow stresses largely decreased with an increase in strain under the relatively low *Z* deformation conditions after reaching the peak flow stresses. Therefore, the derived activation energies significantly decreased with an increase in strain, showing the dependence of the activation energy on the deformation conditions.

References

[1] Y.J. Li, A.M.F. Muggerud, A. Olsen, T. Furu, Precipitation of partially coherent α-Al(Mn,Fe)Si dispersoids and their strengthening effect in AA 3003 alloy, Acta Mater. 60 (2012) 1004–1014.

[2] K. Liu, X.-G. Chen, Development of Al–Mn–Mg 3004 alloy for applications at elevated temperature via dispersoid strengthening, Materials and Design, 84 (2015) 340–350.

[3] A.R. Farkoosh, X.-G. Chen, M. Pekguleryuz, Dispersoid strengthening of a high temperature Al–Si–Cu–Mg alloy via Mo addition, Mater. Sci. Eng. A 620 (2015) 181–189.

[4] D. H. Lee, J. H. Park, S. W. Nam, Enhancement of mechanical properties of Al–Mg–Si alloys by means of manganese dispersoids, Mater. Sci. Technol 15 (1999) 450–455.

[5] Z. Li, Z. Zhang, X.-G. Chen, Microstructure, elevated-temperature mechanical properties and creep resistance of dispersoid-strengthened Al-Mn-Mg 3xxx alloys with varying Mg and Si contents, Mater. Sci. Eng. A 708 (2017) 383–394.

[6] K. Liu, H. Ma, X.-G. Chen, Enhanced elevated-temperature properties via Mo addition in Al-Mn-Mg 3004 alloy, J. Alloy Comp. 694 (2017) 354–365.

[7] Y. J. Li, W. Z. Zhang, K. Marthinsen, Precipitation crystallography of plate-shaped Al_6(Mn,Fe) dispersoids in AA5182 alloy, Acta Mater. 60 (2012) 5963–5974.

[8] R. Zhang, Y. Zhang, Y. Yan, S. Thomas, C. H. J. Davies, N. Birbilis, The effect of reversion heat treatment on the degree of sensitisation for aluminium alloy AA5083, Corros. Sci. 126 (2017) 324–333.

[9] A.R. Farkoosh, X.-G. Chen, M. Pekguleryuz, Interaction between molybdenum and manganese to form effective dispersoids in an Al–Si–Cu–Mg alloy and their influence on creep resistance, Mater. Sci. Eng. A 627 (2015) 127–138.

[10] K. Liu, X.-G. Chen, Improvement in elevated-temperature properties of Al–13% Si piston alloys by dispersoid strengthening via Mn addition, J. Mater. Res. 33 (2018) 3430–3438.

[11] Y. Birol, J. Mater. The effect of processing and Mn content on the T5 and T6 properties of AA6082 profiles, Process Technol. 173 (2006) 84–91.

[12] L. Lodgaard, N. Ryum, Precipitation of dispersoids containing Mn and/or Cr in Al–Mg–Si alloys, Mater. Sci. Eng. A 283 (2000) 144–152.

[13] C. Liu, PhD thesis, Microstructure evolution during homogenization and its effect on the high temperature deformation behaviour in aa6082 based alloys, The University of British Columbia (2017) 74−92

[14] C. Liu, Q. Du, N. Parson, W. Poole, The interaction between Mn and Fe on the precipitation of Mn/Fe dispersoids in Al-Mg-Si-Mn-Fe alloys, Scripta Mater. 152 (2018) 59–63.

[15] C. Li, Master thesis, Precipitation behaviors of dispersoids induced from transition elements (Mn, Sc and Zr) and their effect on recrystallization resistance in aa6082 alloys, University of Quebec at Chicoutimi (2018), 53−63.

[16] H. J. McQueen, S. Spigarelli, M. Kassner, E. Evagelista, Hot Deformation and Processing of Aluminum Alloys, CRC Press, Bradenton, FL, (2011) 87–233.

[17] M. Shakiba, N. Parson, X.-G. Chen, Effect of homogenization treatment and silicon content on the microstructure and hot workability of dilute Al–Fe–Si alloys, Mater. Sci. Eng. A 619 (2014) 180–189.

[18] G. Avramovic-Cingara, D.D. Perovic, H. J. McQueen, Hot deformation mechanisms of a solution-treated Al-Li-Cu-Mg-Zr alloy, Metall. Mater. Trans. A 27 (1996) 3478.

[19] C. Shi, X.-G. Chen, Effect of vanadium on hot deformation and microstructural

evolution of 7150 aluminum alloy, Mater. Sci. Eng. A 613 (2014) A 596 (2014) 183–193.

[20] C. Shi, X.-G. Chen, Mater. Evolution of activation energies for hot deformation of 7150 aluminum alloys with various Zr and V additions, Sci. Eng. A 613 (2014) A 613 (2014) 91–102.

[21] M. Shakiba, N. Parson, X.-G. Chen, Hot deformation behavior and rate-controlling mechanism in dilute Al–Fe–Si alloys with minor additions of Mn and Cu, Mater. Sci. Eng. A 636 (2015) 572–581.

[22] C.M. Sellars and W.J. McTegart, La relation entre la resistance et la structure dans la deformation a chaud, Mem. Sci. Rev. Met. 63 (1966) 731–746 (in French).

[23] B. Zhang, T. Baker, Effect of the heat treatment on the hot deformation behaviour of AA6082 alloy, J. Mater. Proc. Tech. (2004) 153–154, 881–885.

[24] C. Shi, W. Mao, X.-G. Chen, Evolution of activation energy during hot deformation of AA7150 aluminum alloy, Mater. Sci. Eng. A 571 (2013) 83–91.

[25] Peng, X., Su, W., Xiao, D. and Xu, G., Investigation on Hot Workability of homogenized Al-Zn-Mg-Cu alloy based on activation energy and processing map, JOM 70 (2018) 993-999.

[26] W. Geertruyden, W. Misiolek, P. Wang, Grain structure evolution in a 6061 aluminum alloy during hot torsion, Mater. Sci. Eng. A 419 (2006) 105–114.

[27] R. Kaibyshev, O. Sitdikov, A. Goloborodko, Grain refinement in as-cast 7475 aluminum alloy under hot deformation, Mater. Sci. Eng. A 344 (2003) 348–356.

[28] S. Gourdet, F. Montheillet, An experimental study of the recrystallization

mechanism during hot deformation of aluminium, Mater. Sci. Eng. A 283 (2000) 274–288

[29] H.E. Hu, L. Zhen, L. Yang, W.Z. Shao, B.Y. Zhang, Deformation behavior and microstructure evolution of 7050 aluminum alloy during high temperature deformation, Mater. Sci. Eng. A 488 (2008) 64.

[30] R. Hu, T. Ogura, H. Tezuka, T. Sato and Q. Liu, Dispersoid Formation and Recrystallization Behavior in an Al-Mg-Si-Mn Alloy, J. Mater. Sci. Technol. 26(3) (2010) 237−243.

[31] D. Samantaray, S. Mandal, C. Phaniraj, A. Bhaduri, Flow behavior and microstructural evolution during hot deformation of AISI Type 316 L(N) austenitic stainless steel, Mater. Sci. Eng. A 528 (2011) 8565.

[32] H. Liao, Y. Wu, K. Zhou, J. Yang, Hot deformation behavior and processing map of Al–Si–Mg alloys containing different amount of silicon based on Gleebe-3500 hot compression simulation, Mater. Des. 65 (2015) 1091–1099.

[33] S. Spigarelli, E. Evangelista, H. J. McQueen, Study of hot workability of a heat treated AA6082 aluminum alloy, Scr. Mater. 49 (2003) 179–183

[34] S. Gourdet, E.V. Konopleva, H. J. McQueen, F. Montheillet, Recrystallization during Hot Deformation of Aluminium, Mat. Sci. Forum 217 (1996) 441-446.

[35] F. J. Humphreys, M. Hatherly, 2nd ed., Recrystallization and related annealing phenomena, Elsevier, Oxford (2004) 169–213, 415–450.

[36] H. J. McQueen, W.A. Wong, and J. J. Jonas, Deformation of aluminium at high temperatures and strain rates, Can. J. Phys. 45 (1967) 25–1234.

[37] J. J. Jonas, D.R. Axelrad, J.L. Uvira, Trans. On substructure strengthening and the high temperature deformation of cubic metalsJpn. Inst. Met. 9 (1968) 257–267.

[38] S. B. Brown, K. H. Kim, L. Anand, An internal variable constitutive model for hot working of metals, Int. J. Plast. 5 (1989) 95–130.

[39] H. J. McQueen, J. E. Hockett, Microstructures of aluminum compressed at various rates and temperatures, Met. Trans. 1 (1970) 2997–3004.

[40] G. Avramovic-Cingara, D. D. Perovic, H. J. McQueen, Metall. Mater. Trans. A 27 (1996) 3478.

[41] D. H. Lee, J. H. Park, S.W. Nam, Hot deformation mechanisms of a solution-treated Al-Li-Cu-Mg-Zr alloy, Mater. Sci. Technol. 15 (1999) 450–455.

[42] X. Kai, C. Chen, X. Sun, C. Wang, Y. Zhao, Hot deformation behavior and optimization of processing parameters of a typical high-strength Al–Mg–Si alloy, Mater. Des. 90 (2016) 1151–1158.

[43] M. Shakiba, N. Parson, X.-G. Chen, Effect of iron and silicon content on the hot compressive deformation behavior of dilute Al-Fe-Si alloys, JMEPEG 24 (2015) 404–415.

[44] Q. Yang, D. Yang, Z. Zhang, L. Cao, X. Wu, G. Huang, Q. Liu, Flow behavior and microstructure evolution of 6A82 aluminium alloy with high copper content during hot compression deformation at elevated temperatures Trans. Nonferrous Met. Soc. China 26 (2016) 649−657.

[45]C. Shi, X.-G. Chen, Evolution of activation energies for hot deformation of 7150 aluminum alloys with various Zr and V additions, Mater. Sci. Eng. A 650 (2016)

97−209.

[46] S. Wang, L. G. Hou, J. R. Luo, J. S. Zhang, L. Z. Zhuang, Characterization of hot workability in AA 7050 aluminum alloy using activation energy and 3-D processing map, J. Mater. Process. Tech. 225 (2015) 110−121.

Chapter 6 Effects of Mn and dispersoids on recrystallization resistance of 6082 aluminum alloys during post-deformation annealing

Abstract

The effects of different Mn contents (0.05–1 wt%) and its related dispersoids on recrystallization resistance of 6082 aluminum alloys during post-deformation annealing (at 500 ℃ up to 8 h) were investigated. The microstructural evolutions at as-homogenized, as-deformed conditions and after post-deformation annealing were studied using optical, scanning electron and transmission electron microscopes. The results revealed that the presence of a large amount of α-Al(Mn,Fe)Si dispersoids in Mn-containing alloys significantly improved the recrystallization resistance. In the base alloy free of Mn and dispersoids, after 2 h annealing the partial static recrystallization occurred and the grain growth appeared after 4 h annealing, whereas in Mn-containing alloys, even after 8 h annealing the recovered grain structure was well retained. The alloy with 0.5% Mn exhibited the best recrystallization resistance, while the further increase of Mn levels to 0.75% and 1% resulted in a gradual reduction of recrystallization resistance despite of the higher number density of dispersoids. The reason was that the recrystallization occurred only in the precipitation free zones (PFZs) and the increased PFZ fraction with Mn content led to an increase in recrystallization fraction. The variations in dispersoid number density and coarsening of dispersoids during annealing had limited influence on static

recrystallization in Mn-containing alloys.

Keywords: 6082 aluminum alloys, Mn addition, Dispersoids, Precipitation free zone, Post-deformation annealing, Recrystallization resistance

6.1 Introduction

The traditional hardening mechanism of Al-Mg-Si 6xxx aluminum alloys is via the precipitation of fine nano-scale Mg_2Si particles to reach superior mechanical properties at room temperature [1]. However, in the case of the service temperature over 200 ℃, the mechanical properties deteriorate rapidly due to the coarsening and dissolution of Mg_2Si [2]. In order to develop alloys that could be applied at elevated temperatures, several exploration works have been performed trough inducing a large number of thermally stable dispersoids in the aluminum alloys [3-5]. For 6082 aluminum alloys, one of most common thermally stable dispersoids encountered in the matrix is the α-Al(Mn,Fe)Si, which is partially coherent and could be formed via the decomposition of the supersaturated solid solution in the as-cast state during heating [6, 7]. Li [8] reported that the precipitation of a large amount of α-Al(Mn,Fe)Si dispersoids could be promoted with Mn addition in 6082 alloys after a relatively low temperature treatment at 400-450 ℃, while the number density of dispersoids increased with the increasing Mn levels. The strong effect of Mn addition on the precipitation of α-Al(Mn,Fe)Si dispersoids during high temperature

homogenization (550-580 ℃) in 6082 based alloys was also reported by Liu [9, 10].

After casting and homogenization, Al-Mg-Si 6xxx aluminum alloys are usually subjected to a thermomechanical process, such as rolling or extrusion to achieve desirable shape. The deformed structures usually associated with high level of internal stress and high density of substructures. To achieve appropriate and stable mechanical and materials properties, a post-deformation heat treatment (annealing or solution treatment) is performed [11]. Statistic recovery (SRV) and statistic recrystallization (SRX) can occurred during the post-deformation annealing. SRV associates with change of the density and distribution of line defects, while SRX involves the nucleation of new grains and their growth as well as grain boundary migration [12]. The control of SRX plays an important role in some wrought aluminum alloys. It is reported that occurrence of SRX negatively influenced the corrosion resistance in 2xxx alloys [13, 14]. In 5xxx alloys, work hardening effect could be kept only if the unrecrystallized structure can be maintained [15, 16]. In 7xxx alloys, a recrystallized structure can cause the increasing risk of weld cracking, declined fracture toughness, and detrimental effect on corrosion resistance [17-19].

The pre-existed thermally stable dispersoids in the aluminum matrix can significantly control grain growth and retard the recrystallization due to their pinning effect on grain boundary migration [20]. The size, number density, distribution and morphology of dispersoids have significant influence on the recrystallization resistance [21-25]. It is well recognized that the presence of a number of fine Al_3Zr dispersoids can greatly increase the recrystallization resistance during high

temperature annealing in 7xxx alloys [21, 22]. Li et al [23] studied the effects of Er and Zr on recrystallization in pure aluminum and found that the Al_3(Er,Zr) dispersoids could be formed during heat treatment at 400 ℃ for 48 h, resulting in a remarkable enhancement of the recrystallization resistance during the 350-525 ℃ annealing. Birol [24] reported that the superior recrystallization resistance of a 6082 alloy was obtained via a large population of the Cr-rich Al(Cr,Mn,Fe)Si and $(Al,Si)_3Zr$ dispersoids. However, the individual addition of Mn or Zr fails to offer any improvement in the recrystallization resistance in 6082 tube extrusions. Tsivoulas et al [25] investigated the effect of Mn and Zr additions on recrystallization resistance in Al–Cu–Li 2198 sheets, and found that with a constant Zr level the recrystallization resistance was diminished with the addition of Mn and it became progressively worse with a decrease in Zr content, as more Mn was added.

The above reported results about the dispersoid effect on the recrystallization resistance in aluminum alloys appear to be somewhat spread and inconsistent due to the complication of the recrystallization mechanism attributed to many factors involved, such as alloying element type and content, deformation and annealing conditions. Up to date, no systemically study on the effect of Mn dispersoid-forming addition on recrystallization resistance of 6082 alloys after hot deformation could be found in open literature. The evolution of the deformed microstructure during post-deformation annealing due to the presence of a large number of dispersoids, namely the development of static recovery (SRV) and static recrystallization (SRX), should be better understood.

In the present study, the effect of different Mn additions and its related dispersoids on the recrystallization resistance of 6082 aluminum alloys was investigated. The samples of direct chill cast billets were subjected to a low temperature homogenization at 450 ℃ for 6 h to promote the precipitation of Mn-containing dispersoids. The samples were then hot-deformed and followed by post-deformation annealing at 500 ℃ up to 8 h. The microstructural evolutions at as-homogenized, as-deformed conditions and after post-deformation annealing were studied. Quantitative microstructure analyses were performed on the dispersoids, particle free zone, SRV and SRX to better understand the effect of dispersoids on recrystallization resistance.

6.2 Experimental

FFour 6082 alloys with Mn additions of 0.05%–1.0% (designated as the base, 0.5Mn, 0.75Mn and 1Mn alloys) were used for investigation. The chemical compositions are shown in Table 6. 1. The materials were taken from direct chill cast billets with a diameter of 101 mm, provided by the Arvida Research and Development Center of Rio Tinto Aluminum, based in Saguenay, Quebec. To promote the precipitation of a large amount of dispersoids, a relatively low temperature homogenization of 450 ℃ for 6 h with a heating rate of 100 ℃/h, followed by water quenching at room temperature, was applied in DC cast billets prior to hot deformation.

Table 6.1 Chemical composition (wt.%) of the experimental alloys

Alloy	Mg	Si	Fe	Mn	Al
Base	0.79	1	0.18	**0.05**	Bal.
0.5Mn	0.83	1.01	0.22	**0.50**	Bal.
0.75Mn	0.84	1.02	0.23	**0.72**	Bal.
1Mn	0.81	1.02	0.24	**0.99**	Bal.

After homogenization, cylindrical specimens of 10 mm in diameter and 15 mm in length were machined for the uniaxial hot compression tests, which were performed in a Gleeble 3800 thermomechanical testing unit. Specimens were heated to 400 ℃ with a rate of 2 ℃/s and held for 180 s to ensure a homogeneous temperature distribution. The compression tests were carried out at 400 ℃ with the strain rate of 0.1 s^{-1} and the total true strain of 0.75. After hot deformation, a post-deformation annealing was conducted at 500 ℃ for 2, 4 and 8h to study the recrystallization resistance of 6082 alloys.

To reveal the details of microstructure, the polished samples were etched with a 0.5% HF solution for 40 seconds. An Optical microscopy (Nikon, Eclipse ME600) and a scanning electron microscopy (SEM, JEOL-6480LV) were used to examine the microstructure. All the deformed samples were sectioned parallel to the compression axis along the centerline and metallographically prepared. Electron back-scattered diffraction (EBSD) analysis under SEM was applied to examine the grain structure after hot deformation and post-deformation annealing. The step size of EBSD analysis was set to 0.5 μm. All Euler orientation maps were used in EBSD image analysis, the

boundaries misorientation angles of 2-5°, 6-15° and greater than 15° was used to represent low-angle boundaries, medium-angle boundaries and high-angle boundaries respectively. To avoid the noises caused by the sample surface and polishing conditions, misorientation angles below 2° were not taken into account. A transmission electron microscopy (TEM, JEM−2100) operating at 200 kV was used to observe the details of Mn-containing dispersoids. Twin-jet polishing with 30% nitric acid and 70% methanol solution at 15 V and - 20 ℃ was employed to prepare the TEM thin foils.

6.3. Results

6.3.1. Microstructure after homogenization

Fig. 6. 1 shows typical microstructures of 0.5Mn and 1Mn alloys after homogenization at 450 ℃ for 6 h. As indicated, the microstructures were composed of aluminum dendrite cells (Al matrix), Fe-rich intermetallics (white color in inset images) distributed along the dendrite boundaries, and primary Mg_2Si particles (black color in inset images) mostly co-located with Fe-rich intermetallics. In the base alloy with only trace of Mn, there was no precipitation in the aluminum matrix after homogenization. In Mn-containing alloys, a large number of precipitates were observed inside aluminum dendrite cells and they were identified as α-Al(MnFe)Si dispersoids in our previous work [6]. In the 0.5Mn alloy, dispersoids distributed uniformly and only very narrow precipitation free zones (PFZs) was observed in the interdendritic regions (Fig. 6. 1a). However, with increase Mn levels, the PFZs

became enlarged and more recognizable. The 1Mn alloy possessed the highest amount of PFZs (Fig. 6. 1b).

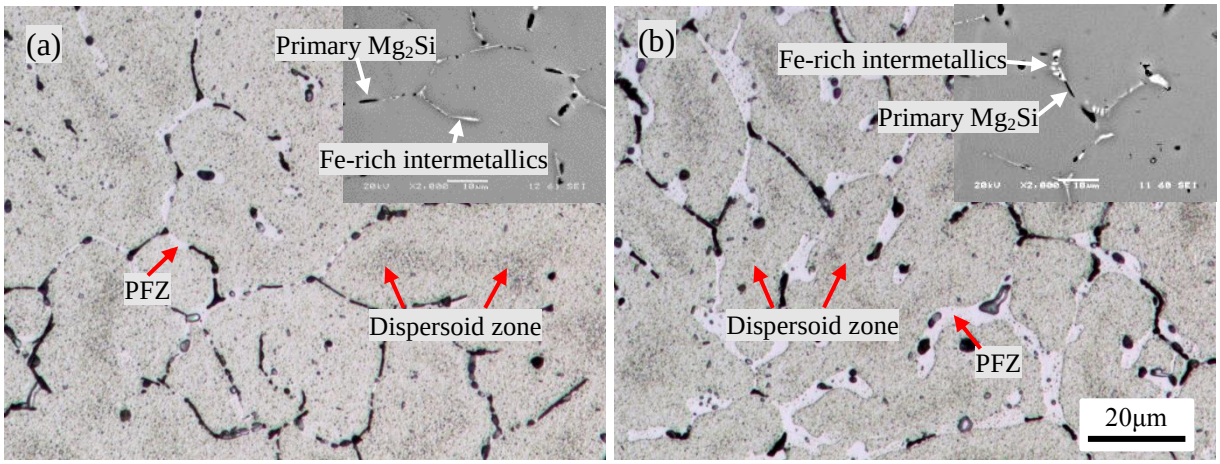

Fig. 6.1 Optical micrographs of: (a) 0.5Mn alloy and (b) 1Mn alloy after 0.5% HF etched for 40s. The inset images are SEM micrographs of original surface (without etching).

6.3.2. Microstructure after hot deformation

After homogenization, the experimental alloys were hot-compressed at 400 ℃ with a 0.1 s^{-1} strain rate. Fig. 6. 2 shows the microstructures after hot deformation of four alloys. Elongated grains perpendicular to the compression direction were mainly observed in all deformed samples. The intermetallics were fragmented along the aluminum dendrite boundaries. In the base alloy, there are only few separate Mg_2Si (black points) in the aluminum matrix but no dispersoids. In the Mn-contianing alloys (0.5Mn, 0.75Mn and 1Mn alloys), fine and dense dispersoids were observed in the aluminum matrix. PFZs were also elongated along the compression direction and they

are more obviously in the 0.75Mn and 1Mn alloys. Quantify analysis on dispersoids was performed based on a series of SEM images (not shown here, see the example in Fig. 6. 9). The amount of PFZs was analyzed based on a series of optical images. Fig. 6. 3 shows the number density of dispersoids and PFZ area fraction in three Mn-containing alloys. The number density of dispersoids increased with increasing Mn content from 8.6 μm^{-2} in the 0.5Mn alloy to 10.2 μm^{-2} and 15.3 μm^{-2} in the 0.75Mn and 1Mn alloys, respectively. For PFZ area fraction, the 0.5Mn alloy had as low as 2.7%, while it increased significantly to 6.8% and 16.7% in 0.75Mn and 1Mn alloys respectively. Additionally, the mean equivalent diameter of dispersoids remained nearly unchanged (~ 75 nm) in the three alloys.

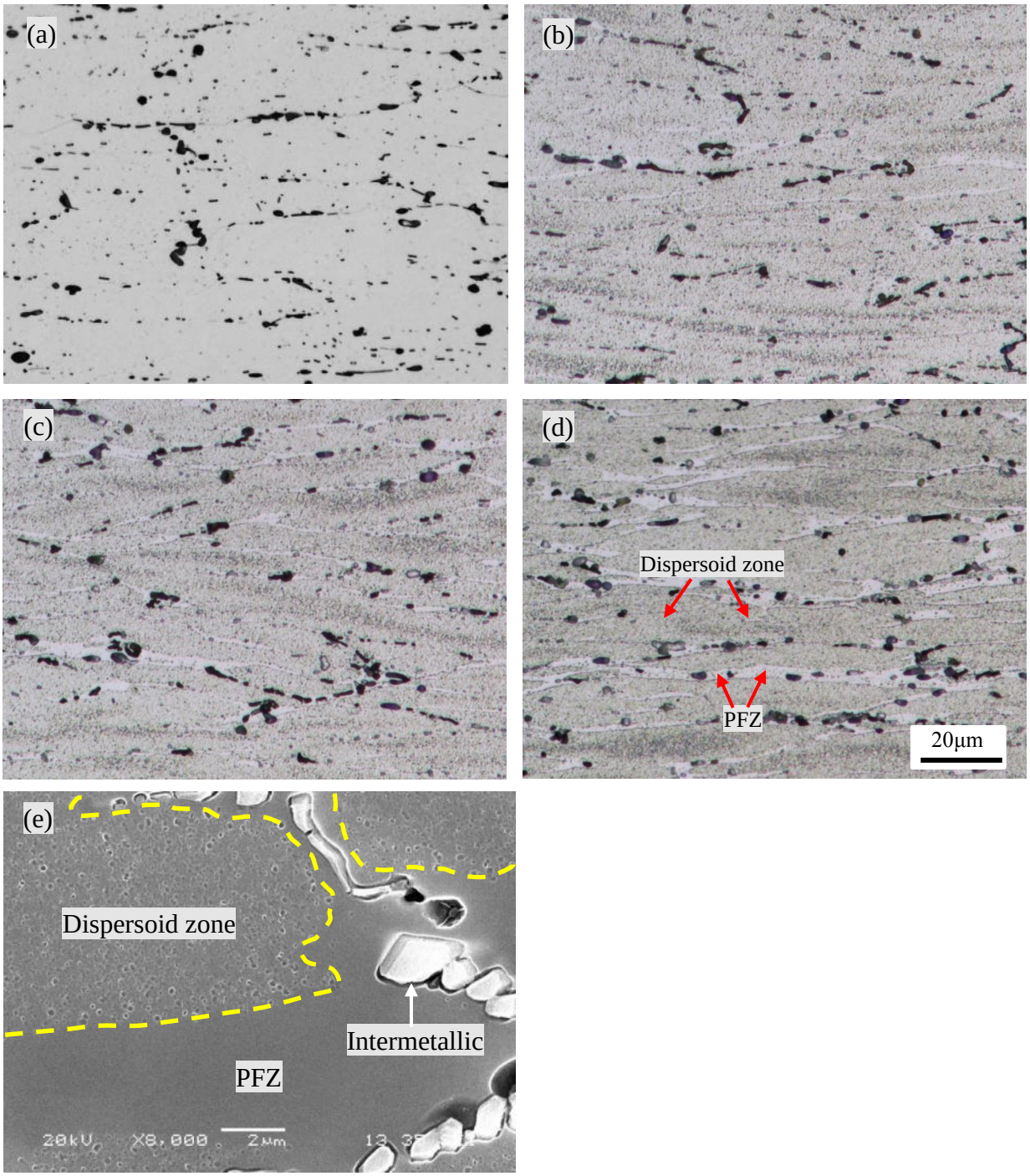

Fig.6.2 Microstructures after hot deformation: base alloy(a), 0.5Mn alloy(b), 0.75Mn alloy(c), 1Mn alloy(d); (e) SEM image of 1Mn alloy; (f) EDX spectra image of dispersoids in 1Mn alloy.

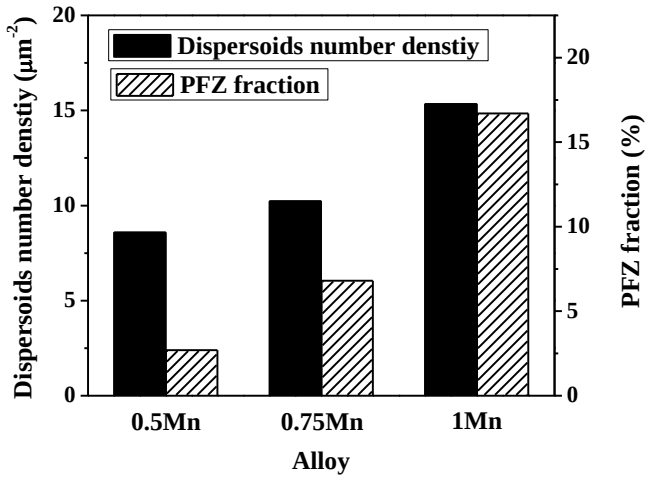

Fig. 6.3 The number density of dispersoids and PFZ area fraction in the different alloys after heat treatment of 450 ^{o}C for 6 h

The grain structures were investigated using EBSD technique. Fig. 6. 4 shows all Euler orientation maps of the four experimental alloys after hot deformation. Besides of the elongated grains, a large amount of low- and medium-angle boundaries were observed, indicating the presence of high densities of dislocation and subgrains. The deformed microstructures of all four alloys were typically the dynamically recovered structure without dynamic recrystallization [26]. Different densities of low- , medium- and high angle boundaries in various alloys were observed, representing the different DRV levels [27].

The misorientation angles boundaries were analyzed based on EBSD mappings, the results of four alloys are plotted in Fig. 6. 5. The densities of misorientation angle greater than 15 ^{o} in all four alloys were similar (in rang of 0.14-0.19 μ m^{-1}), since the DRV during hot deformation had limit influence on the high angle grain boundaries.

However, the density of misorientation angle of 2-15^{o} (subgrain boundaries) increased from 0.35 μ m^{-1} in the base alloy to 0.69 μ m^{-1} in 1Mn alloy. The increased density of misorientation angle of 2-15^{o} indicated the decline of DRV levels with increasing Mn contents and was believed to be related to the presence of a large amount of dispersoids. During hot deformation, dispersoids acted as strong barrier to dislocations movement and subgrains migration [6, 28, 29]. With increasing dispersoid number density in alloys, strong effect of dispersoids was applied on the retardation of DRV and thus the DRV levels became lower with an increase of Mn content (Fig. 6. 5).

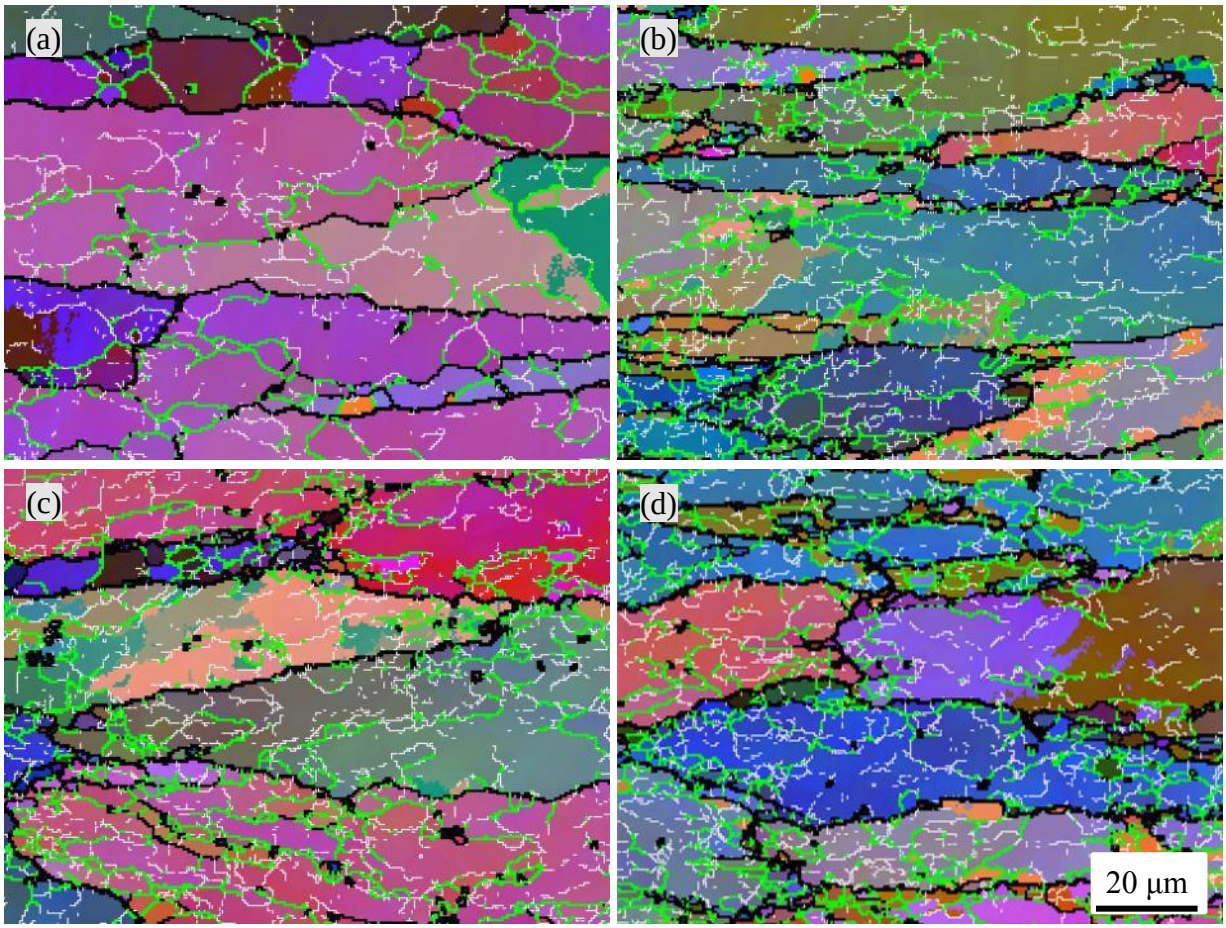

Fig. 6.4 All Euler orientation maps of the four experimental alloys after hot deformation: (a) base alloy, (b) 0.5Mn alloy, (c) 0.75Mn alloy and (d) 1Mn alloy; white lines are 2-5 °, light green lines are 5-15 ° and black lines are ＞15 °.

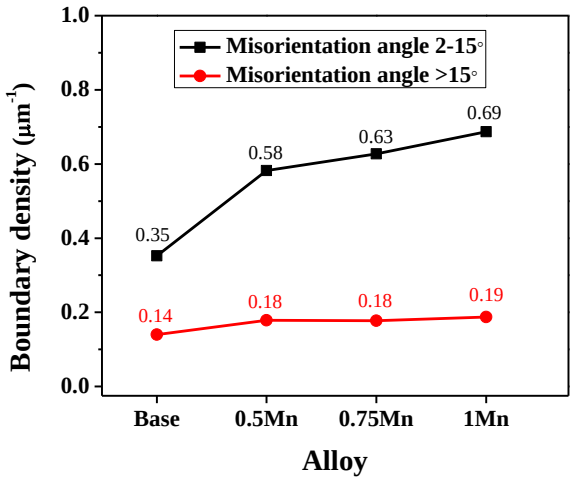

Fig. 6.5 Misorientation angle boundary density of experimental alloys after hot deformation.

6.3.3 Microstructure evolution during post-deformation annealing

Post-deformation annealing was performed at 500℃ for 2h, 4h and 8h. All Euler orientation maps of the annealed microstructures obtained by EBSD technique are shown in Fig. 6. 6 as a function of annealing time. Besides, more specific data on the boundary densities of misorientation angles of 2-15^{o} and >15^{o} for the four alloys were analyzed and the results are plotted in Fig. 6. 7.

In the most cases, elongated grains perpendicular to the compression direction were still observed after annealing. For the base alloy after 2h of annealing, the substructures became better organized (Fig. 6. 6a) with less substructure comparing with the condition before annealing (Fig. 6. 4a). Moreover, some newly formed grains were observed near the original grain boundaries (as indicated by the arrows in Fig. 6. 6a). These new grains were featured as free of internal substructure, indicating that partial statistic recrystallization (SRX) occurred during annealing [30, 31]. The

density of the boundary between 2-15^{o} was reduced to 0.23 μm^{-1} (Fig. 6. 7a) comparing with that of 0.35 μm^{-1} (Fig. 6. 5) before annealing, while the density of boundary greater than 15^{o} increased slightly (from 0.14 to 0.16 μm^{-1}) due to the occurrence of SRX, which is attributed to the formation of some new grains with high angle boundaries. With increasing annealing time to 4 and 8 h, the growth of grains took place that the grains size reached up to several hundred micrometers and millimeters scale (Fig. 6. 6b, c). Accordingly, the density of the boundary between 2-15 ° dropped to zero, indicating no substructure within grains, while the boundary density greater than 15 ° decreased to close zero (Fig. 6. 7a) due to severe grain growth.

For three Mn-containing alloys (0.5Mn, 0.75Mn and 1Mn alloys), a large amount of substructures was always presented after 2-8h of annealing (Fig. 6. 6d-l), no grain growth was observed after even 8h of annealing, suggesting the much better recrystallization resistance than that of base alloy. In the 0.5Mn alloy, the structure of elongated grains was well retained (Fig. 6. 6a-c). However, the densities of boundary between 2-15^{o} (0.33-0.38μm^{-1}, Fig. 6. 7b) were considerably lower than that of the condition before annealing (0.58μm^{-1} Fig. 6. 5b), implying that the occurrence of SRV during annealing. Besides, very few of new equiaxed grains without internal substructure could be observed at the original grain boundaries (as indicated by the arrows in Fig. 6. 6e-f), suggesting the start of SRX in a very limited extent. These recrystallized grains were much smaller comparing those appeared in the base alloy after 2h annealing. The SRX resulted in only a small increase in the densities of

boundary greater than 15^{o} (0.19-0.20μm^{-1}, Fig. 6. 7b) comparing with the condition before annealing (0.18μm^{-1}, Fig. 6. 5). A small amount of recrystallized grains became recognizable but still remained at a low level in the 0.75Mn alloy (see the arrows in Fig. 6. 6 g-i). With further increasing Mn to 1%, a slightly larger amount of recrystallized grains appeared (see the arrows in Fig. 6. 6 j-l) compared to the 0.75Mn alloy. These newly formed recrystallized grains brought the increase in the boundary density of misorientation angles over 15^{o} correspondingly (0.21-0.23μm^{-1} in Fig. 6. 7c and 0.30-0.32μm^{-1} in Fig. 6. 7d). Meanwhile, densities of the boundary between 2-15^{o} also increased with increasing Mn content (Fig. 6. 7c, d) due to the increasing dispersoids number density, which led to stronger retardation effect on SRV.

Regarding the three Mn dispersoids-forming alloys, another fact was found that the boundary structures did not exhibit obvious change along with the annealing time (Fig. 6. 6d-l), which was also reflected by the stability of boundary densities along with annealing time (Fig. 6. 7b, c and d).

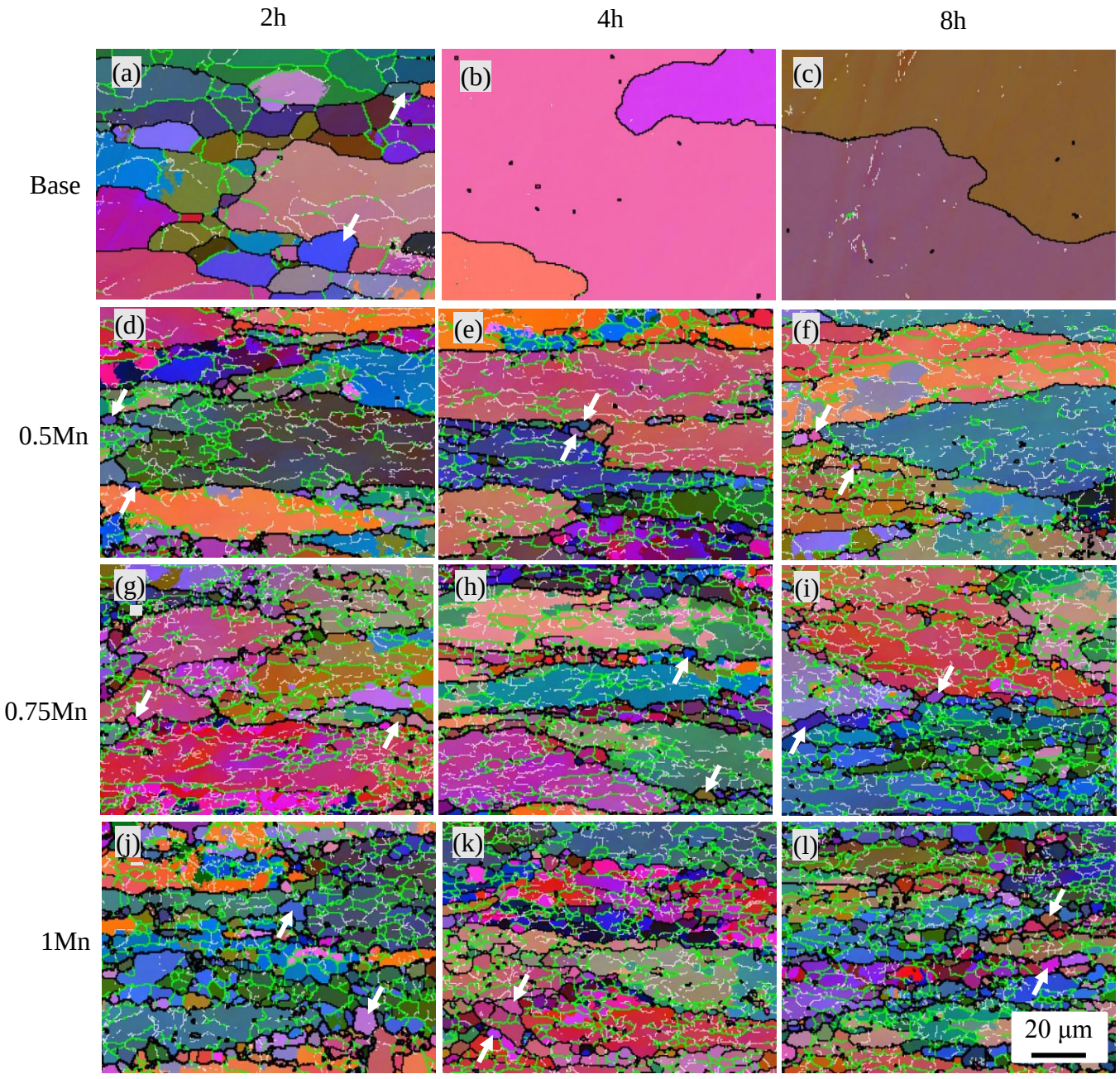

Fig.6. 6 All Euler orientation maps of the experimental alloys after different annealing time; white lines are boundaries of 2-5 °, light green lines are 5-15 °and black lines ＞ 15 °.

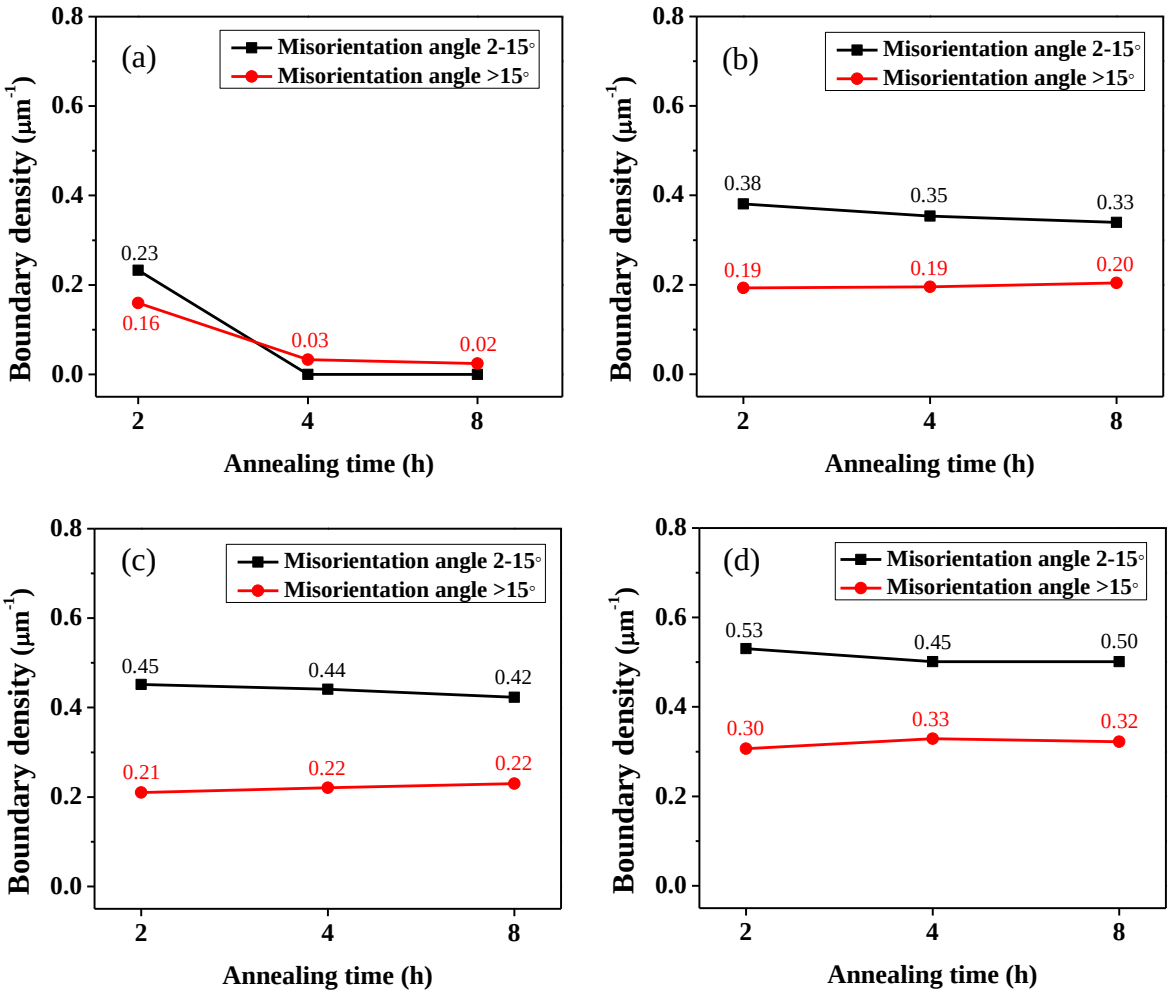

Fig. 6.7 Boundary density of misorientation angles of 2-5° and over 15° in (a) base alloy, (b) 0.5Mn alloy, (c) 0.75Mn alloy and (d) 1Mn alloy with different annealing time.

Quantitative image analysis was performed on the recrystallized grain size and recrystallization fraction for 0.5Mn, 0.75Mn and 1Mn alloys and the results are shown in Fig. 6. 8. Both the recrystallized grain size and recrystallization volume fraction of all three alloys increased with increasing Mn addition but remained nearly unchanged with annealing time. For instance, after 4h of annealing, the recrystallized grain size increased from 3.8 μm in the 0.5Mn alloy to 4.4 and 6.5 μm in the 0.75Mn and 1Mn

alloys, respectively, while the recrystallization fraction increased from 2.1% in the 0.5Mn alloy moderately to 5.2% in the 0.75Mn alloy and considerably to 14.7% in the 1Mn alloy. It should be noticed that although SRX occurred at three Mn-containing alloys, the proportion of recrystallized grains is quite low and the deformed microstructure after post-deformation annealing remains mainly the recovered grain structure.

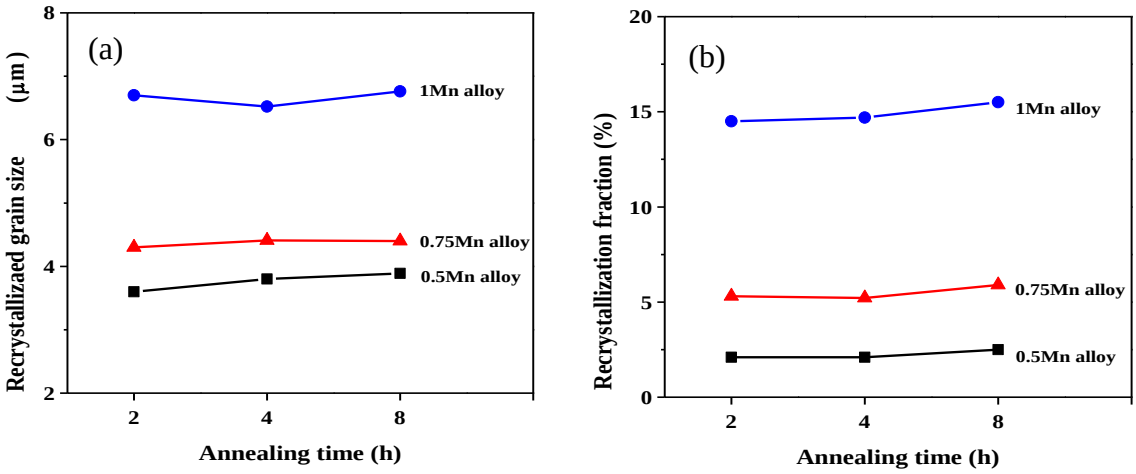

Fig. 6.8 Recrystallization grain size (a) and volume fraction (b) of experimental alloys at different annealing time.

The evolution of dispersoids in the 1Mn alloy during annealing is shown in Fig. 6. 9. During annealing, a gradual coarsening and dissolution of dispersoids took place, implied by the less population and larger size of dispersoids with increased annealing time. The α-Al(MnFe)Si dispersoids are thermally stable at the temperature range of 300-350 ℃ and above those temperatures they become less stable [3,5]. The results

obtained here confirmed that the dispersoids during annealing at 500 ℃ were no more stable. The changes of dispersoids number density in the 0.5Mn, 0.75Mn and 1Mn alloys during annealing were shown in Fig. 6. 10. The decrease in the dispersoid number density with annealing time occurred in all three alloys. However, the decline of the number density was mostly significant in the 1Mn alloy and became less distinct in the alloy with lower Mn content.

The PFZ area fraction in the 0.5Mn, 0.75Mn and 1Mn alloys during annealing was also measured. The results revealed that the PFZ area fraction after annealing in the three alloy remained nearly unchanged when compared with that before annealing (Fig. 6. 3), suggesting the coarsening and dissolution of dispersoids occurred only in the dispersoid zone and the PFZs remained the same as the initial states.

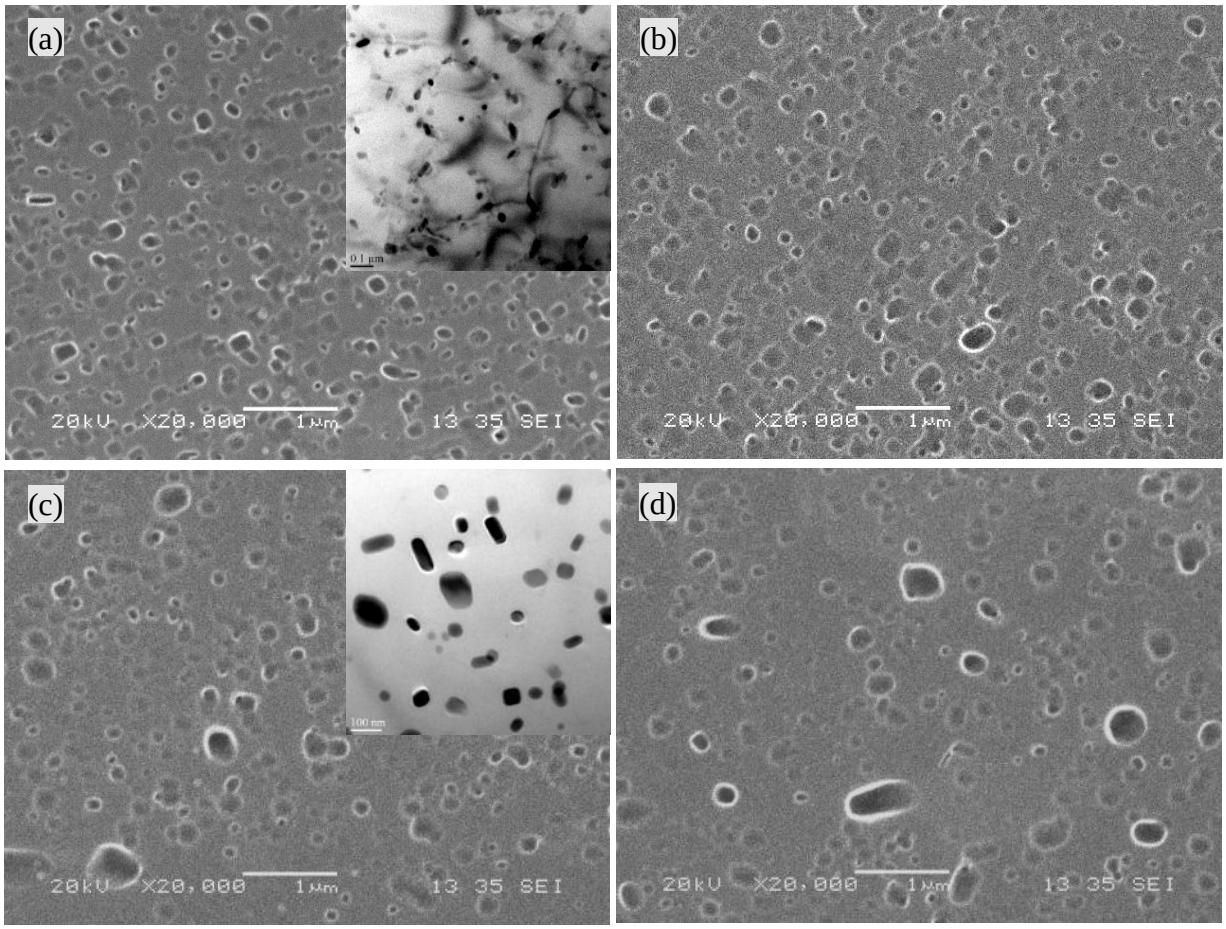

Fig. 6.9 Dispersoids in the 1Mn alloy of (a) before annealing and after annealing at 500℃ for 2 h (b), 4 h (c) and 8 h (d). TEM images are inset in (a) and (c).

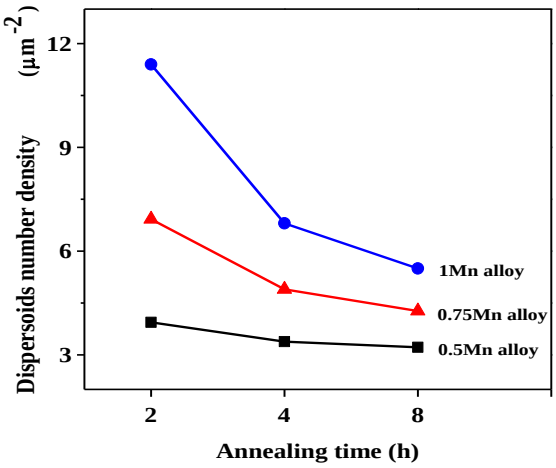

Fig. 6.10 The number density of dispersoids in 0.5Mn, 0.75Mn and 1Mn alloys at different annealing time.

6.4 Discussion

Effect of Mn and its related dispersoids on the recrystallization resistance of 6082 aluminum alloys was studied. A large amount of dispersoids were introduced via Mn addition and a low temperature homogenization at 450 ℃/6h. The presence of a large amount of dispersoids greatly improved the recrystallization resistance and avoided the severe grain growth during post-deformation annealing compared with the base alloy. For the three Mn-containing alloys, the recrystallization resistance slightly decreased with increasing Mn addition.

In the industrial practice, excellent recrystallization resistance is desirable because a poor recrystallization resistance may cause or partially recrystallized structure or coarse grain structure during post-deformation heat treatment, which has detrimental effect not only on strength, toughness and formability, but also on surface

quality and corrosion resistance [25]. Therefore, the control of grain structure is of paramount importance for deformed materials.

In the current study, when the dispersoids was absent in the base alloy, 2 h of annealing at 500 ℃ already resulted in the occurrence of partial SRX, while after 4 h of annealing the abnormal grain growth were observed, resulting in a very coarse grain structure (Fig. 6. 6b and c). After introduction of dispersoids in 0.5Mn, 0.75Mn and 1Mn alloys, the deformed microstructure was stabilized and the recovered grain structure was retained (Fig. 6. 6d-l), showing excellent recrystallization resistance at high temperature annealing treatment.

Regarding the three dispersoids-containing alloys, the number density of dispersoids increased with increasing Mn content after homogenization (Fig. 6. 3). This increase in the dispersoid number density leads to an increase of substructure density during hot deformation (Fig. 6. 4 and 5). In theory, a high dispersoids number density could contributed to a better recrystallization resistance during annealing due the strong pining ability on the grain boundary migration and grains rotation [24, 32]. However, a contrary result in the present study was observed: the 0.5Mn alloy exhibited the best recrystallization resistance with the lowest SRX fraction, whereas the 0.75Mn alloy possessed higher SRX fraction and the 1Mn alloy had even the highest SRX fraction (Fig. 6. 6 and 8b).

The decreased recrystallization resistance with increasing Mn content was believed to be related to the PFZ. Fig. 6. 11 shows the TEM bright field image of recrystallized grains in the 1Mn alloy after 8h of annealing. Newly formed and

recrystallized grains, which featured as free of internal substructures, can be clearly observed in the interdendrite region where the large intermetallic particles presented. The location of these recrystallized grains was actually the PFZ where nearly no dispersoids existed. However, in the neighbor regions, a large amount of dispersoids interacted with dislocations and subgrains was remained, representing high density of substructures in unrecrystallized grains. This result implies that during annealing, the newly recrystallized grains always preferred to nucleate and grow at the PFZ where the pinning effect of dislocations was the weakest [33]. Once the recrystallized grains encountered the dispersoid zone, the growth was arrested and thus the growing of recrystallized grains were restricted in the PFZ.

Fig. 6. 12 gave another evident that SRX took place only in PFZs. Compared the enlarge EBSD map with the optical image, it can be seen that the recrystallized grain band well matched the PFZ shape and distribution in the matrix. Furthermore, the size of recrystallized grains (about 7μm, Fig. 6. 12a) was very close to the PFZ width (Fig. 6. 12b), confirming SRX mainly occurred at PFZs. In addition, the PFZ area fractions of individual alloys are well corresponded with the recrystallization fractions. As mentioned above, the PFZ area fraction increased from 2.7% in the 0.5Mn alloy to 6.8% and 16.7% in the 0.75Mn and 1Mn alloys (Fig. 6. 3), while the recrystallization fraction increased from 2.1% in the 0.5Mn alloy to 5.2% and 14.7% in the 0.75Mn and 1Mn alloys (Fig. 6. 8b), respectively.

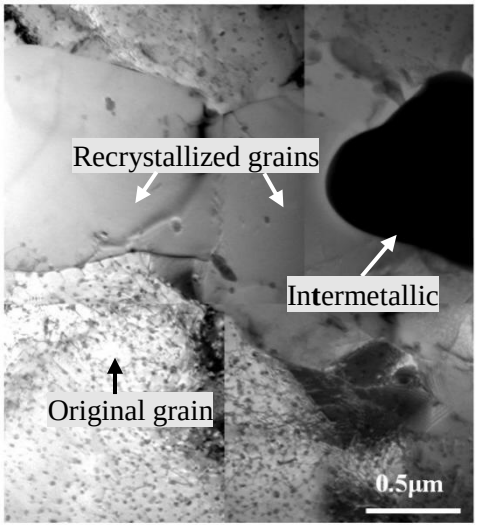

Fig. 6.11 Recrystallized grain in the 1Mn alloy after 8h of annealing

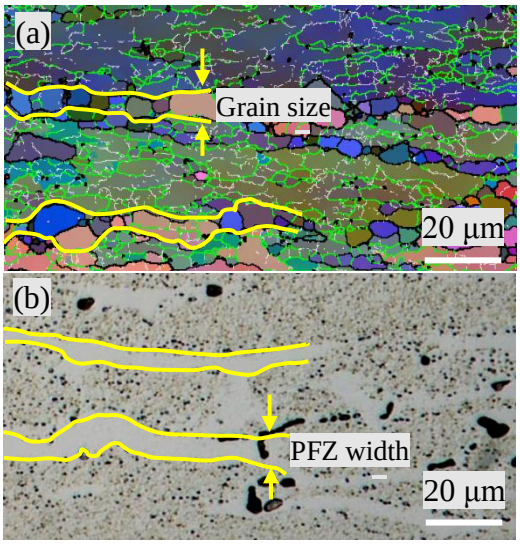

Fig. 6.12 EBSD orientation map (a) and optical image (b) of the 1Mn alloy after 8h of annealing

Fig. 6. 13 shows a schematic of how the recrystallization took place. After hot deformation, a large amount of substructures was induced at both dispersoids zones

and PFZs (Fig. 6. 13a), which is represented in Fig. 6. 4. During post-deformation annealing (Fig. 6. 13b), a high temperature provided driving force for the motion of dislocations and subgrains. In the dispersoids zone, owing to the strong pinning effect of dispersoids on dislocations and subgrain boundaries, only SRV was able to take place. However, in PFZs, SRX can started via the diminish or coalescence of dislocations into subgrains due to the absence of dispersoids and the weakest pinning effect (Fig. 6. 13b). In addition, within PFZs the regions surrounding the large intermetallic particles were highly strained during hot deformation, resulting in a higher density of dislocations and subgrains compared to other interdendrite regions. During annealing, the nucleation of new grains preferred to occur in those regions near the intermetallic particles where driving force were higher, which was known as particle-stimulated nucleation of recrystallization [2, 34, 35]. As a result, PFZs acted as the preferred regions where SRX started and propagated. The fully recrystallized grains in PFZs formed when the high angle boundaries formed (Fig. 6. 13c).

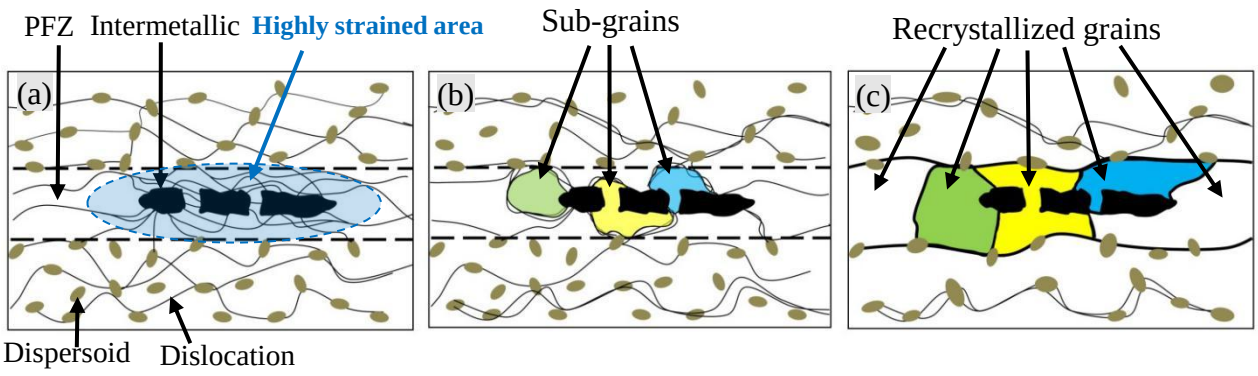

Fig. 6.13 (a) Orientation imaging maps and (b) optical microscope image of the 0.1Mn alloy after 8h of annealing

It should be noticed that the coarsening and dissolution of dispersoids occurred during post-deformation annealing in all three Mn-containing alloys owing to less thermally stable of dispersoids at 500 ℃ (Figs. 6. 9 and 10). However, the above results indicate that the recrystallization resistance was mainly controlled by the PFZ fraction and less influenced by the number density and the coarsening of dispersoids. It was reported that even a low density of dispersoids of 0.003 μm^{-2} could have great influence on the recrystallization resistance in Al-Mg-Si alloys [33]. The dispersoid densities even after 8 h annealing at 500 ℃ still ranged from 3.2 μm^{-2} to 5.5 μm^{-2} in three Mn-containing alloys (Fig. 6. 10), which were probably far enough for inhibiting recrystallization. Therefore, the distribution of dispersoids associated with PFZ is in fact the predominant factor controlling the recrystallization resistance during annealing.

6.5. Conclusions

(1) By the addition of Mn and the low temperature homogenization treatment at 450 °C, a large amount of α-Al(Mn,Fe)Si dispersoids were generated and retained in the aluminum matrix of Mn-containing 6082 aluminum alloys.

(2) During post-deformation annealing at 500 ℃, the base alloy free of Mn and dispersoids exhibited the worst recrystallization resistance. After 2 h annealing a partial static recrystallization occurred, whereas after 4 h annealing the grain growth appeared.

(3) The presence of a large amount of dispersoids greatly stabilized the deformed structure and thus significantly improved the recrystallization resistance. Even after 8 h at 500 ^{o}C annealing, the recovered grain structure was well retained in all Mn-containing 6082 aluminum alloys.

(4) In the Mn–containing alloys, a small amount of recrystallized grains can be observed. The static recrystallization took place in the precipitation free zones (PFZs) and the recrystallization resistance was mainly controlled by the PFZ fraction. The increased PFZ fraction with increasing Mn content led to an increase in the recrystallization fraction. Among three Mn-containing alloys, the alloy with 0.5% Mn exhibited the best recrystallization resistance due to the minim PFZs. With further increase in the Mn content to 0.75% and 1%, the recrystallization resistance moderately deteriorated due to the increased PFZ fraction.

References

[1] A. Cuniberti, A. Tolley, M.V. Castro Riglos, R. Giovachini, Influence of natural aging on the precipitation hardening of an AlMgSi alloy, Mater. Sci. Eng. A 527 (2010) 5307–5311

[2] M. Usta, M.E. Glicksman, R.N. Wright The effect of heat treatment on Mg_2Si coarsening in aluminum 6105 alloy. Metall. Mater. Trans. A. 35, 2 (2004) 435-438

[3] K. Liu, X.-G. Chen, Development of Al–Mn–Mg 3004 alloy for applications at elevated temperature via dispersoid strengthening, Mater. Des. 84 (2015) 340–350.

[4] Z. Li, Z. Zhang, X.-G. Chen, Microstructure, elevated-temperature mechanical properties and creep resistance of dispersoid-strengthened Al-Mn-Mg 3xxx alloys with varying Mg and Si contents, Mater. Sci. Eng. A 708 (2017) 383–394.

[5] K. Liu, H. Ma, X.-G. Chen, Enhanced elevated-temperature properties via Mo addition in Al-Mn-Mg 3004 alloy, J. Alloy Comp. 694 (2017) 354–365.

[6] X. Qian, N. Parson, X.-G. Chen, Effects of Mn addition and related Mn-containing dispersoids on the hot deformation behavior of 6082 aluminum alloys, Mate. Sci. Eng. A 764 (2019) 138253.

[7] C. L. Liu, H. Azizi-alizamini, N. C. Parson, W. J. Poole, Q. Du, Microstructure evolution during homogenization of Al−Mg−Si−Mn−Fe alloys: Modelling and experimental results, Trans. Nonferrous Met. Soc. China 27(2017) 747−753

[8] C. Li, Precipitation Behaviors of dispersoids induced from transition elements (Mn, Sc and Zr) and their effect on recrystallization resistance in AA6082 alloys, Master theses, University of Quebec at Chicoutimi (2018).

[9] C. Liu, Microstructure evolution during homogenization and its effect on the high temperature deformation behaviour in aa6082 based alloys, PhD thesis, The University of British Columbia (2017) 74−92

[10] C. Liu, Q. Du, N. Parson, W. Poole, The interaction between Mn and Fe on the precipitation of Mn/Fe dispersoids in Al-Mg-Si-Mn-Fe alloys, Scripta Mater. 152 (2018) 59–63.

[11]. S. Lin, Z. Nie, H. Huang, B. Li, Annealing behavior of a modified 5083 aluminum alloy, Mater. Des. 31 (2010) 1607–1612

[12]. H.J. McQueen, S. Spigarelli, M.E. Kassner, and E. Evagelista, Hot Deformation and Processing of Aluminum Alloys, CRC, Bradenton, FL, (2011) 383-403

[13] J. Corral, E.A. Trillo, Y. Li, L.E. Murr, Corrosion of friction-stir welded aluminum alloys 2024 and 2195, Journal of Mater. Sci. Letters, 19 (2000), 2117–2122.

[14] I.N. Fridlyand, A.M. Drits, A.A. Yeliseyev, Lightweight and high-temperature alloys and the processing of them, Nauka, Moscow (1986) 126-130.

[15] Y.W. Riddle, T.h. Sanders, Jr., A study of coarsening, recrystallization, and morphology of microstructure in Al-Sc-(Zr)-(Mg) alloys, Metal. Mater. Trans. A 35a (2004) 341-350.

[16] R.R. Sawtell, C.L. Jensen, Mechanical properties and microstructures of Al-Mg-Sc alloys, Metal. Trans. A, 21a, (1990) 421-430.

[17] K.H. Chen, H.C. Fang, Z. Zhang, X. Chen, G. Liu, Effect of of Yb, Cr and Zr additions on recrystallization and corrosion resistance of Al–Zn–Mg–Cu alloys, Mater. Sci. Eng. A 497 (2008) 426–431

[18] M. B. Kannan, V.S. Raja, Enhancing stress corrosion cracking resistance in Al‐Zn-Mg-Cu-Zr alloy through inhibiting recrystallization, Eng. Fracture Mech. 77 (2010) 249‐256

[19] F.-S. Lin, E. A. Starke, Jr., The effect of copper content and degree of recrystallization on the fatigue resistance of 7xxx type aluminum alloys: I. low cycle corrosion fatigue, Mater. Sci. Eng. A, 39 (1979) 27-41

[20] Y. Birol, Impact of partial recrystallization on the performance of 6005A tube

extrusions, Eng. Fail. Anal. 17 (2010) 1110–1116.

[21] Z. Guo, G. Zhao, X. G. Chen, Effects of two-step homogenization on precipitation behavior of Al3Zr dispersoids and recrystallization resistance in 7150 aluminum alloy, Mater. Charact. 102 (2015) 122–130.

[22] Z. Guo, G. Zhao, X. G. Chen, Effects of homogenization treatment on recrystallization behavior of 7150 aluminum sheet during post-rolling annealing, Mater. Charact. 114 (2016) 79–87

[23] H. Li, Z. Gao, H. Yin, H. Jiang, X. Sua and J. Bin, Effects of Er and Zr additions on precipitation and recrystallization of pure aluminum, Scripta Mater. 68 (2013) 59–62

[24] Y. Birol, Effect of Cr and Zr on the grain structure of extruded EN AW 6082 alloy, Met. Mater. Int., Vol. 20, No. 4 (2014) 727-732

[25]. D. Tsivoulas, P.B. Prangnell, The effect of Mn and Zr dispersoid-forming additions on recrystallization resistance in Al–Cu–Li AA2198 sheet, Acta Mater. 77 (2014) 1–16

[26] M. Shakiba, N. Parson, X.-G.Chen, Hot Deformation Behavior and Rate-controlling Mechanism in Dilute Al–Fe–Si Alloys with Minor Additions of Mn and Cu, Mater. Sci. Eng. A, 636, (2015) 572-581

[27] M. Shakiba, N. Parson, and X.-G. Chen, Effect of Iron and Silicon Content on the Hot Compressive Deformation Behavior of Dilute Al-Fe-Si Alloys, J. Mater. Ene. Perform, 24(1) (2015) 405

[28] C. Shi, W. Mao, X.-G. Chen, Evolution of activation energy during hot

deformation of AA7150 aluminum alloy, Mater. Sci. Eng. A 571 (2013) 83–91

[29] C. Shi, X.-G. Chen, Effect of vanadium on hot deformation and microstructural evolution of 7150 aluminum alloy, Mater. Sci. Eng. A 613 (2014) 91–102

[30] O.V. Mishin, D. Juul Jensen, And N. Hansen, Evolution of Microstructure and Texture during Annealing of Aluminum AA1050 Cold Rolled to High and Ultrahigh Strains, Metall. Mater. Trans. A, 41A, (2010), 2936-2948

[31] C. Schafer, V. Mohles, G. Gottstein, Modeling of non-isothermal annealing: Interaction of recrystallization, recovery, and precipitation, Acta Mater. 59 (2011) 6574–6587

[32] J. D. Robson And P. B. Prangnell, Dispersoid Precipitation and Process Modelling in Zirconium Containing Commercial Aluminium Alloys, Acta mater. 49 (2001) 599–613

[33] R. Hu, T. Ogura, H. Tezuka, T. Sato and Q. Liu, Dispersoid formation and recrystallization behavior in an Al-Mg-Si-Mn alloy, J. Mater. Sci. Technol., 26(3), (2010) 237-243.

[34] F.J. Humphreys, The nucleation of recrystallization at second phase particles in deformed aluminium, Acta Metall. 25 (1977) 1323–1344.

[35] D.P. Field , L. Behrens and J.M. Root, Identification of Particle Stimulated Nucleation during Recrystallization of AA 7050, CMC, 14, 3, (2009) 171-183.

Chapter 7 Conclusions & Recommendations

7.1 Conclusions

This research was carried out to investigate effect of Mn as well as the different heat treatment on the microstructure and hot deformation behavior and 6060 and 6082 alloys. The results obtained were divided into three parts.

In part Ⅰ, the effect of the homogenization treatment and micro-alloying of Mn on the evolution of microstructure and hot workability of AA6060 aluminum alloys were investigated. The effect of homogenization temperature and cooling rate as well as micro-alloying of Mn on Mg_2Si precipitation and hot workability of 6060 aluminum alloys were investigated in part Ⅱ. The main focus of part Ⅲ is the effects of Mn-containing dispersoids on the hot deformation behavior of 6082 aluminum alloys. In Part Ⅳ effect of Mn and dispersoids on recrystallization resistance of 6082 aluminum alloy during post-deformation annealing was studied. Based on the results from Chapter 3 to Chapter 6, the following conclusions could be drawn:

Part Ⅰ: Effect of the homogenization treatment and micro-alloying of Mn on the evolution of microstructure and hot workability of AA6060 aluminum alloys

(1) The β-AlFeSi intermetallic was the dominant phase in the as-cast microstructure of AA6060 alloys containing up to 0.10 wt.% Mn. During the homogenization, intermetallic fragmentation occurred, and plate-like β-AlFeSi transformed into rod-like α-AlFeSi. The micro-alloying with Mn promoted the transformation of

β-AlFeSi into α-AlFeSi at lower temperatures.

(2) α-Al(FeMn)Si dispersoids were precipitated during the homogenization of the 0.1 wt.% Mn variant. The highest number density was observed at 520 ℃, and coarsening and dissolution occurred above 550 ℃. Owing to their low number density and relatively large size, the effect of dispersoids on the flow stress was determined to be negligible.

(3) The flow stress behavior of homogenized AA6060 alloys was mainly determined by the solid solution level. The increase in the homogenization temperature resulted in higher flow stresses owing to the increase in Fe, Si solute levels released from intermetallics in the aluminum matrix.

(4) The incremental Mn addition from 0 to 0.1% moderately increased the flow stress by up to 3%. In Mn-containing alloys, the flow stress decreased with increasing soaking time owing to the long-range diffusion of Mn to the constituent particles, which exhibited a corresponding increase in the Mn/Fe ratio.

(5) The abnormal grain growth occurred in alloys with low Mn contents (<0.03Mn) during the high-temperature homogenization (580–610 ℃), which resulted in a reduced flow stress and non-uniform deformation. Higher additions of Mn (>0.06%) effectively prevented this effect.

Part Ⅱ: Effect of homogenization treatment and micro-alloying with Mn on Mg_2Si precipitation and hot workability of 6060 aluminum alloys

(1) During post homogenization cooling of AA6060 alloys at commercially relevant rates, Mg_2Si particles precipitated in the aluminum matrix, and their number

density and size had a significant effect on the solid solution level and high temperature flow stress.

(2) At lower post homogenization cooling rates, the flow stress decreased due to the precipitation of Mg_2Si and the reduction of solid solution levels. The lowest cooling rate tested (100 ^oC/h), produced the lowest flow stress corresponding to the maximum precipitation of Mg_2Si.

(3) Micro-alloying of 0.1% Mn in AA6060 alloys generated a reasonable number of α-Al(FeMn)Si dispersoids during homogenization. These acted as favorable nucleation sites for Mg_2Si and promoted the precipitation of Mg_2Si during post homogenization cooling, resulting in a higher number density and smaller size of Mg_2Si compared to the base alloy free of Mn.

(4) The benefits of the 0.10wt%Mn addition varied with the homogenization temperature applied, reflecting the relative effects on Mg, Si and Mn solid solution levels:

a) At 515℃ the flow stress was reduced compared to the base alloy and the Mg_2Si particle size was reduced

b) At 545℃ the flow stress was similar to the base alloy but the Mg_2Si particles size was still reduced

c) At 575℃ the flow stress was increased due to the Mn solid solution level but the Mg_2Si particle size was still finer than the base alloy.

Part Ⅲ : Effect of Mn addition and its related Mn-containing dispersoids on the hot deformation behavior of 6082 aluminum alloys

(1) Treated at a low temperature homogenization of 450 ℃ for 6 h, a large amount of α-Al(FeMn)Si dispersoids precipitated and retained in the microstructure of Mn-containing 6082 aluminum alloys. With increasing Mn content, the number density of dispersoids increased, whereas the equivalent diameter remained nearly unchanged.

(2) With the addition of 0.5% Mn, the peak flow stresses increased significantly due to the strong strengthening effect of dispersoids comparing with the base alloy free of dispersoids. With further increase in the Mn content from 0.5 to 1%, the peak flow stresses increased moderately.

(3) The materials constants and activation energy for hot deformation were calculated using the hyperbolic-sine constitutive equation and experimental peak flow stress data. The hot deformation activation energy of 6082 alloys increased sharply from 191.2 kJ/mol for the base alloy to 285.6 kJ/mol for the alloy containing 0.5% Mn. With further increasing the Mn content, the activation energy increased moderately to 301.2 and 315.4 kJ/mol in the 0.75% Mn and 1% Mn alloys respectively.

(4) The addition Mn in 6082 alloys promoted the retardation of dynamic recovery and the inhibition of recrystallization during hot deformation due to the strong pinning effect of Mn-containing dispersoids on dislocation slips and subgrain rotations.

(5) It was found that in the Mn-containing alloys, the flow stresses decreased largely with increase strain at relatively low Z deformation conditions after reaching the peak flow stress. Depending on which flow stresses taking into account in the

calculation of the activation energy, the derived activation energy values decreased significantly with increasing strain, showing the dependence of the activation energy on the deformation condition.

Part Ⅳ : Effect of Mn and dispersoids on recrystallization resistance of 6082 aluminum alloys during post-deformation annealing

(1) By the addition of Mn and the low temperature homogenization treatment at 450 °C, a large amount of α-Al(Mn,Fe)Si dispersoids were generated and retained in the aluminum matrix of Mn-containing 6082 aluminum alloys.

(2) During post-deformation annealing at 500 ℃, the base alloy free of Mn and dispersoids exhibited the worst recrystallization resistance. After 2 h annealing a partial static recrystallization occurred, whereas after 4 h annealing the grain growth appeared.

(3) The presence of a large amount of dispersoids greatly stabilized the deformed structure and thus significantly improved the recrystallization resistance. Even after 8 h at 500 ^{o}C annealing, the recovered grain structure was well retained in all Mn-containing 6082 aluminum alloys.

(4) In the Mn–containing alloys, a small amount of recrystallized grains can be observed. The static recrystallization took place in the particle free zones (PFZs) and the recrystallization resistance was mainly controlled by the PFZ fraction. The increased PFZ fraction with increasing Mn content led to an increase in the recrystallization fraction. Among three Mn-containing alloys, the alloy with 0.5% Mn exhibited the best recrystallization resistance due to the minim PFZ. With

further increase in the Mn content to 0.75% and 1%, the recrystallization resistance moderately deteriorated due to the increased PFZ fraction.

7.2 Recommendations

In the present study, the alloys investigated were mainly refers to Mn addition, heat treatment and hot deformation behavior of 6060 and 6082 alloys. Effects of the homogenization temperature, time, cooling rats as well as micro-alloying of Mn on the evolution of microstructure and hot workability of AA6060 aluminum alloys were investigated. Effects of Mn-containing dispersoids on the hot deformation behavior and recrystallization resistance of 6082 aluminum alloys were investigated. Hot deformation flow stresses and activation energies as well as DRV, DRX, SRV and SRX were investigated. Based on the present study following recommendations can be made for future work:

(1) Study of Mn-dispersoids strengthening, solid solution strengthening and T5/T6 aging strengthening in 6082 alloys. By conducting different heat treatment, the alloy could be strengthened via three hardening mechanism, the alloys could be strengthened through different ways and achieve the optimum mechanical properties at room or elevated temperatures.

(2) Investigation of mechanical properties failure mechanism of 6082 alloys. With a certain heating procedure, mechanical properties failure takes place via dissolution of nano-scale Mg_2Si and dispersoids. Whereas the solid solution strengthening is always effective. The strengthening mechanism on function of Mn and heating

procedure deserves to be studied systemically.

(3) Recrystallization resistance in the four 6082 alloys. Different initial deformation conditions could be selected to respond the different energy storage level, with the different dispersoids amount in alloys, recrystallization resistance during different annealing treatment could be further studied.

(4) Analysis of the dispersoids dissolution process during hot deformation and annealing. The relationship between dispersoids dissolution and deformation flow stress curve as well as the properties after deformation and annealing could be investigated systemically.

(5) Constitutive modeling based on the flow stress curves. The entire flow stress curves could be used as the typical flow stress during constitutive analyses, so that a map of activation energies could be established based on the flow stress curves, which reflecting the dynamical relationship between activation energies and flow stresses.